7-2016

Configuration and Optimization of a Novel Compressed-Air-Assisted Wind Energy Conversion System

Jie Cheng
University of Nebraska-Lincoln, chengjiecc@gmail.com

CONFIGURATION AND OPTIMIZATION OF A NOVEL COMPRESSED-AIR-ASSISTED WIND ENERGY CONVERSION SYSTEM

by

Jie Cheng

A DISSERTATION

Presented to the Faculty of

The Graduate College at the University of Nebraska

In Partial Fulfillment of Requirements

For the Degree of Doctor of Philosophy

Major: Electrical Engineering

Under the Supervision of Professor Fred Choobineh

Lincoln, Nebraska

July, 2016

CONFIGURATION AND OPTIMIZATION OF A NOVEL COMPRESSED-AIR-ASSISTED WIND ENERGY CONVERSION SYSTEM

Jie Cheng, Ph.D.

University of Nebraska, 2016

Advisors: Fred Choobineh

The increasing concerns over the environmental impact of carbon emissions and the unsustainability of conventional fossil fuel power plants are stimulating interest in the implementation of renewable energy in current power systems. Among all of the renewable energies, wind energy holds a prominent place because of its high output and the maturity of the technology. However, like all of the other renewable energies, integration of wind energy into the power grid causes some quality and control issues, such as overvoltage or undervoltage and frequency excursion.

Other issues include: 1) wind power generation may require a broader safety margin of the capacity reserve, 2) the excessive energy may be rejected by the transmission because of the mismatch between generation and load demand, and 3) induction wind turbines may not be able to ride through a voltage sag event because a critical voltage has to be guaranteed to produce the fundamental magnetic field.

To mitigate these issues and build a robust wind power system, a novel structure referred to as a compressed-air-assisted wind energy conversion system (CA-WECS) is proposed in this dissertation. The CA-WECS converts the wind-generated mechanical spillage to compressed air when the wind is a surplus and regenerates power from the

compressed air storage when the wind is a deficit. The addition of a compressed air storage subsystem decouples wind power and electric power allowing a higher level of dispatchable generation and providing another degree of freedom for power management. The key component of the new system is a variable displacement machine (VDM), which can work as a compressor or air motor/expander depending on the power gap between wind power and load/command.

This work addresses the configuration of the CA-WECS in detail. The functions of the system components are explained and the fundamentals of the proposed VDM are explicitly described. A regulation policy for dispatchable generation is simulated and studied. The economical issues associated with the implementation of the proposed system are split into two parts, the sizing problem and the offering problem. The sizing problem refers to finding the proper sizes of different components for the proposed system. The offering problem refers to determining the appropriate offer to the day-ahead electricity market for a wind farm consisting of the proposed system. A two-stage stochastic framework is used to solve the optimization model each problem. The simulation studies validate the benefits of the proposed system. The results show that renewable generation is increased by 15-20% under various wind conditions, accounting for a 20-30% revenue increment in a dynamic market environment.

ACKNOWLEDGMENTS

First and foremost, I would like to express my deep gratitude to my advisor, Prof. Fred Choobineh, for his guidance, inspiration, and continuous support for all of the technical and personal aspects of my studies. His advice and suggestions will be of great help in my future career.

I would like to thank my committee members, Dr. Jerry Hudgins, Dr. Sohrab Asgarpoor, Dr. Qing Hui, and Dr. Kevin Cole, for their suggestions and advice. I would never have been able to finish my Ph.D. study without their motivations on creative and critical thinking.

I sincerely thank Paul Marxhausen from the Engineering Electronics (EE) Shop, Jim McManis from the Engineering & Science Research Support Facility (ESRSF), Tom Davlin from Lincoln Electric System (LES), and Michele Suddleson from American Public Power Association (APPA), for their technical and financial help during the research.

I would like to thank my fellow lab mates, Omid, Mehdi, Milad, Jairo, and all others, for their discussion and help. I would also thank my friends and coworkers, Xiaojian, Desmond, Bo, Shiyuan, and Hao, for their kind help during the early stages of the experiment.

Last but not the least, I would like to acknowledge my parents for their unconditional love and support throughout my life. I thank my wife, Lan, for bringing me two little lovely daughters, Chelsea and Ella, during this beautiful journey.

TABLE OF CONTENTS

LIST OF ACRONYMS

a_0	Power density discount factor of the selected wind generator in the wind farm
a_i	Power density discount factor of the i^{th} option of the generator
A^w	Blade swept area
b_0	Friction loss of the selected wind generator in the wind farm
b_i	Friction loss of the i^{th} option of the generator
B_L	Lower bound of the transmission ratio of the CVT
B_U	Upper bound of the transmission ratio of the CVT
c_1	Scale factor for the deviation while sampling wind speed from a distribution
c_2	Torque discounting factor on fluid friction loss
C	Discounted cost through the planning horizon
$CVaR$	Conditional Value-and-risk
CI	Unit price
CM	Annual operation and maintenance cost
C^{IC}	Upper limit of the initial capital
C^{TU}	Discounted cost of the tank unit in the planning horizon
C_p	Coefficient of the power for wind energy
C_i^G	Discounted cost of the i^{th} option of the generator through the planning horizon

C_j^V Discounted cost of the j^{th} option of the variable displacement machine through the planning horizon

C_m^D Discounted cost of the m^{th} option of the compressed-air-assisted wind energy conversion system in the planning horizon

C_n^U Discounted cost of the n^{th} option of the generator in the planning horizon

$C_{t,\omega}^{PT}$ Cost of the penalty at time t in scenario ω

CI^{TU} Unit price of the tank unit

CI_i^G Unit price of the i^{th} option of the generator

CI_j^V Unit price of the j^{th} option of the variable displacement machine

CI_m^D Unit price of the m^{th} option of the compressed-air-assisted wind energy conversion system

CI_n^U Unit price of the n^{th} option of the transmission upgrade plan

CM^{TU} Annual operation and maintenance cost of the tank unit

CM_i^G Annual operation and maintenance cost of the i^{th} generator

CM_j^V Annual operation and maintenance cost of the j^{th} variable displacement machine

CM_m^D Unit price of the m^{th} option of the compressed-air-assisted wind energy conversion system

CM_n^U Unit price of the n^{th} option of the transmission upgrade plan

$e_{t,\omega}^{da}$ Day-ahead electricity price in \$/kWh at time t in scenario ω

$e_{t,\omega}^{rt}$ Real-time electricity price in \$/kWh at time t in scenario ω

E^{TU} Energy capacity in an air tank unit

E_t^T Energy state in the air tank at time *t*

$E_{t,\omega}^T$ Energy state in the air tank at time *t* in scenario ω

$E_{t,\omega}^{T,k}$ Energy state in the air tank at time *t* in scenario ω for the k^{th} wind turbine in the farm

E_L^T Energy capacity of the selected storage in the wind farm

f^{loss} Friction loss of the a wind turbine

$f_{H,\delta}^D$ Compression power as a function of the *H* and δ

$f_{H,\delta}^\gamma$ Compression rate as a function of the *H* and δ

F_ζ^D Tangential force component at position ζ on wobble plate

F_ζ^N Orthogonal force component at position ζ on wobble plate

F_ζ^P Piston force at position ζ on wobble plate

h Length of the time within each time step

H Value of the neutral piston displacement

i Index of the i^{th} option of the generator

j Index of the j^{th} option of the variable displacement machine

k Index of the k^{th} wind turbine in the wind farm

m Index of the m^{th} option of the compressed-air-assisted wind energy conversion system

M_{11} Auxiliary constant for either-or constraint elimination

M_{12} Auxiliary constant for either-or constraint elimination

n Index of the n^{th} option of the transmission upgrade plan

n^{cy} Number of the all of the cylinders in the variable displacement machine

n_1^{cy} Number of the closed compression cylinders in the variable displacement machine

n_2^{cy} Number of the open ejection cylinders in the variable displacement machine

N^h Total number of the time step over the planning horizon

N^D Total number of the options of the compressed-air-assisted wind energy conversion system

N^G Total number of the options of the generator

N^K Total number of the wind turbines in the wind farm

N^U Total number of the option of the transmission upgrade plan

N^V Total number of the options of the variable displacement machine

N^φ Total number of the scenarios in the decision tree

p^o Atmospheric pressure

p^T Tank pressure in general case

p_ζ Cylinder pressure at position ζ

p_ω The profit for given solution under scenario ω

p_L^T The rated air pressure of the tank

P^B Mechanical power from the blade in general case

P^{Gi} Mechanical input power to the generator in general case

P^{Go} Electric output power from the generator in general case

P^{Vc} Compression power of the variable displacement machine in general case

P^{Vp} Expansion power of the variable displacement machine in general case

P_i^G Power capacity of the i^{th} option of the generator (output power)

P_j^V Power capacity of the i^{th} option of the variable displacement machine (output power)

P_L^G Power capacity of the wind generator in the wind farm

P_L^V Power capacity of the selected variable displacement machine in the wind farm

P_m^G Power capacity of the m^{th} option of the transmission line

P_m^V Power capacity of the m^{th} option of the transmission line

P_n^U Power capacity of the n^{th} option of the transmission line

P_t^r Power offer to the day-ahead market at time *t*

P_t^B Mechanical power from the blade at time *t*

P_t^{Gi} Mechanical input power to the generator at time *t*

P_t^{Go} Electric output power from the generator at time *t*

P_t^{Vp} Expansion power of the variable displacement machine at time *t*

P_t^{Vc} Compression power of the variable displacement machine at time *t*

$P_{t,\omega}^{dF}$ Wind farm power deviation at time *t* in scenario ω

$P_{t,\omega}^{dF^+}$ Positive balance of the wind farm power deviation at time *t* in scenario ω

$P_{t,\omega}^{dF^-}$ Negative balance of the wind farm power deviation at time *t* in scenario ω

$P_{t,\omega}^{B}$ Mechanical power from the blade at time *t* in scenario ω

$P_{t,\omega}^{B,k}$ Mechanical power from the blade at time *t* in scenario ω for the k^{th} wind turbine in the farm

$P_{t,\omega}^{B,L,i}$ Pretreated maximum blade power for the i^{th} options of the generator at time *t* in scenario ω

$P_{t,\omega}^{B,L,k}$ Pretreated mechanical power limit of the blade for the k^{th} wind turbine in the farm at time *t* in scenario ω

$P_{t,\omega}^{F}$ Wind farm output power at time *t* in scenario ω

$P_{t,\omega}^{Gi}$ Mechanical input power to the generator at time *t* in scenario ω

$P_{t,\omega}^{Gi,k}$ Mechanical input power to the generator at time t in scenario ω for the k^{th} wind turbine in the farm

$P_{t,\omega}^{Go}$ Electric output power from the generator at time *t* in scenario ω

$P_{t,\omega}^{Go,k}$ Electric output power from the generator at time *t* in scenario ω for the k^{th} wind turbine in the farm

$P_{t,\omega}^{LD}$ Microgrid power load demand at time *t* in scenario ω

$P_{t,\omega}^{Vc}$ Compression power of the variable displacement machine at time *t* in scenario ω

$P_{t,\omega}^{Vc,k}$ Compression power of the variable displacement machine at time *t* in scenario ω for the k^{th} wind turbine in the farm

$P_{t,\omega}^{Vp}$ Expansion power of the variable displacement machine at time *t* in scenario ω

$P_{t,\omega}^{Vp,k}$ Expansion power of the variable displacement machine at time *t* in scenario ω for the k^{th} wind turbine in the farm

r	Annual interest rate
r^{TR}	CVT transmission ratio
$r_{t,\omega}^{+}$	Positive imbalance ratio at time *t* in scenario ω
$r_{t,\omega}^{-}$	Negative imbalance ratio at time *t* in scenario ω
R^{B}	Length of the blade or radius of the swept area
R^{D}	Wobble plate radius; the distant from plate shaft to piston joint on wobble plate
R_1	Effective radius of the primary shaft of the CVT
R_2	Effective radius of the Secondary shaft of the CVT
R_ζ	Arm at position ζ
s_ω	Auxiliary variable for the calculation of the Conditional Value-and-risk (CVaR)
S	Piston head area
t	Index of the time step
t_0	Time-lag constant for the deviation of the wind speed while sampling wind speed from a distribution
T^{D}	Variable displacement machine average torque
T_{1a}	Torque on the left side of the primary shaft of the CVT
T_{1b}	Torque on the right side of the primary shaft of the CVT
T_2	Torque on the secondary shaft of the CVT
$T_{\zeta,1}$	Torque at position ζ on the wobble plate during the closed compression phase

$T_{\zeta,2}$ Torque at position ζ on the wobble plate during the open ejection phase

u_1 Auxiliary variable for either-or constraint elimination; also indicating on/off of the clutch

v_{in} Cut-in speed of the a wind turbine

v_{out} Cut-out speed of the a wind turbine

v_{r1} Rated speed of the a wind turbine corresponding to electrical capacity

v_{r2} Rated speed of the a wind turbine corresponding to mechanical/structural capacity

v_t Wind speed at time *t*

v_t^f Wind speed forecasting reference at time *t*

V^T Rated volume of the compressed air storage

V_1 Cylinder volume corresponding to the beginning of the closed compression

V_2 Cylinder volume corresponding to the end of the closed compression

V_ζ Cylinder volume at position ζ

x_i^G Binary decision variable for the i^{th} option of the generator

x_j^V Binary decision variable for the j^{th} option of the variable displacement machine

x_m^D Binary decision variable for the m^{th} option of the compressed-air-assisted wind energy conversion system

x_n^U Binary decision variable for the n^{th} option of the transmission upgrade plan

y^T Integer number of the tank unit

Y Component life cycle in year

α Confidence level

β Weighting parameter to quantize the tradeoff between profit and risk aversion attitude

γ^{Vc} Compression ratio for ideal gas corresponding to the end of the closed compression

γ_ζ^{Vc} Compression ratio for ideal gas at position ζ

γ_ζ^{Vp} Expansion ratio for ideal gas at position ζ

δ^B Blade pitch angle

δ^V Angle of the wobble plate in a variable displacement machine

ε Auxiliary variable for zero-product constraint elimination

ζ Polar angle on wobble plate surface for piston position

ζ_1^{cy} Angle coverage of the closed compression cylinders in the variable displacement machine

ζ_2^{cy} Angle coverage of the open ejection cylinders in the variable displacement machine

η^G Efficiency of the generator

η^T Efficiency of the air tank

η^{Vp} Efficiency of the variable displacement machine as an expander

η^{Vc} Efficiency of the variable displacement machine as a compressor

θ_t Wind power density at time *t*

$\theta_{t,\omega}$ Wind power density at time *t* in scenario ω

$\theta_{t,\omega}^{k}$ Wind power density at the k^{th} wind turbine location in the wind farm at time *t* in scenario ω

λ Tip speed ratio

ξ Auxiliary variable whose optimal value is equal to Value-and-risk (VaR)

ρ Air density

φ_{ω} Probability of the scenario ω

ω Index of the scenario

Ω^{B} Rotation speed of the blade

Ω_{1} Rotation speed of the primary shaft of the CVT

Ω_{2} Rotation speed of the secondary shaft of the CVT

$\Omega_{p^T}^{V,opt}$ Optimal rotation speed of the variable displacement machine under the tank pressure p^T

LIST OF FIGURES

LIST OF TABLES

CHAPTER 1. INTRODUCTION

1.1. Renewable Energy Exploration Trend

Renewable energy includes solar, the wind, hydro, oceanic, geothermal, biomass, and other sources of energy that are ultimately derived from “nuclear fusion in the sun”, and are thus renewed infinitely as a course of nature [1]. More broadly, renewable energy is derived from a power source that can be replenished repeatedly and sustainably with no or very little adverse side effects.

The renewable energy sources like wind and solar are considered as a promising and sustainable solution to future energy needs due to their abundance and environmental friendliness. In addition, the use of renewable energy technologies is receiving additional attention by power system planners and regulators, because of the depletion of fossil fuel and global warming issue associated with carbon emission. The European Union has a mandate to satisfy 20% of its energy needs from renewable sources [1, 2], while the US Department of Energy envision 20% of electricity needs be satisfied from renewable sources by the year 2030 [3].

Among the renewable sources, wind energy has been the fastest-growing source of electricity in the world [4, 5]. Its ubiquitous availability, environmental friendliness, and strong output make it a competitive energy resource compared to the traditional ones. Lawrence Berkeley National Laboratory of U.S. Department of Energy has reported that the wind-power-purchase agreement price averaged 2.5 cents per kWh in 2013 [6].

The wind power industry has developed attractive technologies for wind energy conversion system (WECS) that has resulted in its adoption across a broad spectrum of applications including small-household-based and large-utility-based turbines.

A configuration of a household scale wind turbine system is depicted in Figure 1.1. A wind turbine consists of blades, gearbox, generator and AC/AC electronics. The electricity is mainly supplying the house load, while the output is still connected to grid through a point of common coupling (PCC). Grid works as a giant reservoir to mitigate any deviation/mismatch between the generation and load.

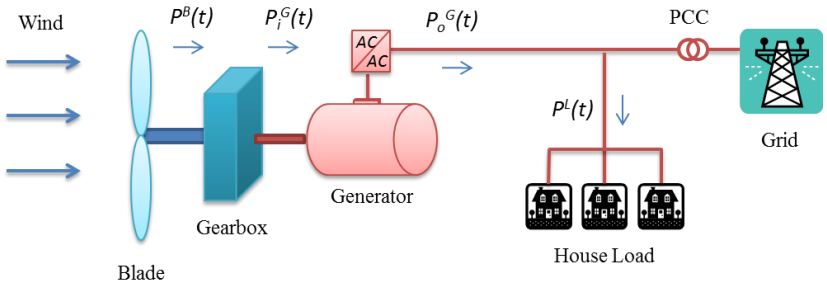

Figure 1.1: Traditional wind energy conversion system.

Solar energy is another widely recognized renewable energy source. Two types of technologies were developed to generate electricity from sunlight, namely, photovoltaics (PV), and concentrating solar power (CSP). Businesses and residential are interested in the first type, while utilities primarily utilize the second type.

PV panels capture the radiation power given off from the sun and convert it into electricity directly. PV panels do not need a rotary machine to operate, and A DC/AC converter could be used to bridge the panels to the grid.

CSP essentially concentrates sunlight to drive a traditional steam turbine, creating electricity on a large scale. The thermal energy from the sunlight is collected by arrays of mirrors or lens and is used to boil the water, in turn, to power the rotary engine.

Other forms of renewable energy include wave and tide energy in the ocean, geothermal energy in the ground, biomass energy from plants and crops. However, the technologies to utilize those energy resources are either premature for large scale applications or cost-ineffective at the current stage of development.

1.2. Issues of Integrating Renewable Energy into Power System

Although integration of renewable energy resources into the power system exhibits advantages such as no fuel cost, zero emission, there are some difficulties associated with those resources. First, availability of most renewable energy is unpredictable for a given period. Second, unlike fossil fueled generated energy, renewable energy is not dispatchable, meaning the system operator could not assign an output adjustment. Third, renewable energy is unable to adapt to the load pattern of the area, and in turn, the imbalance has to be mitigated by other resources.

There are a few ways to solve these problems. One way to limit the renewable energy adverse interference is setting an upper limit on the penetration level of renewables. This way reinforces the system reliability, while sacrificing the capacity of renewables. Forming a hybrid system is another way to alleviate the problem since multiple types of renewable energy could offset the shortage of each other and serve the load more consistently. Taking the wind and PV hybrid, for example, PV generation is dependent on daylight radiation, while the wind increases during the night. This combination smooths

the variation of the supply. However, it may not be sufficient because of the fast dynamic behavior of the power system.

Energy storage is introduced to maintain the power balance and energy effectiveness within the system. It enables the excess energy to be stored for the later deficit of supply. In addition, energy storage fulfills systematic functions like load leveling, power quality, ancillary services, and so forth. The requirement for transmission and distribution could be classified into three categories, response service, grid support, and power management [7, 8].

Response service is a transient regulatory capacity for power quality in the system. It primarily includes frequency control and voltage control. Power system requires the demand and supply to be equal at all times. The system frequency is a measure of this balance, where frequency increases if generation is greater than demand and vice versa. Storage could be a resource to compensate the angular excursion or suppress voltage variation and fluctuation.

Grid support means a short-term regulatory capacity for system security. It includes spinning reserve, non-spinning reserve (standing reserve) and black start capacity. Spinning reserve is a synchronized generation capacity, which could be ordered by the system operator for immediate generation of a certain amount of power. Standing reserve is a standby power generation capacity that could be offered within a short notice. Black start capability is an independent capacity to restore an electricity station or part of the power grid to operation without the support from external transmission network. The medium size storage with high energy density could provide spinning and non-spinning reserve while large-scale storage could be an option for the black start of the power system.

Power management represents strategic methods for system economic operation. It includes peak shaving, load leveling, and seasonal storage. Peak shaving presents a method to reduce the amount of energy demand from the utility during peak hours when the rate is high. Load leveling suppresses power flow fluctuation during a day so that to accommodate constant power output from the power plant, such as a nuclear plant. Seasonal storage is a vague concept for a system of high renewable energy penetration. The storage is built to compensate seasonal fluctuation in renewable power supply under worst case. The large scale long term storage is developed for power management, tackling with the economic operation of power system.

Additional requirements for integration of renewable energy could include forecast hedge, time shifting, and transmission curtailment. Various types of energy storage technologies have been developed to handle those issues [9, 10, 11]. The different application scenarios for those technologies are plotted in Figure 1.2. And the details of those technologies will be introduced in Section 1.3.

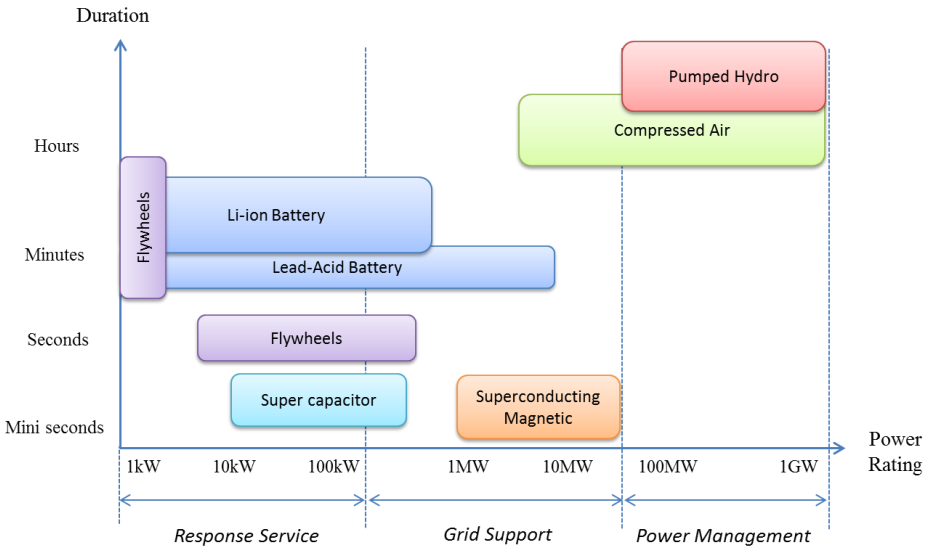

Figure 1.2: Storage for different application categories.

1.3. Storage Technologies for Renewable Energy

Because of the intermittent property of renewable energy resource, several energy storage technologies are coupled with them to form a reliable energy supply. The power industry has several regulations for system safety and stability, such as frequency and voltage regulation, operating reserves, black start capability, and so forth. Some of the storages may be appropriate to fulfill the particular type of regulations, but not all of them. Thus, the choosing of storage technology depends on the system requirement, geographic condition, response performance, space availability, type of energy resource, etc. Typical energy storage technologies include the following options.

1.3.1. Battery Energy Storage (BES)

Batteries have a long history serving as the storage for electricity, and they are considered as a responsive and reliable form of storage. Different types of batteries have been developed, including lead-acid, nickel-cadmium, lithium ion, sodium sulfur, and so on. Several battery storage systems have been implemented in the power system for load leveling, power stabilizing and frequency control.

The lead-acid battery is a mature technology in energy storage. The advantages include the quick response time, inexpensive mass production and mature control method. However, the disadvantages are obvious, such as short life span, periodic maintenance, and environmental hazard.

The recent development of battery technology has shown lithium-ion battery has far better performance than lead-acid batteries, including longer life cycle, higher energy and power density, and environmental friendliness. However, the obstacles for its massive

application includes its expansive manufacturing and technical immaturity. Thus, although the battery storage systems are the prevalent choice for power quality, uninterruptable power supply, and short-term spinning reserve applications, further development and improvement are expected.

1.3.2. Pumped Hydro Energy Storage (PHES)

Pumped hydro storage system uses two water reservoirs at a different altitude to shift energy while required. When the wind is surplus and demand is low, it works as a load to pump water from lower reservoir to the upper one. In contrary, while the wind is low but demand is high, the energy is regenerated by running the water through the hydro turbine from the upper reservoir to the lower one, supporting the peak load.

PHES is an excellent option for large-scale energy storage. It is reported by the Electric Power Research Institute (EPRI) that PHES accounts for more than 99% of bulk storage capacity worldwide [12]. The benefits include, fast ramping rate, high efficiency, and high reliability with long life cycle [13].

However, siting PHES needs a rough terrain condition for high-low reservoirs, which creates a conflict with the flat topography requirement of wind energy. Besides the limitation on siting conditions, the disadvantages also include adverse effects on the environment, water rights issues and long term construction. The scarcity of further cost-effective and environmentally acceptable sites in the U.S. explains why there are only 24 pumped storage projects that are constructed and in operation, and most of which are authorized more than 30 years ago [14].

1.3.3. Flywheel Energy Storage (FES)

The flywheel energy accumulator comprised of a massive flywheel that is connected to an electrical machine. Magnetic brackets are widely used to reduce the friction loss or self-discharging. When the demand is low, the electric machine works as a motor to accelerate the flywheel with the excess electricity. When the wind is low, the electric machine turns into a generator to generate electricity, driven by the high spinning flywheel.

The FES is designed for high-power but short duration in several minutes. Therefore, they are mainly for providing the ancillary services, such as microgrid stabilization and short-term spinning reserves. As the wind turbine may experience hours of low wind situation, they are not good for the middle term reserve for wind power [15].

1.3.4. Superconducting Magnetic Energy Storage (SMES)

SMES stores the energy in the form of a continuously circulating current in a superconducting magnetic coil. The charging and discharging philosophy is the same as other storage methods, except it stores the energy in the form of electricity rather than mechanical or chemical forms.

SMES is usually used to provide grid stabilization and voltage and frequency regulation, but for only several seconds. Although the storage process exhibits a high round trip efficiency around 95%, the complexity of the cooling system for superconductor and the large occupation of flat area to construct the coil torus place obstacles to its implementation.

1.3.5. Supercapacitors Energy Storage (SCES)

A supercapacitor is a very large electrochemical capacitor in a circuit, storing and releasing energy due to an applied voltage. The supercapacitors have very high charging and discharging rate, good energy density and a large number of life cycles. However, the short duration of from milliseconds to seconds range is the main drawbacks of this technology. It could be used for power quality regulation to wind energy system.

1.3.6. Compressed Air Energy Storage (CAES)

In CAES, the energy is stored by compressing the air into an above ground vessel or underground cavern, using excess electricity, and is released by driving a natural gas turbine after heated in the combustion chamber. Geologically, there are abundant places for underground caverns, such as salt domes, bedded salt, aquifers, hard rock mines, and natural gas wells [15]. A DOE handbook reported that approximately 80% of the land in the U.S. has suitable sites for CAES deployment, meaning it is less site-specific as pumped hydro does [4, 16, 17, 18]. The benefits also include,

- Long term storage
- High energy density
- Long life cycle
- High reliability with less maintenance intensity
- Less environmental impact
- Cost effectiveness

The disadvantages rest on two issues,

- Low round trip efficiency
- The use of natural gas

A lot of research has been conducted to tackle those issues [19, 20]. Because the efficiency loss of CAES mainly comes from the heat generated from the compression process, the heat recycle technologies has been used to recuperate this amount of heat at compression stage and to preheat the compressed air at expansion stage. The heat recovery technology could also reduce or eliminate the use of natural gas, and help to increase overall efficiency.

Multiple-stage compression technology is another technology to increase the compression efficiency, where the compression process is split into several stages, such as low-pressure compression, middle-pressure compression and high-pressure compression [21] . For each stage, the stroke is reduced, leading to a smaller housing size, less heat generated, and in turn more efficient heat recovery. Also, the same philosophy applies to multiple stage expansion.

1.3.7. Storage Comparison

Different characteristics are considered for the selection of storage system to suit specific power system requirement. Those criteria consist of the following aspects [9, 22].

- Storage capacity – the maximum capacity and duration
- Response time – the ramp up and ramp down rate
- Efficiency – the round trip efficiency
- Energy density – the volume occupation of storage

- Cost – the expense of installation and maintenance
- Lifespan – the length of time for economic operation of system
- Technical maturity – availability of commercial components and the proven reliability
- Geological and environmental concerns – the geological availability and restrictions, and the environmental impact on the surrounding area.

Based on the introduction of previous listed energy storage methods and selection criteria, a comparison of parameters for different storage technologies for renewable energy is summarized from [9, 11, 12, 23], and given in Table 1.1.

Table 1.1: Comparison between Storage Technologies.

	BES		FES	SCES	SMES	PHES	CAES
	Lead-Acid	Lithium-ion					
Typical Capacity	1kW-5MW	1kW-5MW	5kW-20MW	<150kW	10kW-1MW	5MW-2GW	25MW-2.5GW
Energy Density	Good	Very good	Fair	Good	Fair	Very good	Very good
Cost/kW	$1800	$1000-1500	$2000	N/A	N/A	Small $2500 Large $1500	Small $1000 Large $1250
Cost/kWh	$450	$4500-6000	$7800-8800	N/A	N/A	Small $425 Large $260	Small $125 Large $60
Dynamic Response	mini seconds	mini seconds	mini seconds	seconds	mini seconds	1 min from standing still	15 min from cold start
Max Duration	1min-3hour	1min-3hour	4sec-15min	1sec-1min	5sec-5min	4-100hours	2-24hours
Maintenance Cost	High	High	Moderate	High	Low	Low	Low
Life Time	4500 cycles	>100,000 cycles	~20 years	~10 years	~30 years	50+ years	15-40 years
Tech Maturity	Mature	Premature	Mature	Premature	Premature	Mature	Mature
Environmental	Toxic	Benign	Benign	Benign	Health adverse	Adverse	Benign
Round-Trip Efficiency	65-75%%	80-90%	90-95%	85-95%%	90-95%	55-85%	40-70%

The comparison shows that the SCES and SMES are short-term storage solution for angular stability and voltage support. The flywheel could be used for either high power short duration or long duration low power application. It is mostly used as energy recycling

device for short-term power quality. Lead-Acid battery technology is a mature technology for energy storage; however, its performance is largely deteriorated by the depth of discharge. Although the lithium-ion battery technology gets rid of the depth of discharge problem, its high cost prevents the commercially mass production.

Thus, the PHES and CAES are the only attractive options for long-term energy storages for wind power, since they have long life cycles, large power capacity, relatively low cost, reasonable efficiency, and technology maturity. As more attentions have been paid to the environmental impact of man-made structures on the precious but fragile ecosystem, it is difficult to get authorization and licensing for a pumped hydroelectric plant in the recent 30 years [14]. On the contrary, the underground storage of a CAES plant is invisible for human eyes, where the adverse impact is much smaller than that of a pumped hydro plant. The above ground portion uses mature technology as a natural gas power plant does. Additionally, considering its low cost per kWh and high energy density, it is an appealing choice to select to couple with wind energy [24].

1.4. Current Compressed Air Storage Projects

There are two existing large-scale CAES plants in the world and additional two plants under the development. Brief introductions of these plants are presented as follows.

1.4.1. Huntorf Plant

Huntorf plant is the first compressed air storage system in the word. It was commercially opened on Dec. 1978 [25, 26]. Two underground salt caverns form the storage of a total volume of 11 million cubic feet. The operational air pressure ranges from

620 to 1010 psi (converting to 43 to 70 Bar). It requires 12 hours for a full charge and sustains 4 hours for a full capacity generation.

The plant functions primarily for cyclic duty, ramping duty and as a hot spinning reserve for industry. It is upgraded recently and starts to serve as operating reserves for numerous wind turbine plants. The gas turbine equipped with black start capacity, enabling a full generation of 321MW within six minutes.

1.4.2. McIntosh Plant

McIntosh plant is the second CAES plant in the world and the first in the U.S. It is operated since Jun. 1991 [25]. A salt cavern with a total volume of 19 million cubic feet works as the storage to serve 110 MW full power generation for 26 hours. The working air pressure ranges from 650 to 1,080 psi. Three-stage compression and two-stage expansion are applied to the storing and generating processes, respectively. An advanced recuperator is used to recycle the heat from the low-pressure expander exhaust to preheat the outlet of compressed-air to the high-pressure combustor. With this technology, the fuel consumption is reduced by approximately 25%. Compared to conventional gas turbines, the CAES plant is able to ramp to its full power with 15 minutes notice rather than 30 minutes from the black start and consumes 60%-70% less natural gas to achieve equivalent generation.

1.4.3. Other Proposed Projects

Additional two CAES plants have been proposed and are still under development. First Energy Corp. proposed the development of a CAES power plant in an abandoned limestone mine, Norton, Ohio in 2009. The project could involve 268 MW of rated capacity in the initial phase, and has the potential to expand to 2,700 MW with proposed 9.6 million

cubic meters of compressed air storage, making it a key role in the regional renewable energy deployment.

APEX Matagorda Energy Center, LLC is planning to construct a 317MW CAES power plant in Matagorda County, Texas. The storage is supposed to use an underground salt formation dome to provide bulk energy storage for enhancing both the renewable energy and conventional fossil generation.

1.5. Objectives of Research

The primary objective of this research is to offer a novel compact system to utilize wind energy optimally, while taking advantage of compressed air storage technology, for a dispatchable power supply.

The secondary objective of the research is twofold. First, is the optimal sizing of components of the proposed system while considering wind resource uncertainty. Second, is the optimal offering strategy for a wind farm consisting of a group of the proposed systems while considering risk management.

The rest of this dissertation is organized as follows. Chapter 2 reviews the current applications of or proposals for compressed air energy storage projects coupled with wind energy. In Chapter 3, a new configuration of a compressed-air-assisted wind energy conversion system is proposed; and the system model is explained in detail. Chapter 4 investigates the sizing problem for different components of the proposed system. Chapter 5 addresses the optimal offering problem for a wind farm consisting of a group of the proposed wind energy conversion systems. Chapter 6 presents a case study where the proposed system is applied to a microgrid expansion. Conclusions are drawn in Chapter 7.

CHAPTER 2. COMPRESSED AIR ENERGY STORAGE REVIEW

Government mandates, subsidies and public awareness of the need for clean renewable energy are currently the driving factors in the wind energy industry. However, since utility companies already place much stress on generator control to meet fluctuating demand, the intermittent nature of wind introduces additional complexity to the problem [27].

The problems caused by the integration of wind energy include power quality issues, such as undervoltage, overvoltage, and frequency excursion. In addition, wind forecasting errors require a broad safety margin of capacity reserve, and excessive energy may be rejected by the transmission line while experiencing a congested network.

Induction wind turbines may not be able to ride through a voltage sag event because a critical voltage has to be guaranteed to produce the fundamental magnetic field on which the rotor operates. Thus, external power is needed to restore an induction wind turbine to generation and operation after experiencing a network failure.

Building energy storage for wind energy could be a good solution to the aforementioned problems. The analysis in Chapter 1 has shown that pumped hydro energy storage (PHES) and compressed air energy storage (CAES) are the only options for large-scale, long-term, high-power, low-cost storage. Compared to water rights issues and the adverse environmental impact caused by pumped hydro, compressed air has a much smaller visible footprint and fewer limitations.

Moreover, wind-rich areas are generally remote places with geographic conditions qualifying them for CAES installations. Coupling a wind farm with a CAES can turn the wind farm into a dispatchable resource, whose power output is more predictable or the power prediction is more reliable and credible because the forecasting error could be mitigated by its accompanying CAES, resulting in a large operational margin. If the wind farm is serving a local community, the CAES could also provide load shaving and peak shifting to avoid the highest electric rate and alleviate transmission congestion.

A sketch of a CAES plant for a wind farm is depicted in Figure 2.1. The wind farm is connected to the power grid through the power line (in red). A CAES plant consists of a compression plant and an expansion plant. The compression plant is linked to the wind farm side of the power line, consuming the excess power from the wind farm and compressing air into a reservoir through an injection well. The expansion plant is connected to the grid side of the power line, generating electricity to supply the grid when it is commanded. The combination of wind energy and CAES provides an additional energy source that is both environmentally friendly and cost competitive with existing energy options [28, 29].

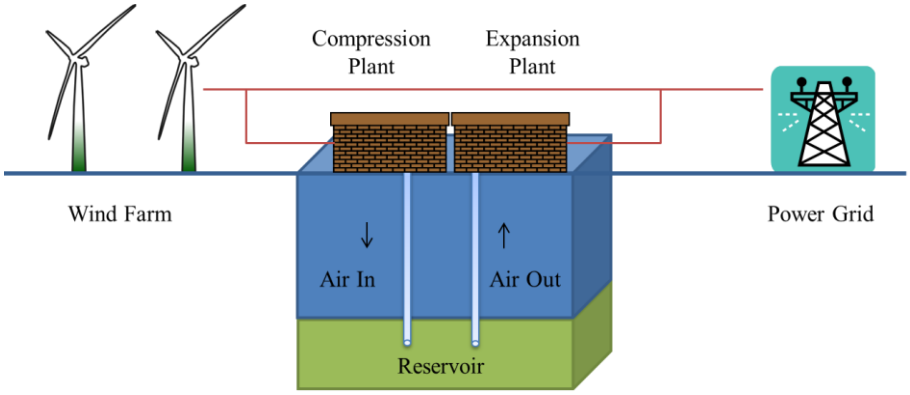

Figure 2.1: Sketch of CAES for a wind farm.

2.1. Compressed Air Energy Storage with Onshore Wind Energy

The compressed air storage technology derives from the concept of natural gas storage in the petroleum industry, where a depleted natural gas well is converted into a storage facility to hedge against price fluctuation in the natural gas market. The concept is shifting to the electric power industry to hedge against the imbalance between demand and supply, electricity rate fluctuation, and market penalties.

The CAES system is essentially a variation of the natural gas power generation system. In principle, a standard gas turbine generation cycle includes a compression process, where the air is compressed by the combustion shaft and guided to the generation turbine, acquiring about two-thirds of the combustion power. A CAES system separates the compression and combustion cycles into two islands. Since the air is compressed before entering the combustion cycle, the gas supply is supposed to be reduced by 66% to generate the same amount of electric power [30].

The components and cycles of a CAES are described in Figure 2.2. The principal equipment in the facility could be split into four components: the compression island, the generation island, the underground portion, and the plant accessories [30].

A typical compression cycle contains a series of axial or centrifugal compressors, compressing the atmospheric air to the desired high pressure. Because a quick, high-ratio compression can generate a great amount of heat, which leads to efficiency loss, the compression process is split into multiple stages to reduce the compression ratio for each stage. The intercoolers are placed between multiple compression stages to normalize the

temperature of the compressed air for the next stage. The high-pressure air is injected into the reservoir through the injection well.

A generation plant contains the combustion turbines, the generator, and heat exchangers. Two-level turbines are typically used in a CAES, namely, a high-pressure turbine and a low-pressure turbine. They are connected in series so that the residual energy in the exhaust of the high-pressure turbine can be reused by the low-pressure turbine. The waste heat in the exhausts of the low-pressure turbine is used to preheat the incoming compressed air to the inlet of the high-pressure turbine. The required air volume (or flow rate) is supplied to the combustion chamber through the production well as long as the pressure allows.

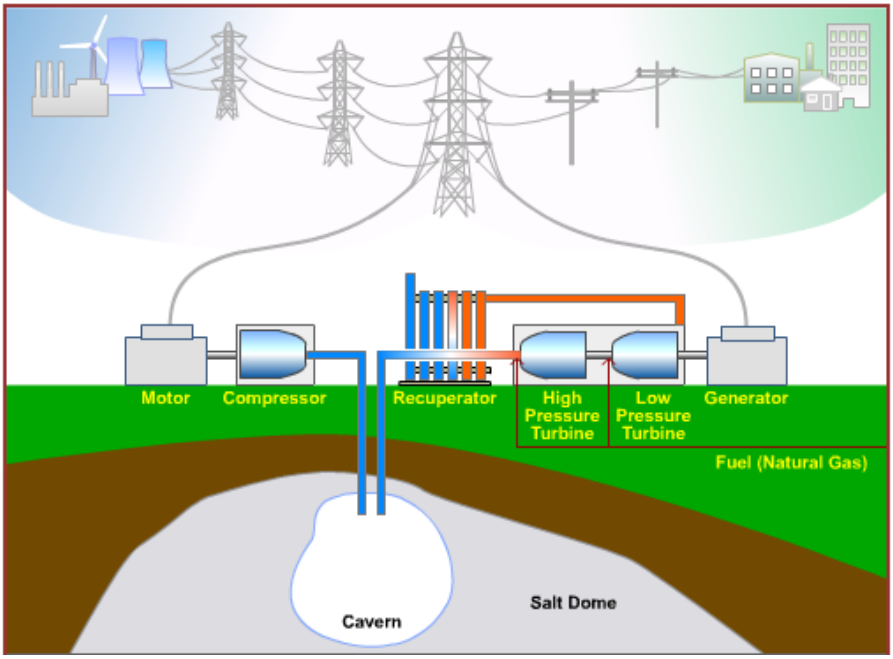

Figure 2.2: Layout of a CAES facility and its operation [30].

The underground facility is used to contain the storage medium with minimal energy loss. The choice of storage container really depends on the scope of the project.

Typically, a solution-mined salt cavity, a mined hard rock cavity, or an aquifer could be used for a large volume of underground storage. However, an aboveground tank or vessel could be an alternative in small applications although it can be costly [31, 32].

The plant accessories include the remaining equipment that is necessary for power plant operation, such as transformers, AC buses, breakers, and batteries, etc. This equipment is responsible for the power and energy management of the whole plant.

Since the combustion of a fossil fuel is needed in a conventional CAES facility, the system is not completely emission free. It is essentially an air compression station plus a gas turbine generator. In order to eliminate the external fuel consumption, adiabatic storage was proposed in [25].

In an adiabatic CAES, a thermal energy storage (TES) system is deployed between the above-ground plant and underground storage, as shown in Figure 2.3 [25]. The heat from compression could be stored in a TES system, and this heat could be recovered to preheat the compressed air during expansion. The use of TES eliminates the need for the combustion system, turning it into an absolute emission-free storage system.

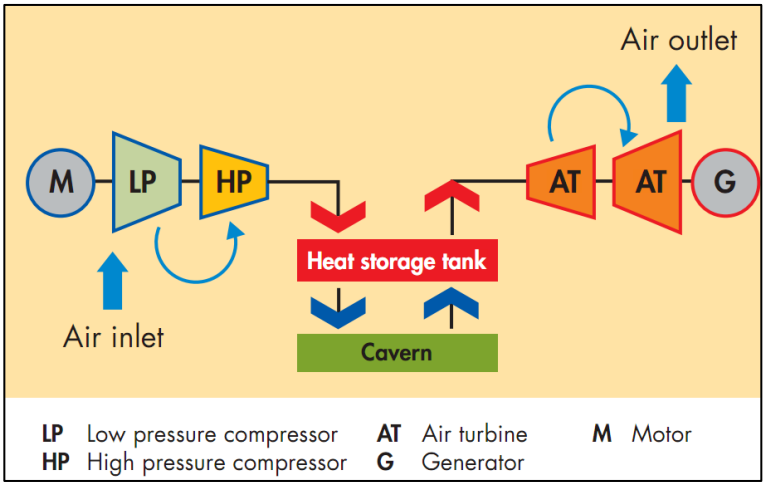

Figure 2.3: Sketch of an adiabatic CAES system [25].

2.2. Compressed Air Energy Storage with Offshore Wind Energy

Offshore wind resources are regarded as more advantageous than land-based wind energy for several reasons. Because the roughness of the sea level is much smaller than the land surface, the intensity of the turbulence and eddies can be largely reduced. Thus, offshore winds tend to be more consistent than these on land. Consequently, the turbine's tower frame can be lower as strong wind occurs at a lower height with less turbulence [8]. Because turbulence-related wind shear is reduced, the fatigue load can be reduced accordingly, resulting in the extension of the unit life cycle. Finally, there are fewer restrictions on noise, landscape impact, electromagnetic interference, and other environmental issues in the development and utilization of sea wind energy.

Moreover, the offshore breezes are stronger in the afternoon, matching the peak hour demand of the power system. Since the offshore turbines are close to high demand areas along the coast where the generation could meet the load immediately, long-distance transmission lines could be omitted [33].

Therefore, interest in the research and application of offshore wind energy has increased significantly around the world. However, offshore wind turbines still face the same shortcomings of nondispatchability caused by intermittency and spillage caused by congestion as an onshore wind turbine faces.

Many ocean energy storage systems have been designed to solve these problems. More emphasis will be placed on compressed air storage solution since this is the main focus of continuing research.

The basic concept of ocean compressed air energy storage (OCAES) was first introduced by [20, 34] to level the load. In contrast to conventional land-based CAES, where the underground caverns could only operate within a certain range of pressure levels, OCAES is able to maintain a constant pressure due to the fixed hydrostatic pressure at a particular water depth. The air container could be an open-ended reservoir or a flexible bladder installed on the seafloor or at the desired water depth [20, 35, 36]. The compressed air delivered to the underwater container displaces the same amount of seawater from the container and stores the energy.

A typical schematic of an OCAES is shown in Figure 2.4. The OCAES system is mounted on a floating platform, coupled with wind turbines and wave generators. An adiabatic TES is placed between the generator and compressor. The overall efficiency could be improved by extracting heat from the compression process and retrieving the heat to reheat the compressed air before it enters into the turbine generator for expansion. An air storage tank is anchored on the seabed. A power line is connected from the wind turbines to the grid. The compressor is linked to the wind turbine side of the power line, and the turbine generator is linked to the grid side of the power line. Air pipes between the storage and the platform are used to inject and retrieve air to and from air storage, respectively. Actually, the concept of OCAES with wind turbines is similar to CAES with wind turbines on land, except the constant pressure could be managed by the fixed depth of the sea.

Another proposed wind energy OCAES system integrates an open accumulator between the wind turbine and generator through hydraulic links, as shown in Figure 2.5, converting the wind power into both electric power and storage [37, 38].

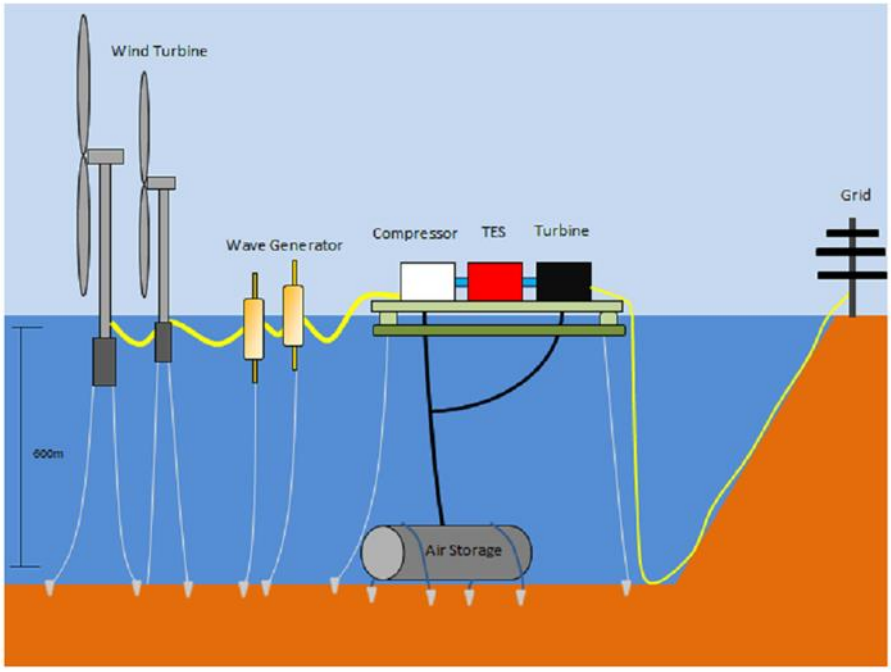

Figure 2.4: Ocean-compressed air energy storage with thermal energy storage [20].

In this configuration, a variable displacement hydraulic pump is directly driven by the turbine blades, converting all captured wind power to hydraulic power. All other components are moved to the ground level, including an open accumulator with storage tank, liquid piston chambers, hydraulic transformer, hydraulic control valves, electrical generator, etc.

The open accumulator provides two energy storage branches: the energy-dense pneumatic branch and a power-dense hydraulic branch. While the wind power is low, the compressed air in the accumulator tank is released to drive air expanders through liquid pistons, assisting the power generation. The hydraulic motor compensates the pressure drop in the tank by injecting liquid into the tank. While the wind is high, the excess power is used to drive the air compressors, accumulating the compressed air in the tank. The pressure increment is compensated by releasing liquid through the hydraulic motor.

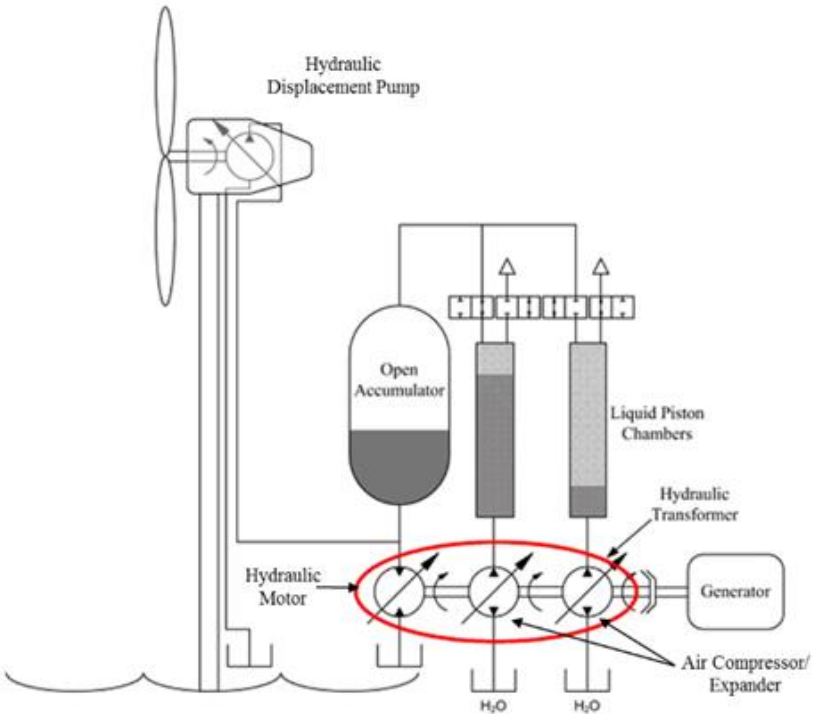

Figure 2.5: Ocean wind energy conversion system coupled to open accumulator storage [37].

In this way, the system can benefit from the high energy density of the pneumatic branch and the high power density of the hydraulic branch. The quasi-isothermal process could be achieved by the large contact surface of specially designed liquid pistons in the chambers. Two additional advantages of this design include constant air pressure management and hydraulic transient overload capacity.

Although the system is able to manage the power and harvest energy from the wind, it introduces several complex subsystems, such as a hydraulic pump and motor, liquid pistons, etc., which could incur problems, such as sealing, lubrication, filtering, and so forth. Its complexity could also increase the maintenance cost and the failure rate of the system.

Besides the air storage in the underwater tank, a pipeline could be an alternative storage medium for OCAES. A layout of pipeline storage of compressed air is shown in Figure 2.6, where the compression plant is located offshore and linked to the onshore expansion plant through a distant pipeline. The low-value wind power is used to compress the air, while the high-value wind power is supplied directly to the power grid.

However, it is difficult to apply TES because the compression and expansion processes are at separate locations. Moreover, the length and pressure level of the pipeline restricts the storage capacity.

Another alternative solution is to replace the wind turbine generator in the nacelle with a compressor. All of the wind energy is converted to compressed air and transported to an onshore expansion plant. In this case, all of the wind energy would suffer from the low efficiency of the compression process, rendering it as an impractical option for OCAES.

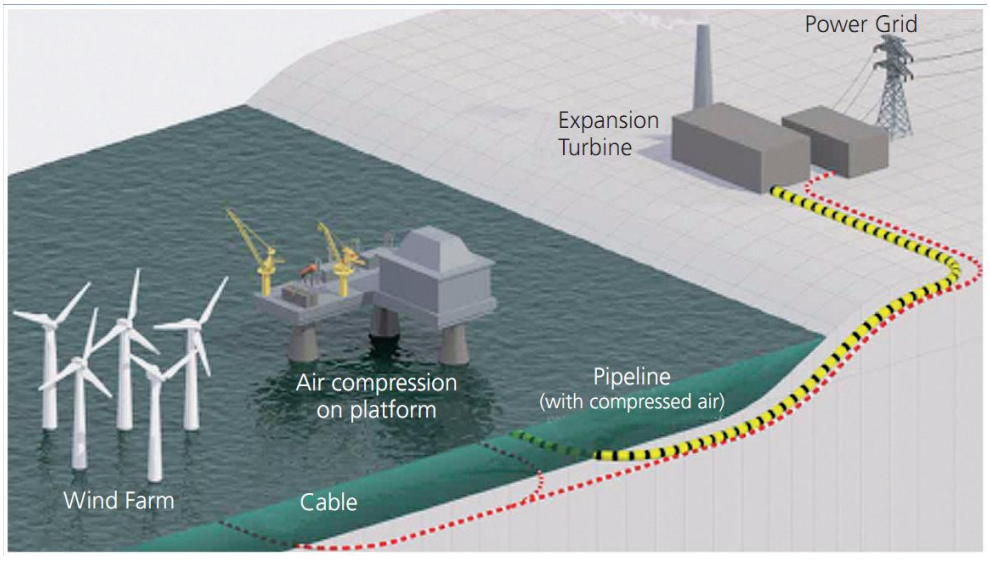

Figure 2.6: Offshore wind energy with compressed air energy storage in the pipeline [39].

2.3. Mini-Compressed Air Energy Storage with Wind Energy

Although CAES typically provides large-scale storage to a power system, small-scale CAES systems still have the economic potential to provide short-term load shifting, forecast hedging, and transmission curtailment for small capacity wind turbines because of their highly flexible deployment. The term mini-CAES often refers to a small CAES that works for a single wind turbine or for an independent regulative unit to the microgrid.

A small-scale hybrid system integrating a pneumatic system with a conventional wind turbine is proposed in [40]. As shown in Figure 2.7, a compressor is linked to the output of a wind generator, consuming electricity to generate compressed air to the tank. An air motor is connected to the tank, consuming compressed-air to supplement electrical power generation. A clutch is placed between the air motor and the main shaft of the generator, engaging the air motor when its rotation speed is synchronized to the speed of the generator.

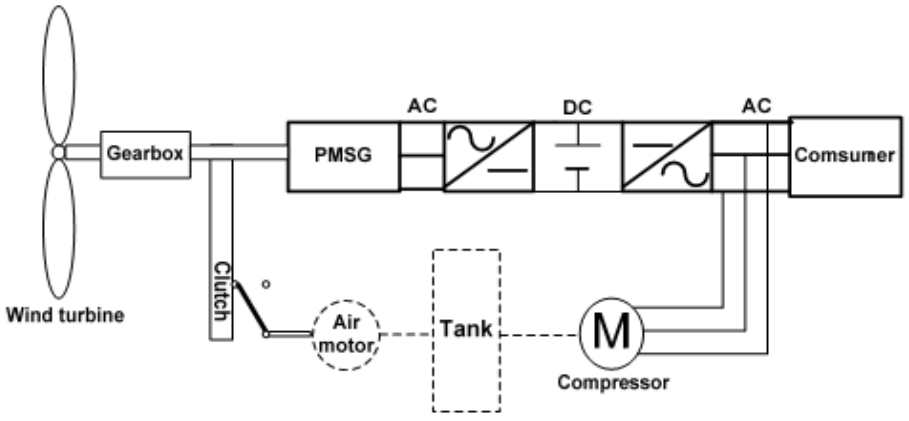

Figure 2.7: Small-scale hybrid wind turbine with CAES [40].

This configuration offers the simplicity of design and direct compensation of torque variation of the wind turbine. However, the system only recycles the electrical spillage

rather than the mechanical spillage. Since the accumulation of the storage consumes the electricity, integrating storage could result in the decrease of overall generation.

An even more compact CAES unit was proposed by [41], consisting of an air tank, a solenoid control valve, an air motor/compressor, an electric motor/generator, and control electronics as shown in Figure 2.8. During charging time, the electricity flows through an electric motor, driving the compressor to store the energy in the air tank. During discharge time, the generator is driven by the air motor, producing electricity to the grid. In addition, a pulse width modulation (PWM) operation is applied to the control valve to obtain the control of power dynamics. However, because of the electric power consumption during the charging period, this configuration also decreases the overall generation.

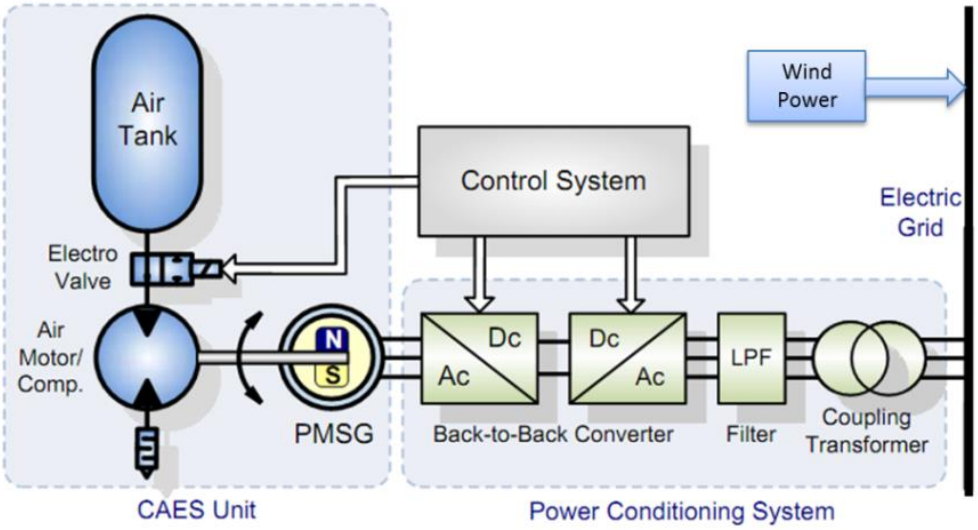

Figure 2.8: Compact CAES unit connected to the electric grid [41].

Small-scale CAES could also be used for an uninterruptible power supply (UPS) as shown in Figure 2.9. In this application, the wind energy is used solely to produce high-pressure compressed air. When the grid experiences an interruption in the power supply,

the air motor drives the generator to supply electricity to the load. This application increases power security at the cost of power production.

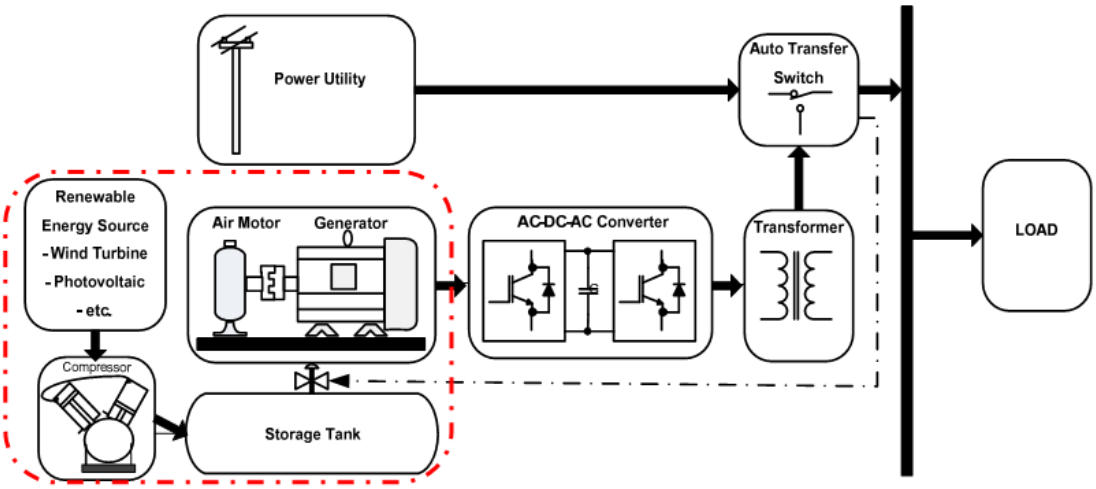

Figure 2.9: CAES unit for UPS application [42].

2.4. Challenges

In order to integrate the wind energy into the power system, large-scale CAES systems have been proposed to achieve long-term, economic energy storage. The addition of TES technology could recycle the heat and eliminate the gas combustion stage. Thus the energy efficiency is increased, and carbon emission is reduced. The underground caverns are utilized as storage for land-based CAES. The open-ended reservoir or a flexible bladder is used in OCAES, where constant pressure can be obtained. Mini-CAES systems are usually used to provide the short-term regulation capacity to small size wind turbines. The CAES systems could cumulate the low-value wind power and transform it into high-value electric power. The benefits would also include mitigating the power fluctuation, hedging against forecasting error, reducing the electrical spillage in a congested network, and so forth.

Currently, the wind turbine and CAES are designed individually. The wind energy and compressed air energy are only related/coupled through the electric linkage, e.g., the wind energy is firstly converted to electric power, and then the electric power is used to produce compressed air. Since none of the storage systems can achieve 100% efficiency, integrating a storage to renewable energy will decrease the overall generation, compared to a system without storage.

On the other hand, a joint design could bring mechanical linkage between wind power and the power of compressed air, giving another degree of freedom to manipulate the storage. The challenges and opportunities for a new joint design configuration depend on how the following issues are addressed.

2.4.1. Mechanical Spillage

The mechanical spillage is defined as the portion of the wind energy that is able to penetrate the blades but not able to be used by the generator because of generator capacity limit. In an uncongested power system, electrical spillage disappears. However, mechanical spillage still exists when wind speed exceeds the rated speed. Recovering this amount of energy would be beneficial.

2.4.2. Overall Generation and Efficiency

Converting electricity to storage and regenerating electricity from the storage decreases the overall power generation efficiency since useful energy is lost through the conversion process. If the energy source for storage is from the previously wasted mechanical spillage, the overall power generation efficiency could be increased.

2.4.3. Capacity Factor

The capacity factor is defined as the ratio of the electric output power over the electric rated power. If the wind speed is below the rated speed, the wind turbine can extract maximum power from the wind, but the quantity of electricity may be less than the rated, and the capacity factor is low. Otherwise, if the wind speed is above the rated speed, the capacity factor reaches its maxima, but wind turbine has to activate pitch control to trim away the extra energy, creating mechanical spillage. Utilizing the idle volume of generator capacity while the wind is low could improve the capacity factor.

2.4.4. Cost Effectiveness

Joint optimal sizing of a wind turbine (or wind farm) and a corresponding CAES is a critical issue for the economic performance of a project.

2.4.5. Dispatchability

Because of the stochastic characteristics of wind energy, the dispatchability of a wind-CAES joint project depends not only on the optimal operation but also the optimal offering strategies. A less reliable offer could also impair its economic effectiveness.

CHAPTER 3. DESIGN OF THE SYSTEM

This chapter briefly reviews the structure and the torque of the traditional wind turbine. By analyzing the difference of mechanical power and electric power and identify the surplus capacities of blades and generators, the structure of a novel compressed-air-assisted wind energy conversion system (CA-WECS) is proposed. Functions of different parts are explained in details. The operation of dispatchable generation is numerically studied. The simulation results give the reference commands for blades, VDM, generator and CVT.

3.1. Wind Turbine Structure Review

Before a new system can be designed, the structure of the traditional wind turbine generation system has to be analyzed. The wind energy harvesting technology can be improved by identifying the blade power capacity and electric power demand and by constructing a flexible mechanism to accommodate the difference.

Modern wind turbines are the device to convert the kinetic power in the wind to the electric power to the grid. The most common design is the upwind horizontal axis wind turbine [43]. The main parts on the top of a wind tower usually include the blade, gearbox, generator, and control system, as shown in Figure 3.1. According to the empirical formula [44], the power that the wind blade can extract under the wind speed of v_t is characterized by (3.1),

$$P_t^B = \frac{1}{2}\rho {v_t}^3 A^w C_p(\delta^B, \lambda) - f^{loss} \tag{3.1}$$

where the air density is ρ, the swept area is $A^w = \pi {R^B}^2$, the rotor radius is R^B, and the power coefficient and friction loss of the turbine are C_p and f^{loss}, respectively [45, 46]. The power coefficient C_p is a function of the blade pitch angle δ^B and tip-speed ratio λ.

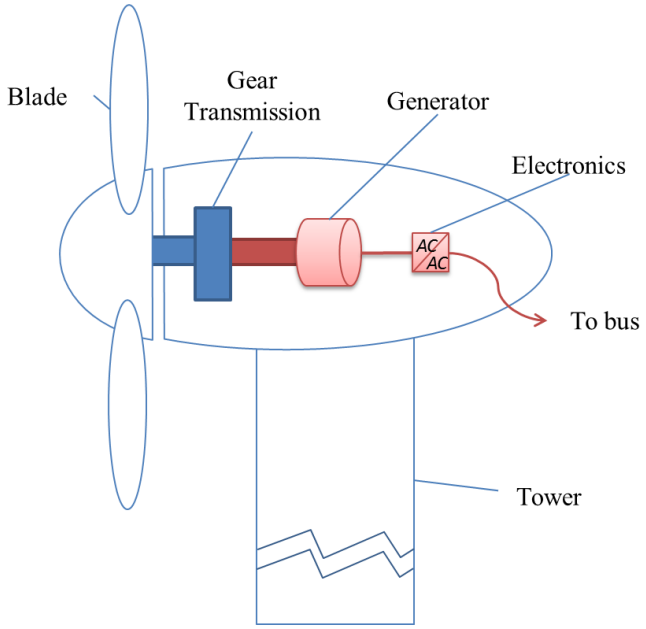

Figure 3.1: The configuration of a traditional wind turbine.

The tip speed ratio is defined as blade tip linear speed over wind speed. If the tip speed ratio is maintained at its optimal value, the power in the wind is proportional to the cube of the wind speed, as the purple curve shown in Figure 3.2. However, because of capacity limitation on the generator and internal friction loss, electrical power curve only occupies a small portion of total wind energy, as shown as the blue power curve in Figure 3.2. As can be seen, the domain is divided into three regions. In Region I, the power output is zero because of the low wind speed. In Region II, output power increases with a cube of the wind speed until generation capacity of the turbine is reached. In Region III, as wind speed surpasses the rated speed, the wind turbine maintains a constant output, while excessive energy in the wind is trimmed away by blade pitching.

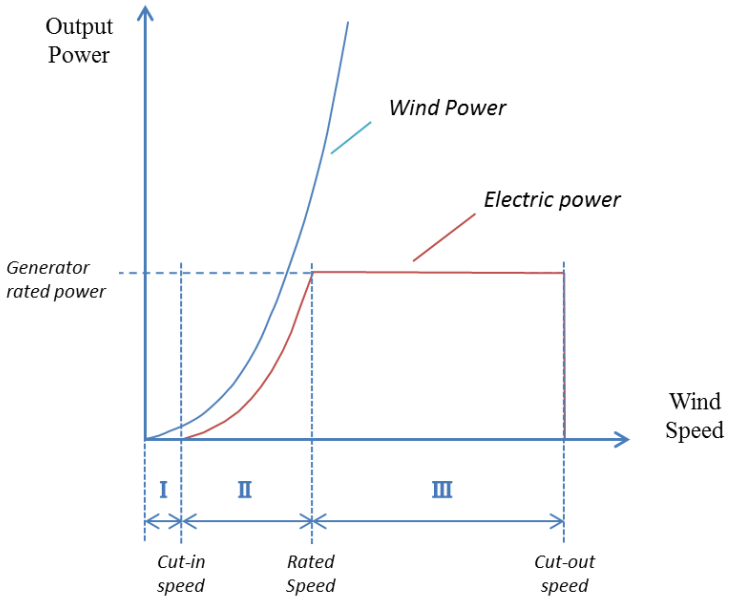

Figure 3.2: Wind power and generator power as a function of wind speed.

Pitching control is a control method for the wind turbine to adjust the power penetration through the turbine blades. In an infinite bus case, the wind turbine power generation follows the electric power curve in Figure 3.2.

When the wind speed is in Region II, the pitch control is deactivated, meaning the blade has to extract maximum kinetic power from the wind. The blade angle is set at zero to obtain maximum efficiency for blade power penetration. When the wind speed is in Region III, the pitch control is activated to reduce the wind power extraction efficiency [44, 47]. The blade angle is increased to trim off the excessive power beyond the capacity of the generator.

In the pitch control framework, if the wind speed is given, there is a unique pairing of the optimal pitch angle and the tip-speed ratio for the blade to approach the reference power point setting [41, 47]. Because the tip-speed ratio is defined as the ratio of the blade tip line speed over the wind speed, as shown in (3.2), where the angular rotation speed of

the blade shaft is represented by Ω, then the pairing of the optimal pitch angle and tip-speed ratio can be converted to the pairing of the optimal pitch angle and optimal rotation speed of the blade shaft. Hence, a statement is derived that, under the given wind speed, the references of the pitch angle and the blade rotation speed Ω^B are determined after the power point is set.

$$\lambda = \frac{\Omega^B R^B}{v_t} \tag{3.2}$$

Since the blade shaft and the generator shaft are coupled through a fixed ratio gearbox, the generator speed reference is determined if the rotation speed of the blade is given. An example of the relationship between the blade rotation speed and the generator speed is given in Figure 3.3 (a), if the gearbox ratio is set as 1:1.

As it is stated through (3.1), the blade power is predetermined by the given wind speed; and the power point of the generator is preset by the system controller. The torque references of the blades and generator can be obtained, given the formula that the power of a rotary machine is calculated as the product of rotation speed and torque in (3.2).

An example of the relationship between the blade torque and the generator torque is depicted in Figure 3.3 (b), given that the power point reference of the generator is set at full capacity generation, and the blade power is preset at the maximum power point.

The torque discrepancy can be calculated as the difference between the blade torque and the generator torque, as shown in Figure 3.3 (c). Thus, the core objective of this design is to propose an adaptive structure to supplement/consume the torque and compensate for the discrepancy on the main shaft.

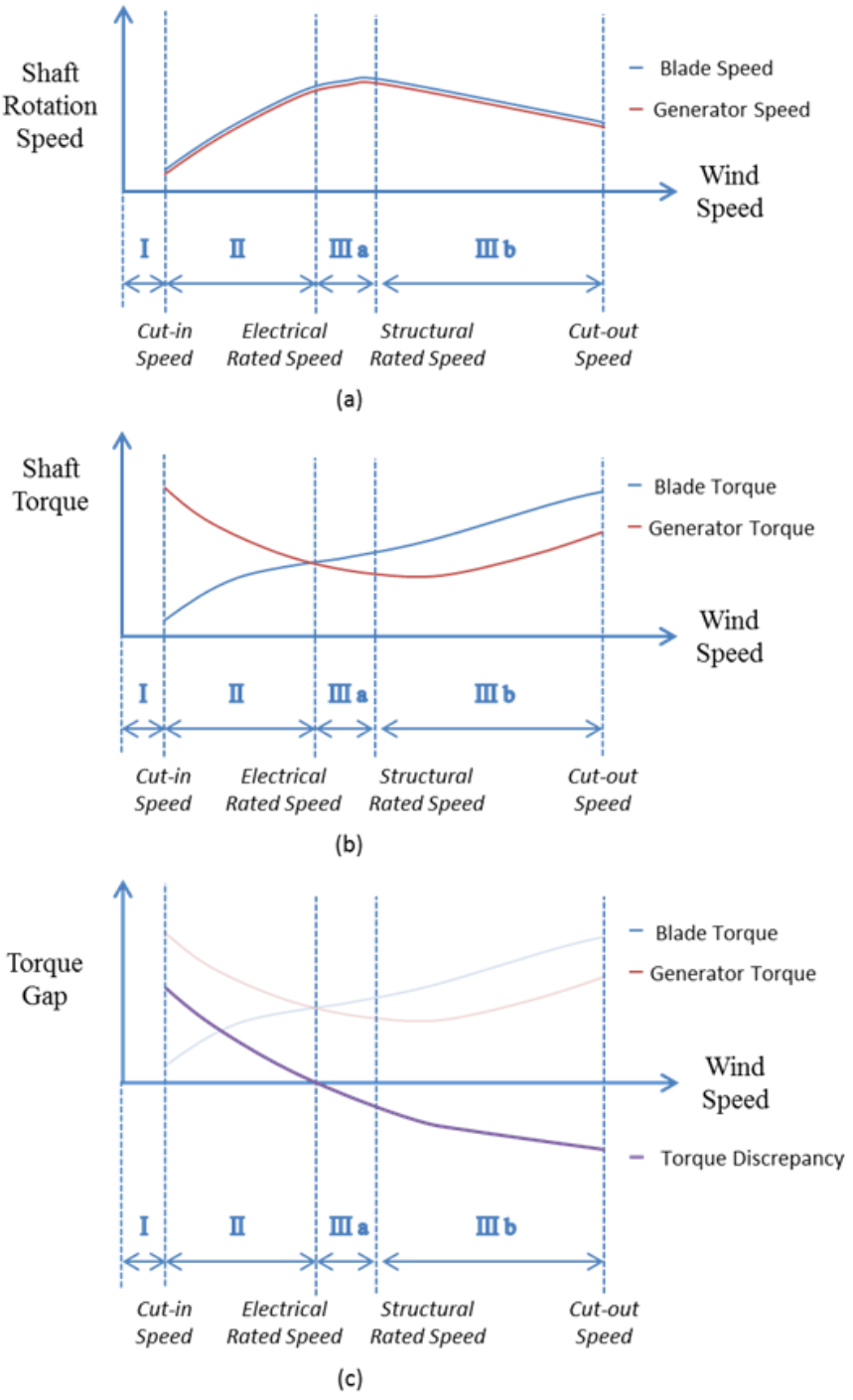

Figure 3.3: Curves of the blade and generator for a) rotation speeds, b) torques, and c) torque discrepancy.

3.2. System Configuration

Currently, the WT and CAES are designed individually. The wind energy and compressed air energy are only related/coupled through the electric linkage, e.g., the wind energy is first converted to electric power, and then the electric power is used to produce compressed air.

The wind power curve for a traditional wind turbine is presented as the red curve in Figure 3.4 [48]. If the electric capacity limit is removed, the wind energy curve can be extended to its mechanical limit, as shown by the blue curve in Figure 3.4.

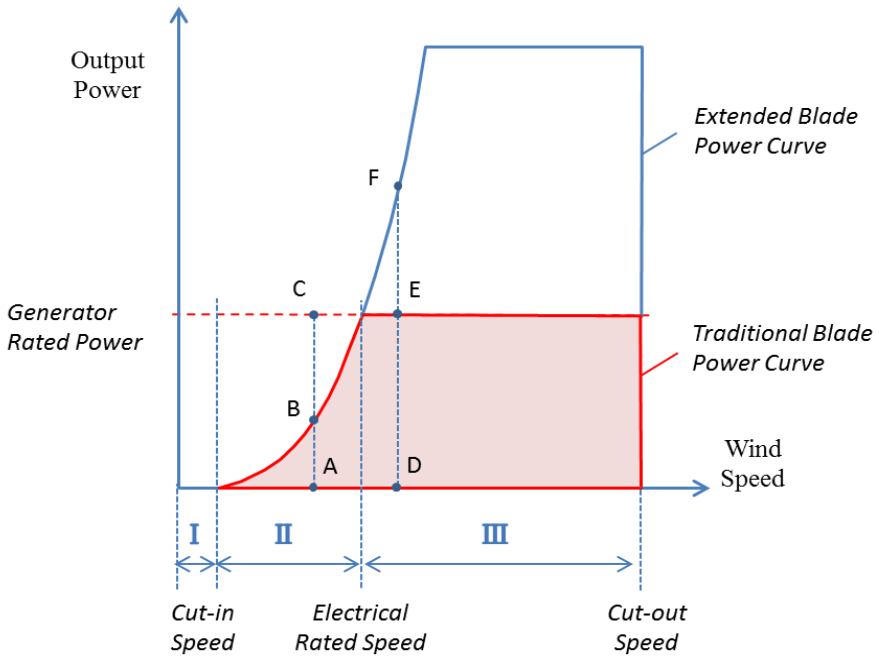

Figure 3.4. The curve of blade power penetration.

The entire area, covered by both red and blue curves, is defined as the capacity of blade power penetration, meaning the maximum power that wind turbine blades can extract from the wind. In this figure, the operational range of a turbine is divided into three regions. Two arbitrary speed points are chosen to explain the *capacity vacancy* and *mechanical*

spillage. While the wind speed is at Point A, the wind power is insufficient to support full capacity generation. This unused portion of generation capacity is defined as the *capacity vacancy*, as the segment BC in Figure 3.4. As the wind speed increases to Point D, the blade capacity exceeds the power capacity of the generator. The *mechanical spillage* is defined as the portion of the wind energy that is able to penetrate the blades but cannot be used by the generator. It is shown as the segment FE in Figure 3.4, while the wind speed is at Point D. It is noted that, in an uncongested power system, electrical spillage would disappear; however, mechanical spillage would still exist.

Since the capacity vacancy in Region II and the mechanical spillage in Region III have been identified, our concept is to divert the mechanical spillage to storage while there is a surplus of wind energy and to generate electricity from the storage while there is a deficit. The expected power curve is shown in Figure 3.5, where the red curve represents the power curve of a wind turbine generator, and the blue curve represents the power penetration throughout the blades. The aforementioned capacity vacancy and mechanical spillage are represented by the shaded area in Regions II and III, respectively.

To achieve the desired power curve shown in Figure 3.5, a joint design for a compressed air system and a wind energy system is proposed, presenting an adaptive structure to compensate for the difference between blade power and electric power [49]. The key feature of the design is that it brings an additional mechanical linkage between wind power and the power of compressed air, providing another degree of freedom for energy management. It is expected to reduce both the mechanical spillage and the capacity vacancy. Because the idea of recycling the mechanical spillage to refill capacity vacancy has not been addressed in prior publications, the literature on this type of system is scant.

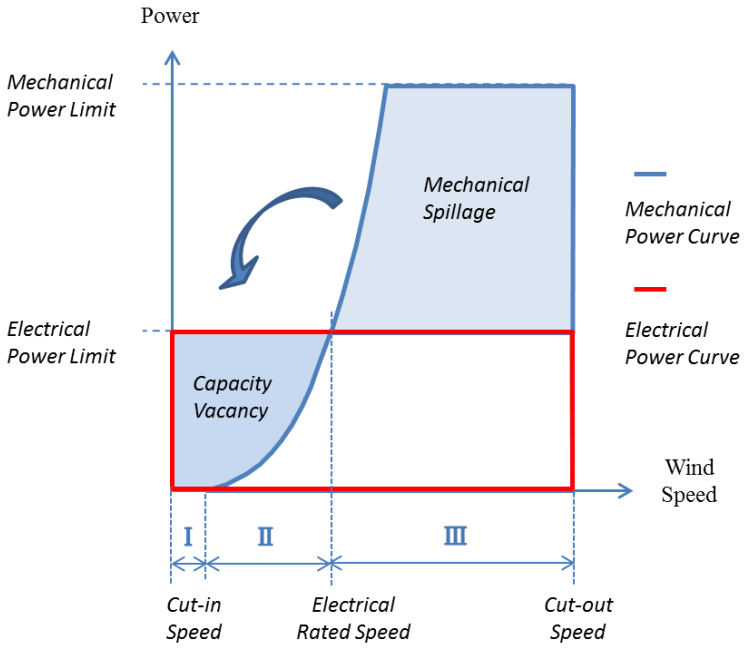

Figure 3.5. Expected power curves of the proposed system.

A mechanical configuration [50] is proposed to reduce both the mechanical spillage and the capacity vacancy by accommodating the aforementioned torque discrepancy. It consists of blades, gearbox, clutch, continuously variable transmission (CVT), variable displacement machine (VDM), generator, air tank, and converter, as shown in Figure 3.6 (a). The additional components used in the proposed system relative to a traditional wind turbine are shown within the boundary of the dashed yellow line in Figure 3.6 (a).

There are three working modes based on different wind and load patterns, as shown in Figure 3.6 (b). First, when the wind is strong enough to supply the load, the extra energy from the wind is recycled by the VDM. Second, when the blade power is lower than the load, the VDM operates in expansion mode to supply the load. Third, when the wind speed experiences high/low extremes and is out of the operational range, the clutch decouples allowing the VDM to drive the generator and supply the load independently. The structure and function of the components are explained as follows.

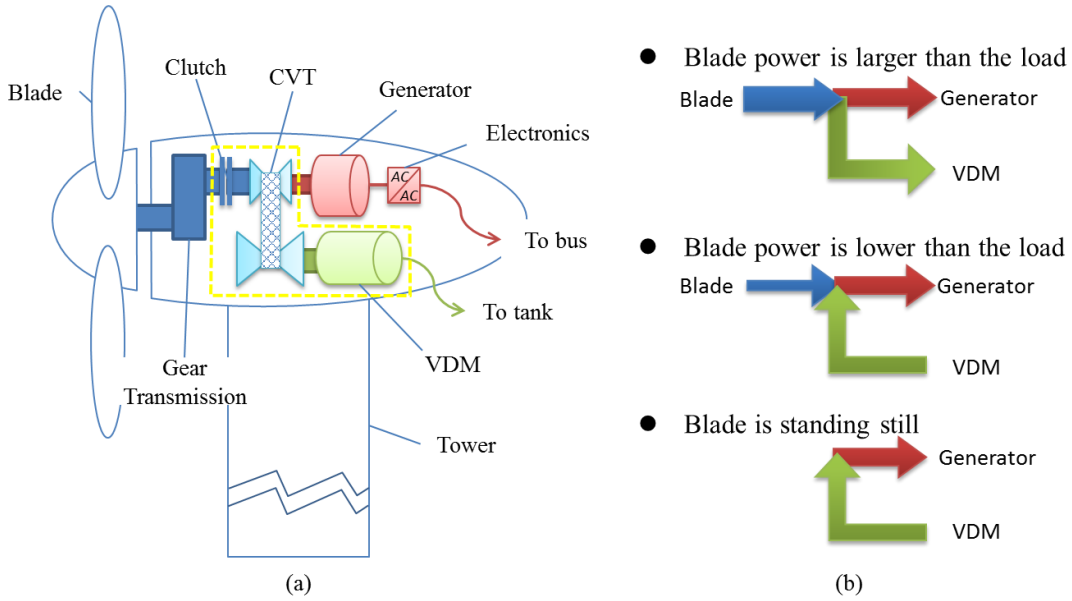

Figure 3.6. The a) configuration and b) energy flows of the proposed wind energy conversion system.

3.2.1. Wind Turbine Blade

The power penetration through the blades under various wind speeds is represented in Figure 3.7. The red curve represents the power curve of a traditional wind turbine, which is identical to the one in Figure 3.2. The blue curve represents the extended power that could be diverted to VDM for compression. Those two parts form the blade power penetration of the proposed system.

The whole operational range is segmented into four regions by four wind speed points, namely, cut-in speed, electrical-rated speed, structural-rated speed, and cut-out speed. Among them, electrical rated speed is the point at which the system reaches its rated electric power output; and the structural rated speed is the point at which the blade power penetration reaches its maximum power that the structure can survive (due to the structural

capability of the design). The space between the electrical rated power and structural-rated power is the area we referred to as the mechanical spillage.

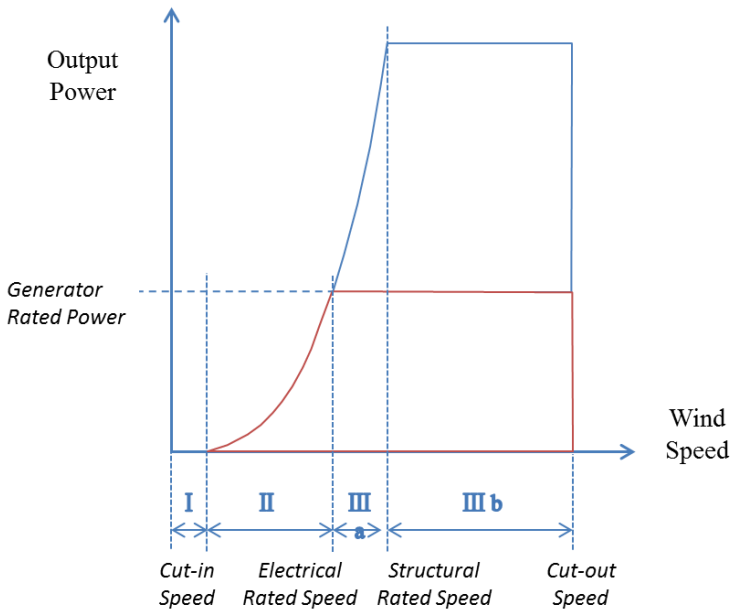

Figure 3.7: Blade power of proposed system.

Compared to a traditional power curve of the blade, the only difference rests in Region III, which is further split into two regions in the proposed system. The operations in Regions IIIa and IIIb are explained as follows.

In Region IIIa, the wind speed is between the electrical-rated speed and structural-rated speed, where the electric power reaches its upper limit but structural power does not. Wind blades still maintain their optimal tip-speed-ratio to extract maximum power from the wind. The blade pitching is deactivated.

In Region IIIb, the wind speed is between the structural-rated speed and cut-out speed, where both electric power and structural power reach their upper limits. Wind blades have to decrease the energy extraction efficiency to maintain structural safety. Thus, the

blade pitching control is activated to maintain the constant penetration power while the wind speed is increasing.

Finally, it is noted that, in Region I, since the blade power penetration is unable to overcome the internal friction, the clutch disengages the blade from the CVT. Thus, the generator and VDM with the air tank form an independent system to generate electricity. This mode is especially meaningful while the system is experiencing a black start.

3.2.2. Variable Displacement Machine

The variable displacement machine (VDM) is the core component of a compressed air subsystem. It provides a mechanical linkage between the blade power and compressed air storage power. A VDM is a reversible machine that can work as a compressor or an expander to produce or consume the compressed air depending on the setting of internal actuators.

A VDM is an axial multipiston device to compress or expand fluid (air), whose structure is represented in Figure 3.8. It consists of a driveshaft, wobble plate, multiple pistons and cylinders, and its housing [50, 51]. The angular and linear adjustment of the wobble plate is represented by the wobble angle and the neutral piston displacement (NPD), represented by δ and H, respectively.

The positive wobble angle corresponds to the compression mode while the negative wobble angle corresponds to the expansion mode. In a traditional VDM, a single adjustment of the wobble angle will drift the compression ratio [51]. The NPD is introduced in this configuration as a complementary control variable to adjust the compression ratio of the air while the wobble angle experiences a change [50]. The VDM acts as a buffer

between the mechanical and electric power of a wind turbine and decouples their direct relationship. The operation issues of VDM will be discussed in Section 3.3.

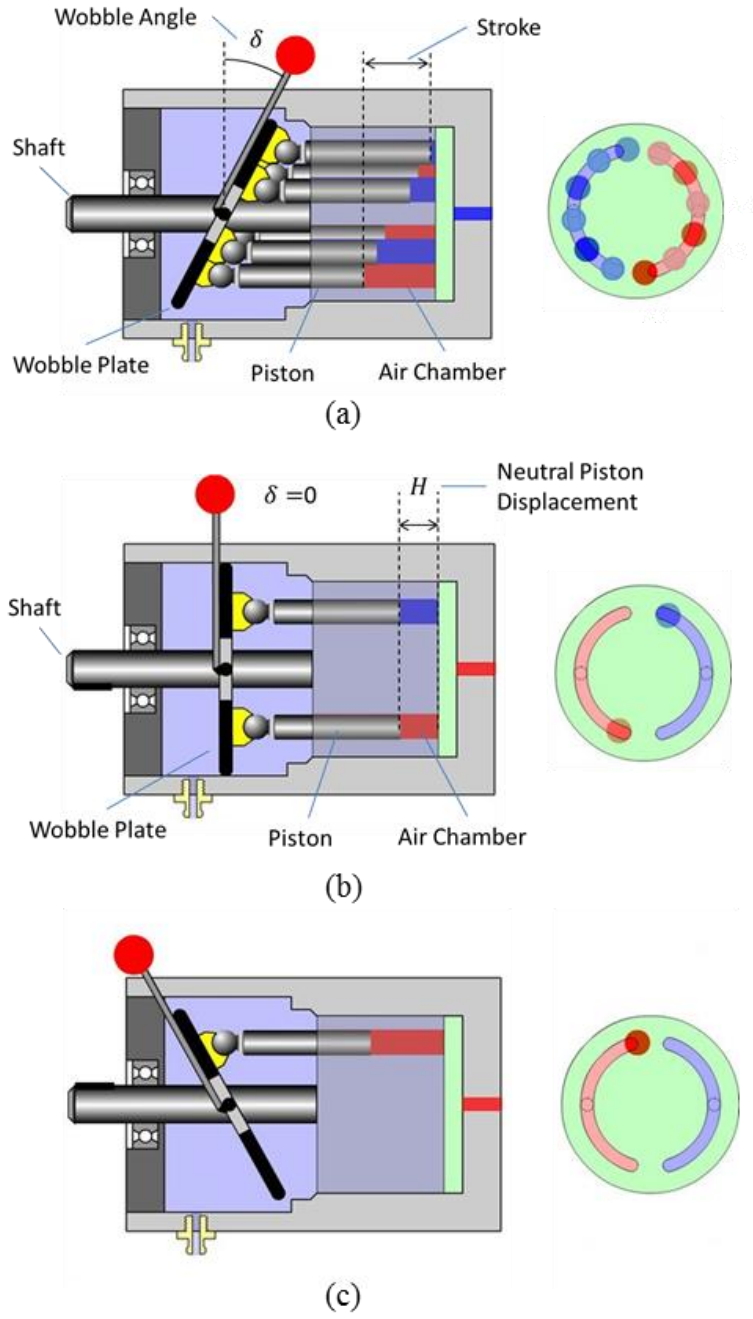

Figure 3.8. Cross-section of VDM in states of a) positive wobble angle, b) neutral, and c) negative wobble angle [52].

3.2.3. Gearbox with Continuously Variable Transmission

In the proposed system, the transmission subsystem consists of the increasing gear, clutch, and CVT, as shown in Figure 3.9. The increasing gear is used to match the rotation speed to the operational range of the generator. A CVT is integrated with the blade's shaft through a clutch enabling flexible power distribution among the shafts of the generator and VDM, as shown in Figure 3.9.

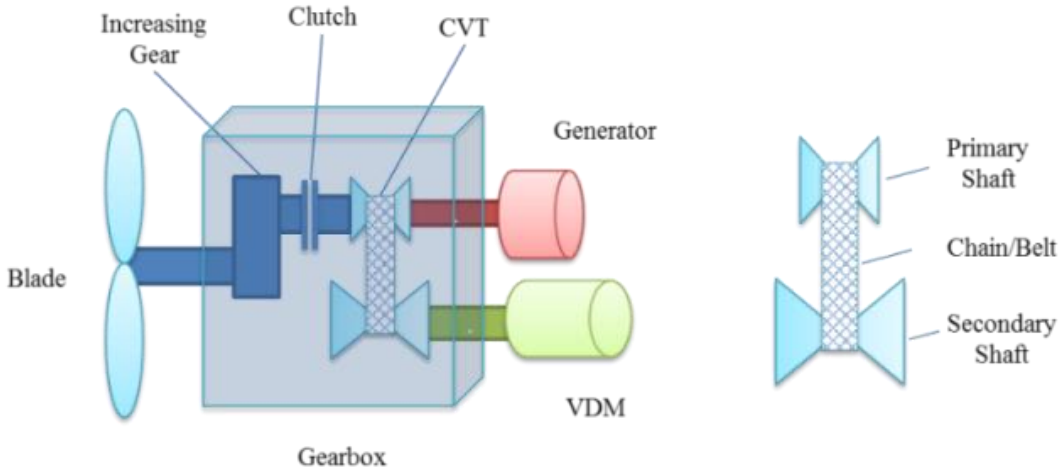

Figure 3.9: The detailed structure of gearbox and its connections.

A CVT enables continuous adjustment of transmission ratio during operation. Various types of CVT are designed and applied in the automobile industry, such as variable-diameter pulley (VDP), Extroid CVT, infinitely variable transmission (IVT), and so forth [53].

The transmission ratio of a CVT is defined as the rotation speed ratio between the primary and secondary shafts. The primary input refers to the turbine blades; and the primary and secondary outputs refer to the generator and VDM load, respectively.

A variable-diameter pulley (VDP) is selected, for example, to demonstrate the fundamentals of a CVT. As shown in Figure 3.10, a VDP consists of a drive pulley, a driven pulley, and a transmission chain/belt [54]. The two pulleys are connected through the chain/belt and operated in the same manner as a drive gear meshes with a driven gear. A pulley is formed of a pair of opposing cones. The effective diameter is varied by adjusting the distance between the cores. As the effective diameters of the primary and secondary shafts are continuously changing, the transmission ratio on the chain is changed accordingly.

As shown in Figure 3.10 (a), moving drive pulley halves closer leads to a larger effective diameter of the primary shaft; and moving driven pulley halves apart gives the secondary shaft a smaller effective diameter. Both operations result in an increasing gear state, meaning the transmission ratio is greater than 1. On the contrary, the opposite operation leads to a reduction gear state as shown in Figure 3.10 (b).

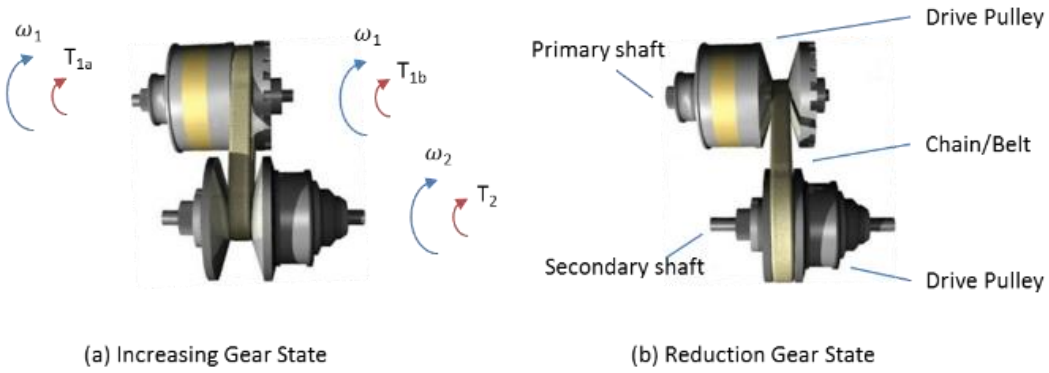

Figure 3.10: Demonstration of variable-diameter pulley CVT [55].

In this application, the CVT is used to adjust the rotation speed of a VDM at its optimal speed, as determined by the tank pressure, and decouple this speed with the optimal blade rotation speed which is determined by the wind speed.

The positive direction reference is arbitrarily selected as the clockwise rotational direction viewed from the right-hand side. The power balance and speed relation of the CVT are characterized by (3.3) and (3.4), respectively; and the transmission ratio of the CVT is defined as the primary speed over the secondary speed in (3.5).

$$T_{1a}\Omega_1 + T_{1b}\Omega_1 + T_2\Omega_2 = 0 \tag{3.3}$$

$$\Omega_1 R_1 = \Omega_2 R_2 \tag{3.4}$$

$$r^{TR} = \frac{\Omega_1}{\Omega_2}, r^{TR} \in (B_L, B_U) \tag{3.5}$$

where the torques from the left and right side of the primary shaft and the torque from the secondary shaft are represented by T_{1a}, T_{1b}, and T_2, respectively; and the rotation speeds of the primary and secondary shafts are represented by Ω_1 and Ω_1, respectively. The effective radiuses of the primary and secondary shafts are represented by R_1 and R_2, respectively. The lower and upper bounds of the transmission ratio of the CVT are represented by B_L and B_U, respectively. Actually, the CVT is used to match the speed ratio of the generator shaft and the VDM shaft and to guarantee that the VDM is operated at its optimal speed under various air pressures. The control scheme of the CVT will be discussed in Section 3.4.3.

In the proposed system, the power distribution curve over wind speed is characterized by Figure 3.11, where the blue area represents wind power penetration through the blades, the red rectangle represents the power that could be delivered to the generator as long as storage allows. The blue shaded area represents the mechanical power

diverted the VDM, and the green shaded area represents the mechanical power supplied by the VDM. (Note: negative output power means supplying power.)

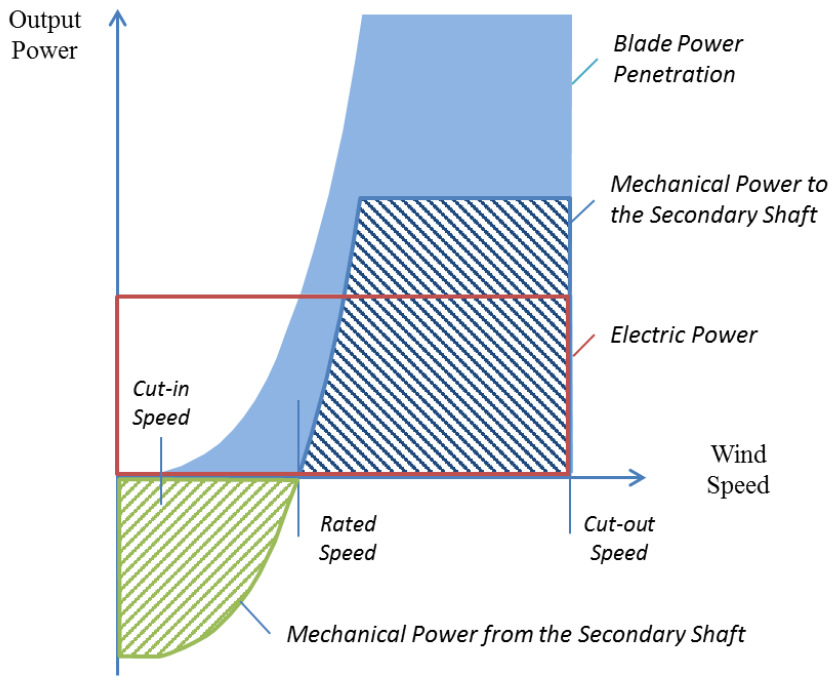

Figure 3.11: CVT power distribution curve vs. wind speed.

The power balance on the gearbox is depicted in (3.6), where terms on the left side of the equation are input power, including the blade power and the VDM expansion power; and terms on the right represent output power, including generator input power and the VDM compression power. In steady state analysis, the input power and output power have to be equal all the time. Additionally, the VDM is subject to additional either-or constraints, as shown in (3.7), because it works either in the compressor mode or in the expander mode.

$$P_t^B + P_t^{Vp} = P_t^{Gi} + P_t^{Vc} \tag{3.6}$$

$$P_t^{Vp} \cdot P_t^{Vc} = 0 \tag{3.7}$$

where compression power and expansion power of VDM are represented by P_t^{Vc} and P_t^{Vp}, respectively. It is assumed there is no power loss on the gearbox because all of the loss on gearbox have been considered and discounted to the efficiency of the component, such as blade loss, VDM loss and the generator loss.

The clutch is disengaged while the wind experiences extreme high or low speeds. In that case, the VDM and generator form an independent power system to generate electricity and blade power and compression power are equal to zero.

3.2.4. Compressed Air Storage Tank

An air tank is a storage component working jointly with the VDM. Each type of tank has its safety pressure threshold beyond which excessive energy is released through a spill valve. Thus, for a given volume and safety pressure and a specified temperature, the maximum energy in a tank is predetermined; and we refer to it as the storage capacity. In this sense, the characteristics of the storage tank are analogous to a battery pack. Large storage can be formed by simply parallelizing the tank units. If the isothermal process is chosen as a reference for the tank storage calculation, the storage capacity E_L^T is calculated by (3.8),

$$E_L^T = p_L^T V^T ln \frac{p_L^T}{p_0} \tag{3.8}$$

where the safety pressure and volume of the tank are $p_L{}^T$ and V^T, and the atmospheric pressure is referred to as p_0.

The energy balance in the tank from one period to the next consists of the portion of energy from the previous period, plus the compressed-air generation minus the

compressed-air consumption during this period, as expressed in (3.9), where the energy in the tank in the current time step and the next time step are represented by E_t^T and E_{t+1}^T, respectively. The efficiencies for the storage tank, compression, and expansion processes are η^T, η^{Vc}, and η^{Vp}. It is noted that the constraint in (3.7) also applies here, as the VDM cannot work on both compression and expansion modes at the same time.

A minimum pressure may be required for normal operation [56]. To avoid the nonlinearity brought by the pressure-to-energy calculation, it is assumed minimum pressure corresponds to 10% of the rated capacity. Thus, the remaining energy in the tank has to be greater than 10% of its rated capacity, as the constraint shows in (3.10).

$$E_{t+1}^T = \eta^T E_t^T + \eta^{Vc} P_t^{Vc}\, h - P_t^{Vp}\, h/\eta^{Vp} \tag{3.9}$$

$$E_t^T \geq 10\% E_L^T \tag{3.10}$$

3.2.5. Generator and Electronics

The configurations of the generator and the electronics are unchanged in the proposed system. However, the capacity factor of the generator is expected to be improved, because the mechanical spillage is recovered to refill the capacity vacancy.

3.2.6. Thermal Management

The thermal storage may be used in compression and expansion phases to improve the efficiency of compressed air subsystem. The operation is out of the scope of this proposal.

3.3. Fundamentals of the Variable Displacement Machine

Variable displacement machine is designed to capture surplus power from the blade shaft or to provide power to the generator shaft, depending on the working mode. The behavior of air in the cylinders of the VDM is analyzed in this section. The piston movements and air dynamic states in both compression mode and expansion mode are depicted in Figure 3.12 (a) and (b), respectively. Each single cylinder will experience the state series from the left to the right in Figure 3.12 (a) while rotating around the VDM shaft during the compression phase.

The compression process is divided into three phases, namely, closed compression, open ejection, and open suction. In the closed compression phase, the air is compressed in the closed chamber. At the end of this phase, the air pressure has to reach the air pressure of the storage tank. As it comes to the open ejection phase, the compressed air is ejected to the storage through the open valve to the tank. After the ejection, the valve is open to the atmosphere and the air is suctioned to the cylinder during the open suction phase.

Because the VDM is a reversible machine, the expansion process is the reverse of the compression process, which is divided into the open exhaust, open injection, and closed expansion phase. The chamber air exhausts to the atmosphere at the first stage, and the compressed air is injected into the cylinder in the second stage. Finally, the compressed air expands in the closed chamber of the cylinder during the third stage; and the pressure in the chamber is expanded to the atmospheric pressure at the end of this stage. The compression process is used, for example, for torque and pressure analysis.

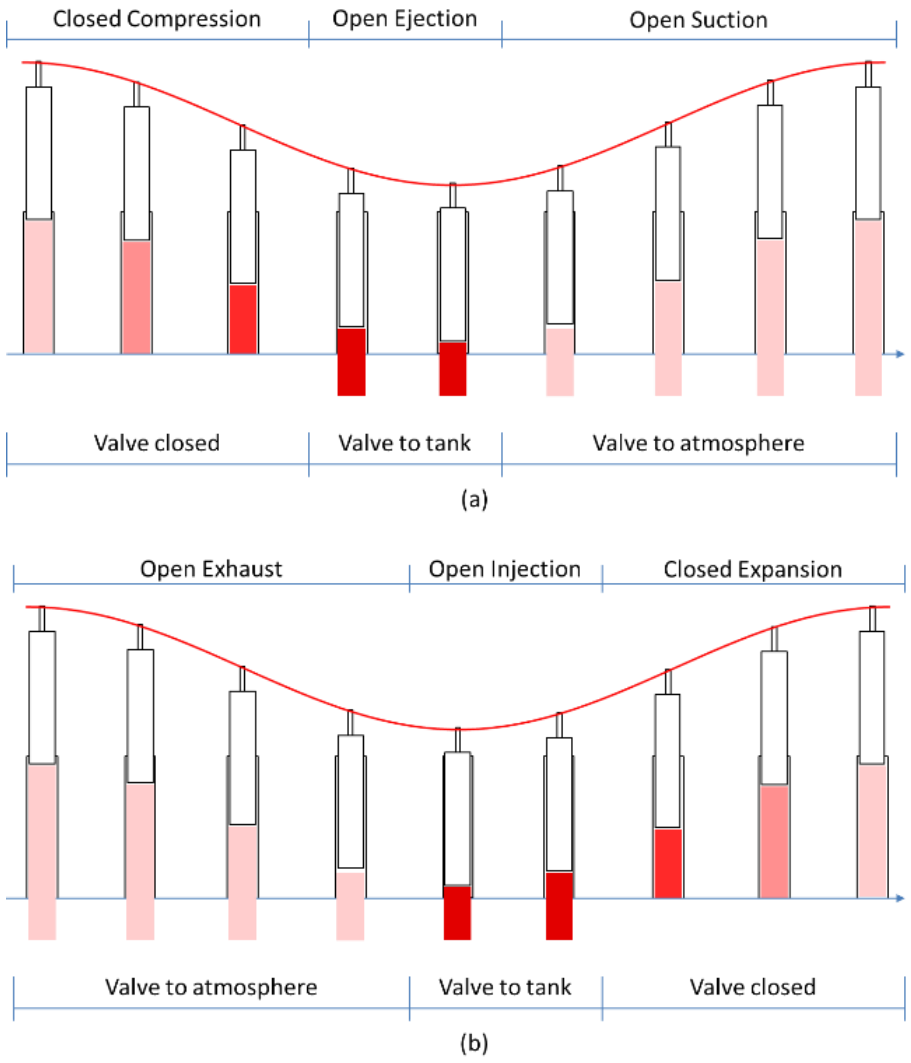

Figure 3.12. The single cylinder performance in a) compression mode and b) expansion mode.

The closed compression phase is taken, for example, to demonstrate the effect of adjustment on wobble plate and neutral piston displacement. The six cylinders in Figure 3.13 (a) correspond to the six red points, A1-A6, on the right half of the cross-section plot of the VDM housing in Figure 3.13 (a). As the piston starts to push the air into the chamber at state A1, the air in the chamber is compressed, leading to a gradual pressure increase, until the chamber pressure reaches the tank pressure at state A6. Then this amount of air

exhausts to the tank. Since the pistons rotate around the VDM shaft, each cylinder would experience the state changes from A1 to A6 while compressing.

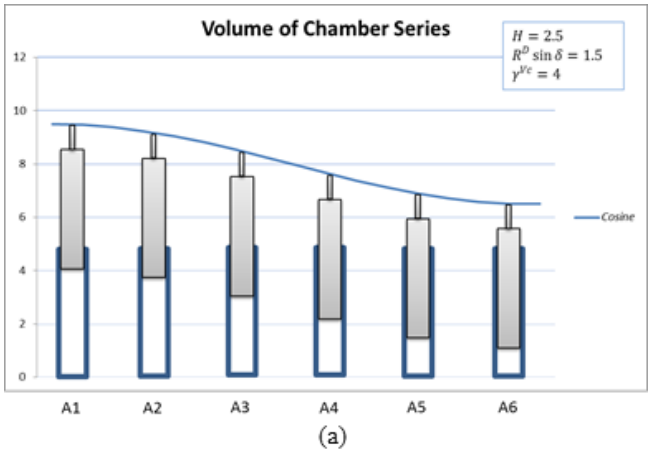

Figure 3.13: Example of the VDM chamber series condition during compression a) $H = 2.5, R^D \sin\delta = 1.5$, b) $H = 2.5, R^D \sin\delta = 0.5$ and c) $H = 0.75, R^D \sin\delta = 0.45$.

The example in Figure 3.13 (a) shows that, while the piston moves from state A1 to A6, the chamber achieves a compression ratio of 4.0. By adjusting the wobble angle while maintaining the value of NPS, the compression ratio is changed from 4.0 to 1.5 as shown in Figure 3.13 (b). Further decreasing the NPS helps to regain the compression ratio from 1.5 to 4.0 as states change from Figure 3.13 (b) to Figure 3.13 (c). Comparison of Figure 3.13 (a) and Figure 3.13 (c) demonstrates that the design of the VDM allows several pairs of 'wobble angle and NPS' achieving the same number of compression ratio. In this way, wobble angle and compression ratio is decoupled. This statement/function is useful in VDM control scheme under various wind speed condition.

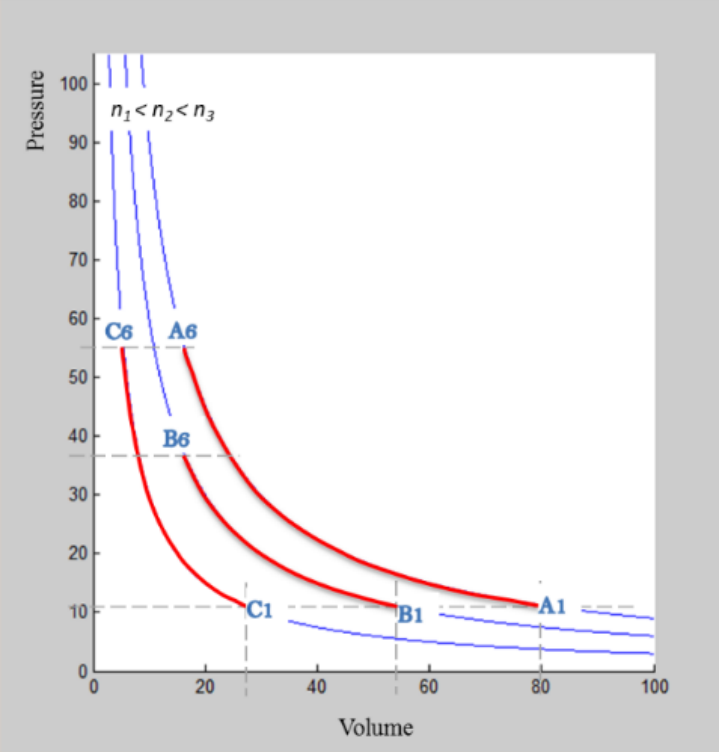

Figure 3.14: Isothermal compression curves for different amounts of gas in moles.

Mapping Figure 3.13 (a) (b) and (c) onto the parallel isothermal curves gives the red curves in Figure 3.14. It is assumed that ideal gas process is achievable. The three blue

curves represent different amounts of substance of the gas in moles as $n_1 < n_2 < n_3$. The energy storage process in Figure 3.13 (a) is represented by the curve A1-A6 in Figure 3.14. The process in Figure 3.13 (b) and (c) are represented as curves B1-B6 and C1-C6 in Figure 3.14, respectively. The comparison between A1-A6 and B1-B6 shows reducing the wobble angle could decrease the final pressure of compression. The comparison between A1-A6 and C1-C6 demonstrates that a shorter stroke could also lead to the same final pressure as a larger stroke does (meaning the same compression ratio).

3.3.1. Torque Analysis

A front view of wobble plate is presented in Figure 3.15 (a), where the polar angular position of Piston 1 is represented by ζ; and the effective radius of the wobble plate is represented by R^D, measuring the distance between the centers of the wobble shaft and piston shaft. A side view of wobble plate is given by Figure 3.15 (b), where the piston force at position ζ is represented by F_ζ^P. This force is decomposed to the orthogonal component F_ζ^N, which is perpendicular to the wobble plate, and the tangential force component F_ζ^D, which is perpendicular to the shaft of the wobble plate.

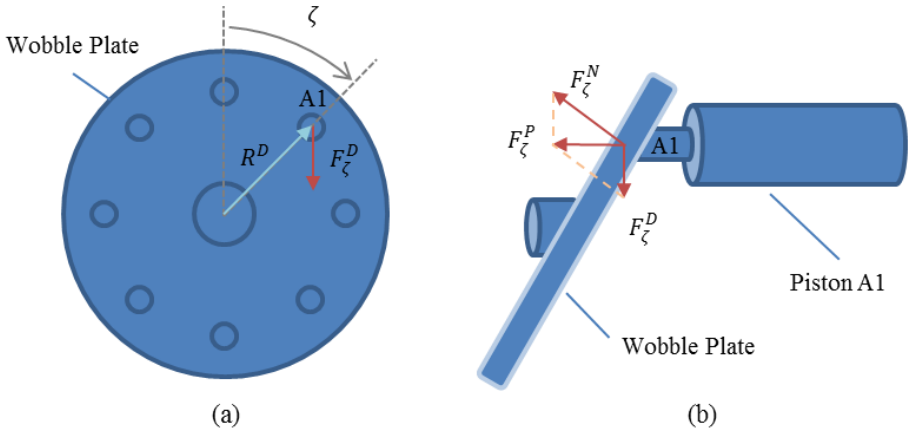

Figure 3.15: The wobble disk force analysis in a) the side view and b) the front view.

Since the compression process is divided into three phases, the force on the wobble plate is derived in each stage. In the closed compression phase, the volume V_ζ of the air chamber at position ζ is calculated by (3.11), where S represents the area of the piston head. The relative compression ratio γ_ζ^{Vc} at position ζ is calculated by (3.12). The piston force F_ζ^P at this point is the product of the compression ratio, atmosphere pressure, and the piston surface area in (3.13). The tangential force component F_ζ^D is then calculated by (3.14). Since the effective arm R_ζ pertaining to position ζ is the product of the effective radius multiplied by the sine of the position angle in (3.15), the torque on the wobble plate is expressed by (3.16). The same calculation process applies to the open ejection phase, where the relative compression ratio is replaced by the constant final compression ratio, as shown in (3.17). In the open suction phase, the torque loss caused by the air friction is negligible.

Since the torque expressions in all three phases are derived, the expected torque from a single piston is calculated by the integration of the piston torque through 2π of the wobble plate divided by 2π, where angles for closed compression and open ejection are represented by ζ_1^{cy} and ζ_2^{cy}, respectively. Thus, the torque from pistons to the wobble plate, T^D, is calculated by the expected torque multiplied by the total number of pistons/cylinders n^{cy}, as shown in (3.18).

$$V_\zeta = (H + R^D \sin\delta^V \cos\zeta) \cdot S \tag{3.11}$$

$$\gamma_\zeta^{Vc} = \frac{H + R^D \sin\delta^V}{H + R^D \sin\delta^V \cos\zeta} \tag{3.12}$$

$$F_{\zeta}^{P} = \gamma_{\zeta}^{Vc} p^{o} S = \frac{H + R^{D} \sin \delta^{V}}{H + R^{D} \sin \delta^{V} \cos \zeta} p^{o} S \tag{3.13}$$

$$F_{\zeta}^{D} = F_{\zeta}^{P} \tan \delta^{V} = \frac{H + R^{D} \sin \delta^{V}}{H + R^{D} \sin \delta^{V} \cos \zeta} p^{o} S \tan \delta^{V} \tag{3.14}$$

$$R_{\zeta} = R^{D} \sin \zeta \tag{3.15}$$

$$T_{\zeta,1} = F_{\zeta}^{D} R_{\zeta} = \frac{H + R^{D} \sin \delta^{V}}{H + R^{D} \sin \delta^{V} \cos \zeta} p^{o} S R^{D} \tan \delta^{V} \sin \zeta \tag{3.16}$$

$$T_{\zeta,2} = p^{T} S R^{D} \tan \delta^{V} \sin \zeta \tag{3.17}$$

$$T^{D} = n^{cy} \frac{1}{2\pi} \left(\int_{\zeta=0}^{\zeta_1^{cy}} T_{\zeta,1} \, d\zeta + \int_{\zeta=\zeta_1^{cy}}^{\zeta_1^{cy}+\zeta_2^{cy}} T_{\zeta,2} \, d\zeta + \int_{\zeta=\zeta_1^{cy}+\zeta_2^{cy}}^{2\pi} 0 \, d\zeta \right) \tag{3.18}$$

According to the fundamentals of fluid dynamics, if the air pressure is predetermined, a unique optimal rotation speed of the fluid machine can be calculated. This optimal rotation speed is determined as $\Omega_{p^T}^{V,opt}$ in respect to the tank pressure p^T. The optimal rotation speed is selected between the maximum power point and the maximum efficiency point, so as to establish the compromise between the power output and efficiency. The flow rate of the fluid also has a frictional effect on the torque, so a discounting factor c_2 is assigned to model this effect. The derivation of the optimal rotation speed and torque discounting factor is out of the scope of this dissertation [57]. Thus, the VDM power, P^{Vc}, is expressed in (3.19). It is noted that the integration in (3.18) eliminates the angular position variable ζ; and the VDM power expression in (3.19) is the function of only the "wobble angle-NPD" pair (H, δ), marked as $f_{H,\delta}^{D}$ in (3.20).

$$P^{Vc} = c_2 \cdot T^D \Omega_{p^T}^{V,opt} \tag{3.19}$$

$$P^{Vc} = f_{H,\delta}^{D} \tag{3.20}$$

3.3.2. Pressure Analysis

In the compression mode, the pressure change occurs only in the closed compression phase. The initial volume V_1 and final volume V_2 are calculated by (3.21) and (3.22), respectively. The compression ratio, γ^{Vc}, is calculated by (3.23), as the ratio of initial volume to the final volume, if the isothermal process applies. The additional constraints on wobble angle and NPD are given by (3.24) and (3.25), modeling the wobble angle limits and physical inference between the piston head and cylinder bottom. Since the closed compression angle ζ_1^{cy} is the constant parameter, the right-hand side of (3.23) is the function of only the "wobble angle-NPD" pair (H, δ), marked as $f_{H,\delta}^{\gamma}$ in (3.26).

$$V_1 = (H + R^D \sin \delta^V) \cdot S \tag{3.21}$$

$$V_2 = \left(H + R^D \sin \delta^V \cos \zeta_1^{cy}\right) \cdot S \tag{3.22}$$

$$\gamma^{Vc} = \frac{V_1}{V_2} = \frac{H + R^D \sin \delta^V}{H + R^D \sin \delta^V \cos \zeta_1^{cy}} \tag{3.23}$$

$$\delta^V \in \left(-\frac{\pi}{4}, \frac{\pi}{4}\right) \tag{3.24}$$

$$H > R^D \sin \delta^V \tag{3.25}$$

$$\gamma^{Vc} = f_{H,\delta}^{\gamma} \tag{3.26}$$

3.3.3. Operation Point Resolving

Equations (3.20) and (3.26) indicate that the (H, δ) pair serves as the control variables to adjust the compression ratio, as well as the VDM power. Because the compression ratio reference is determined by the tank pressure and the VDM power reference depends on the blade power surplus/deficit compared to the load, the VDM power and compression ratio are the known variables for each specific moment. There are two equations for two variables, H and δ; thus, jointly solving the equations gives the result of the reference of H and δ.

However, the equations include the integration function. The analytical solution is not easy to obtain. The numerical solving process is introduced to solve the equations. The 3D surfaces and their contours on the "wobble angle-NPD" plane for the compression ratio and VDM power are plotted in Figure 3.16 (a) and (b), respectively, in which the x-axis represents the wobble angle and the y-axis the NPD.

An overlap of both contours in Figure 3.17 gives the mesh grid and intersections points of the compression ratio and power. Three points are plotted to explain the dynamic working states of the VDM. While the compression ratio is at R2 and VDM power is at L1, the operational point of VDM is at Point A. If the tank pressure decreases from R2 to R1 while the VDM power is constant, the operational point will move from Point A to Point B through Line AB. If the VDM power is increased from L1 to L2 while tank pressure is constant, the operational point will move from Point A to Point C through Line AC. Those movements demonstrate the dynamic working states of the VDM, and the references of the wobble angle and NPD are calculated by the corresponding values on the x- and y-axes.

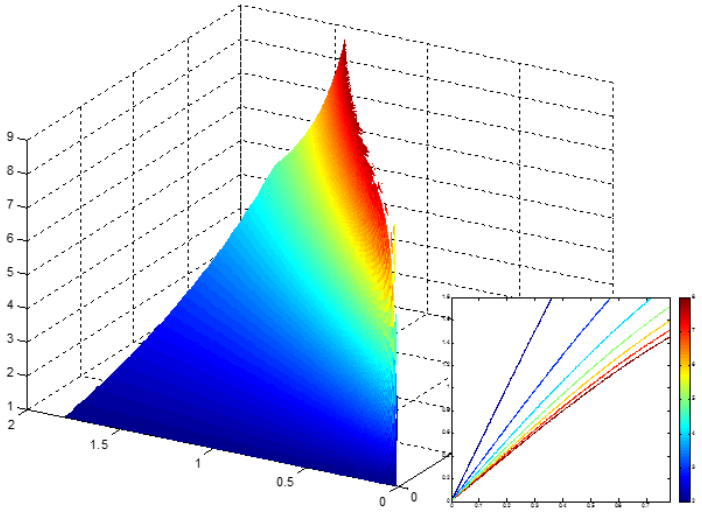

(a)

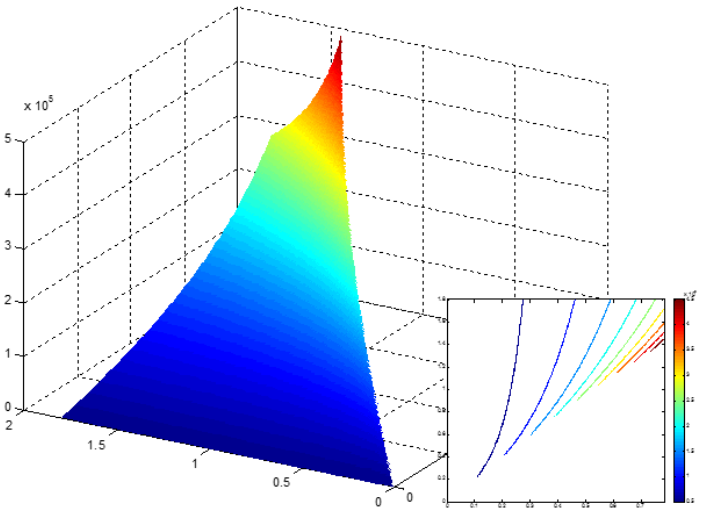

(b)

Figure 3.16: The operational surfaces and contours of the a) compression ratio and b) VDM power.

In case that there is not an intersection between a specific pair of values of compression ratio and power, the VDM output power is reduced to the maximum available power under the current pressure ratio to meet the load, which may create gaps between the power expectancy and power reference of the VDM.

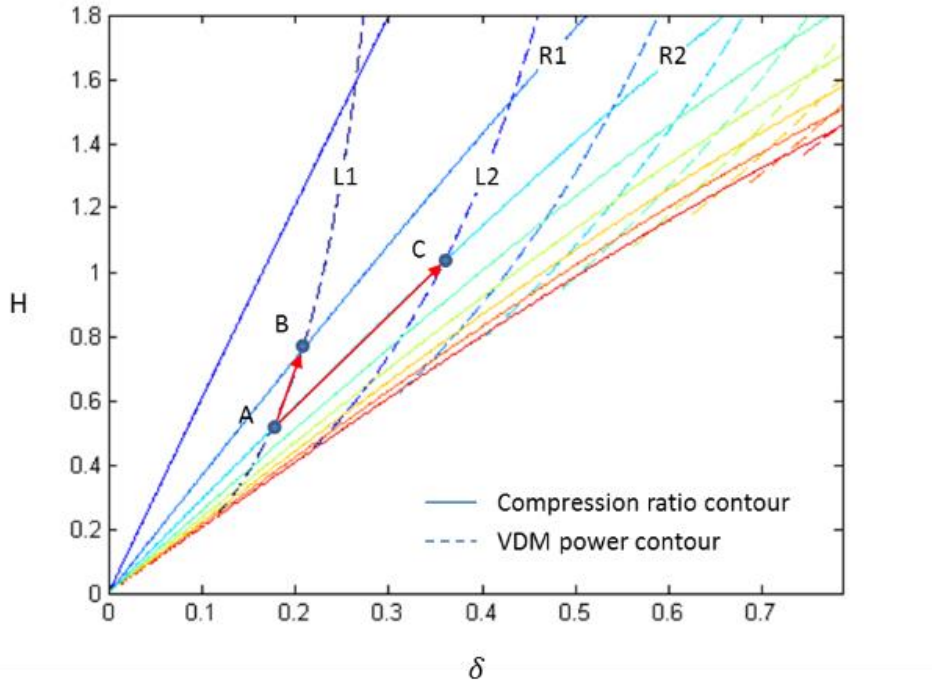

Figure 3.17: The overlapped layout of the mesh grid of the compression ratio and VDM power.

3.4. Dispatchable Generation Strategy

The objective of this section is to generate the references of the control variables for the subsystem of the VDM, blade, and generator. It is noted that the wind speed, load power reference, and tank pressure are assumed to be the known variables obtained from the external commands or measurements. The regulation process is explained as follows.

3.4.1. VDM Regulation

The VDM regulation policy is explained in Figure 3.18. First, the blade power envelope is calculated from the wind speed. Second, the VDM power expectancy is generated by comparing the difference between the blade power envelope and the load power. Then, the limits or constraints, such as VDM rated power and tank storage vacancy,

apply to the VDM power expectancy. Finally, the references of VDM power and speed, as well as “wobble angle-NPD” pair are obtained by the contour mesh grid method as explained in Section 3.3.3.

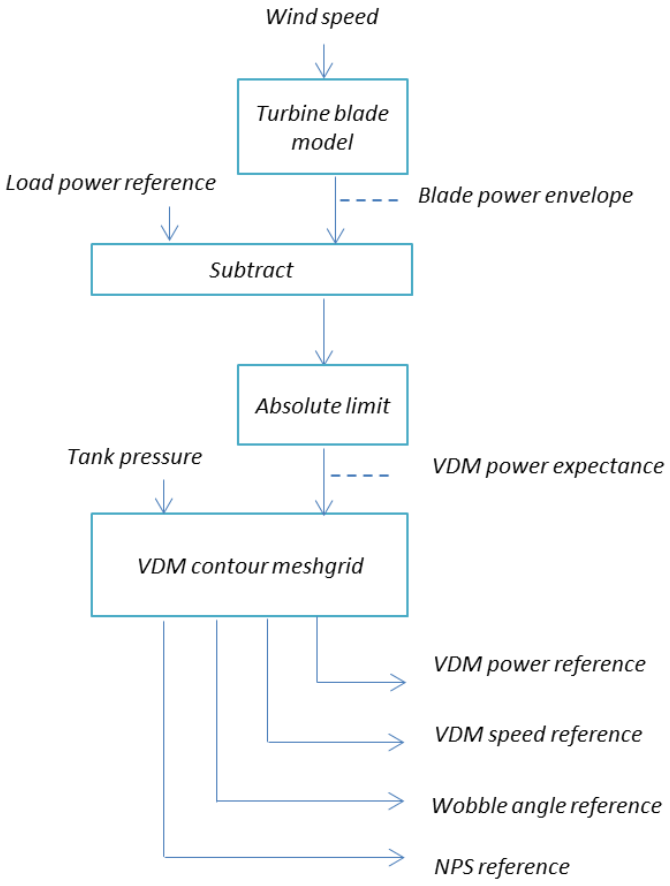

Figure 3.18: The VDM reference generation flowchart.

3.4.2. Blade and Generator Regulation

Since the VDM power reference is determined in the previous section, it is assumed to be a known variable in this section. Because the blade and the generator are coupled through a fixed ratio gearbox, the references of the blade and the generator are obtained simultaneously. Two separate flowcharts apply to the blade and generator regulation.

If the calculated blade power is higher than the load power, the VDM enters the compression mode. As depicted in Figure 3.19 (a), the generator power reference is equal to the load power reference. The blade power reference is the summation of the VDM power and the generator power. Since the blade power reference is derived and the wind speed is a known variable, the references of the blade rotation speed and blade pitch angle are obtained through the turbine blade mode, as discussed in Section 3.2.1. Thus, the generator speed reference is calculated by the blade speed reference multiplying the gear ratio.

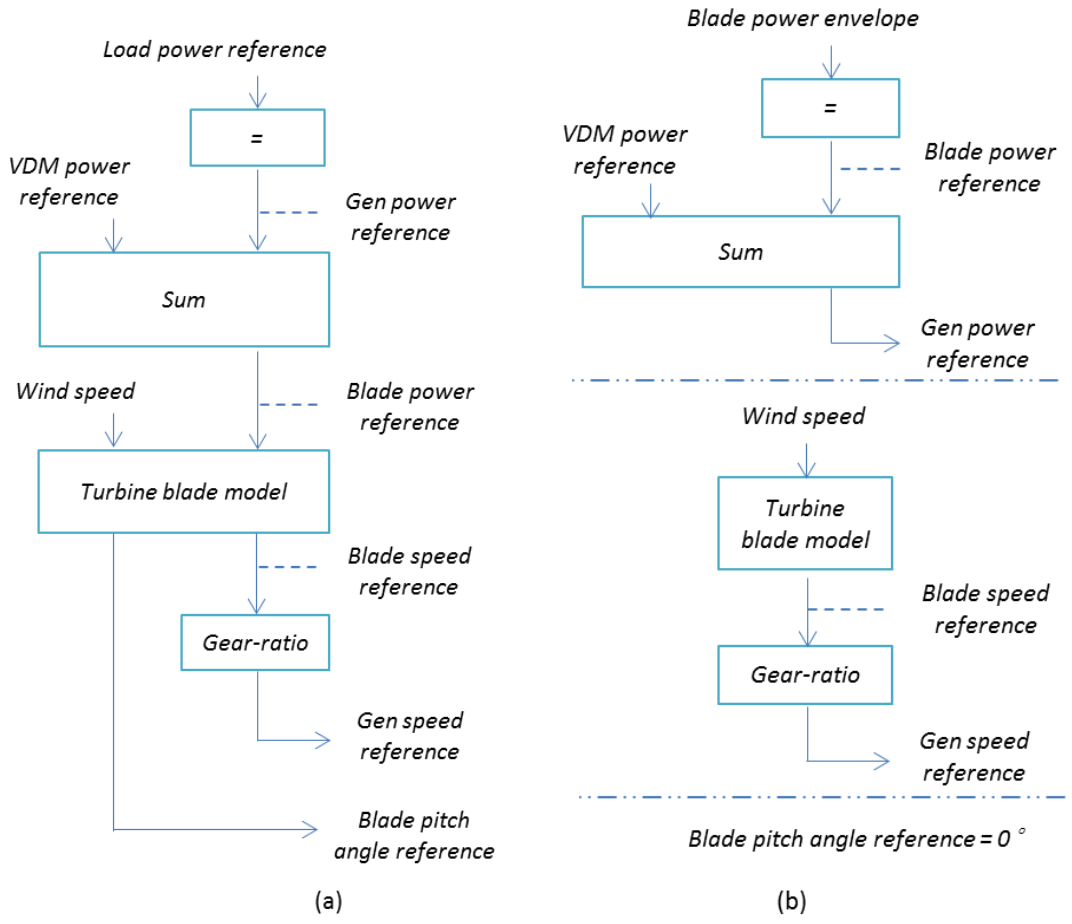

Figure 3.19: The blade and generator reference charts for the a) compression mode and b) expansion mode.

If the blade power envelope is lower than the load power, the VDM enters the expansion mode. Figure 3.19 (b) depicts the control process. In order to extract the maximum power from the wind, the blade angle is set as 0°; and the blade power reference is equal to the blade power envelope. The generator power reference is the summation of the VDM and blade power references. The turbine blade model gives the blade rotation speed reference under the current wind speed. Thus, the generator speed reference is calculated from the blade speed reference.

3.4.3. CVT Regulation

Since the speed references of the VDM and generator were obtained in the previous analysis, the CVT ratio reference is calculated by the ratio of the generator speed reference over the VDM speed reference. The regulation flow chart is shown in Figure 3.20.

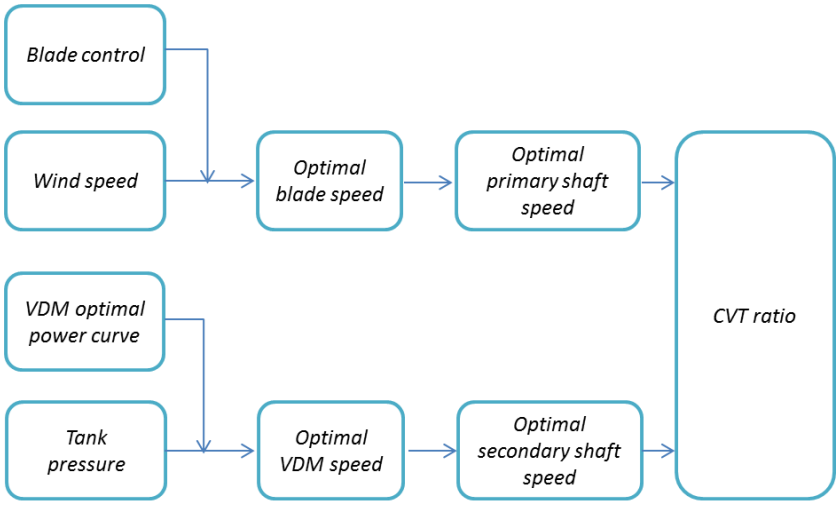

Figure 3.20: The regulation flow of CVT.

3.4.4. Other Constraints

Other constraints include the mechanical power balance in (3.6) and the energy storage update in (3.9).

3.5. Numerical Case Study

A numerical case study is conducted to evaluate the performance of the proposed control for CA-WT in this section. The parameters for the system are given in Table 3.1. The episodes of wind speed and load data with a 10-minute interval for one week were obtained from the Eastern Wind Dataset at NREL and NE-ISO Express real-time maps and charts, respectively [58, 59]. The load data are scaled down to the 0-400kW range to simulate the consumption pattern of a small community. The wind speed and load pattern are shown in Figure 3.21.

Table 3.1: System Key Parameters

PARAMETER	VALUE	PARAMETER	VALUE
Cut-in speed	3.0 m/s	VDM rated power	417 kW
Rated speed	6.5 m/s	Compression efficiency	65%
Cut-out speed	15 m/s	Expansion efficiency	65%
Blade length	32 m	Storage rated capacity	3300kWh
Generator rated power	250 kW	Max pressure	8.0 Bar
Generator efficiency	99%	Min pressure	3.0 Bar

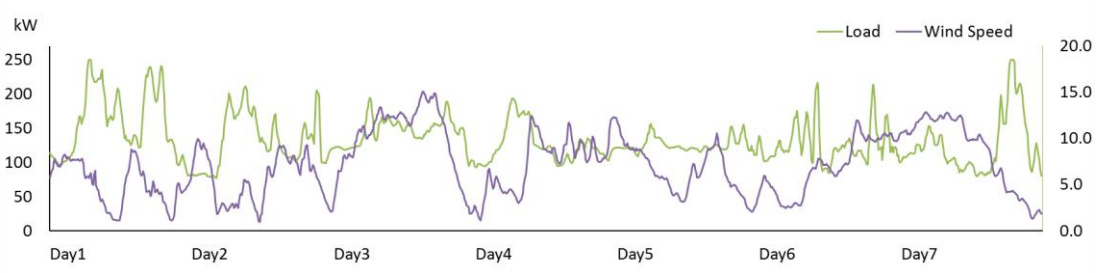

Figure 3.21: The wind speed and load patterns.

Two cases are considered for comparison. In Case 1, the proposed CA-WT is operated to match the maximum load demand. In Case 2, the system is replaced by a traditional WT to serve the load.

3.5.1. Performance Comparison

The power generation comparisons between Case 1 and Case 2 over one week are given in Figure 3.22. The results demonstrate that the traditional WT has severe generation dips as well as downtime under the given wind and load patterns. The proposed system eliminates most of the downtime and dips, although there is still unmet load sometime in Day 1 and Day 2, while the load is high and the wind is low.

The generation for the CA-WT and WT during this period is 21.79 MWh and 15.66 MWh, respectively, indicating 39.2% higher in Case 1 than in Case 2. Load coverage calculates the percentage of load that is covered by the wind power generation system. The CA-WT is able to cover 97.08% of the load while the WT covers 69.76% of the load, as shown in Table 3.2. The generator factor increases from 37.27% to 51.87%.

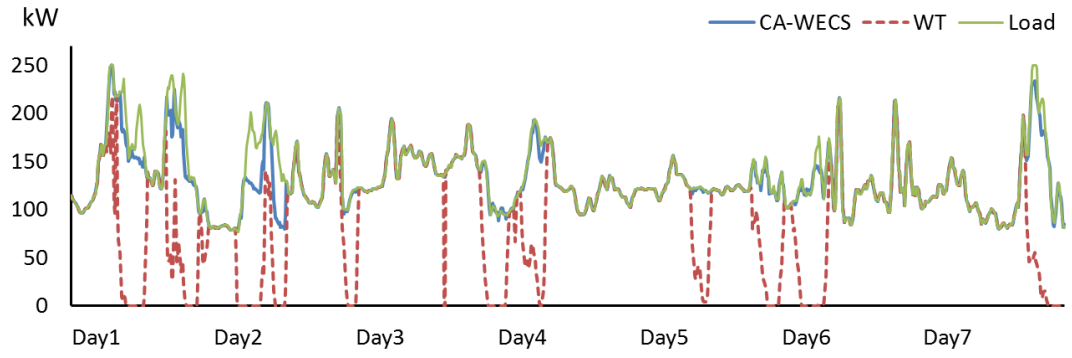

Figure 3.22: The generation comparison between the proposed CA-WT and traditional WT.

Table 3.2: Generation Comparison

PARAMETER	GENERATION	LOAD COVERAGE	GENERATOR FACTOR
Total load	22.44 MWh	100.00%	(53.43%)
CA-WT	21.79 MWh	97.08%	51.87%
WT	15.66 MWh	69.76%	37.27%

3.5.2. Generations profiles

A generation detail in Day 1 is shown in Figure 3.23. From the 7th hour to the 13th hour, the WT is unable to cover the load due to the unavailability of adequate wind energy, including four hours of downtime from the 9th to the 12th hour. In comparison, the CA-WT is able to recover most of the downtime. The maximum gap between the generation and load for CA-WT is 87 kW, compared to 225kW for the WT.

The blade power curve shown in Figure 3.24 explains the energy harvest in the CA-WT. The mechanical spillage is marked as the positive gap between the blade power and the WT generation, and the capacity vacancy is the negative gap between them. The proposed VDM and storage serve as a buffer to mitigate the gap between the wind energy and the load. The VDM consumes the mechanical spillage and produce the compressed air while the wind speed is high and consumes the compressed air to generate electricity while wind speed is low. The corresponding VDM power is shown in Figure 3.25.

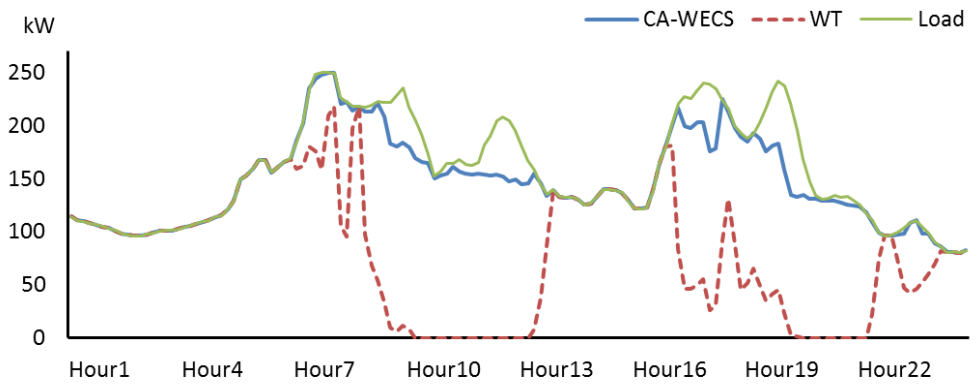

Figure 3.23: The generation curves vs. load curve in Day 1.

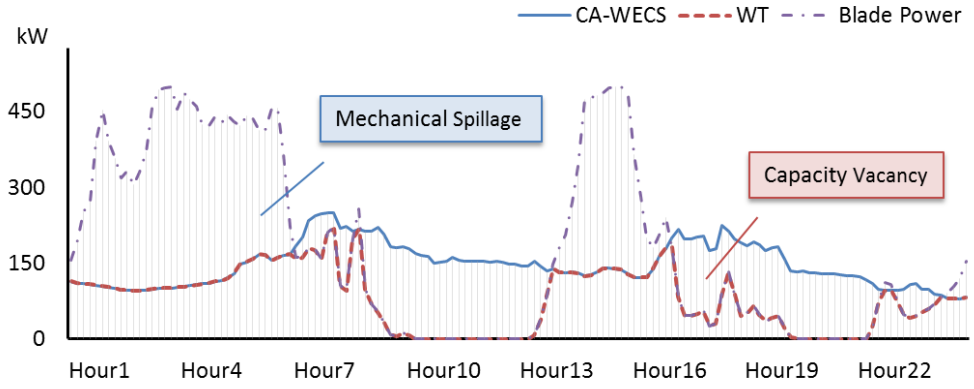

Figure 3.24: The blade power curve vs. generation curves in Day 1.

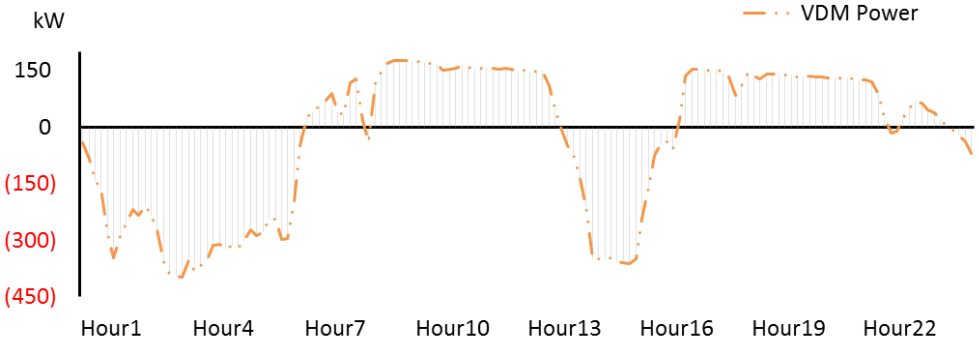

Figure 3.25: The VDM power curve in Day 1.

3.5.3. Operational references

The details of the VDM operation during the Day 1 are depicted in Figure 3.26, where the positive "wobble angle-NPD" pair indicates compression mode; and the negative indicates the expansion mode. The pressure ratio changes corresponding to the VDM operation. According to the algorithms in Section.3.4.3, the CVT ratio in Figure 3.27 indicates a range of 0.45 to 2.00. The speed and torque references for the blade and generator are shown in Figure 3.28 (a) and (b), respectively.

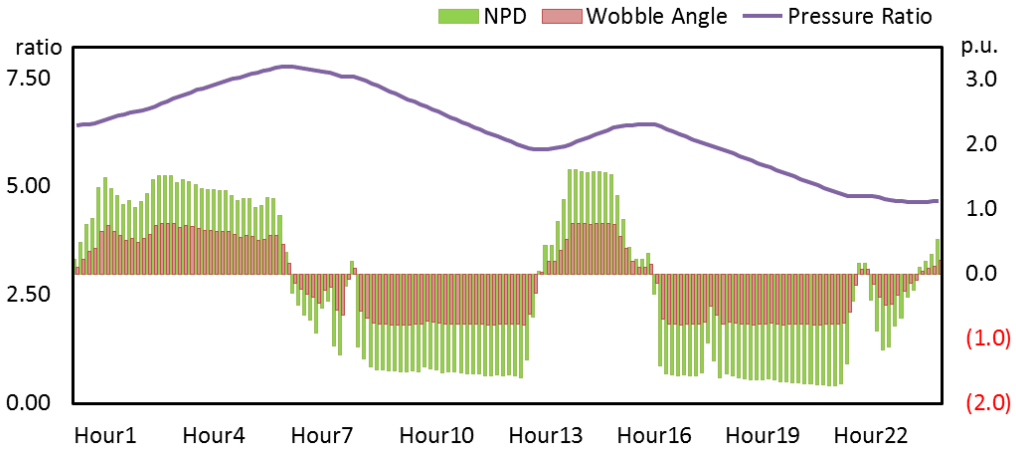

Figure 3.26: The operation of the wobble angle and NPD vs. the corresponding air pressure.

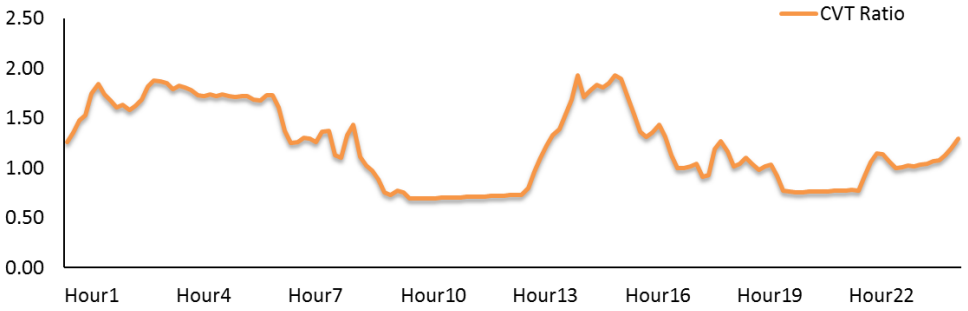

Figure 3.27: The CVT ratio.

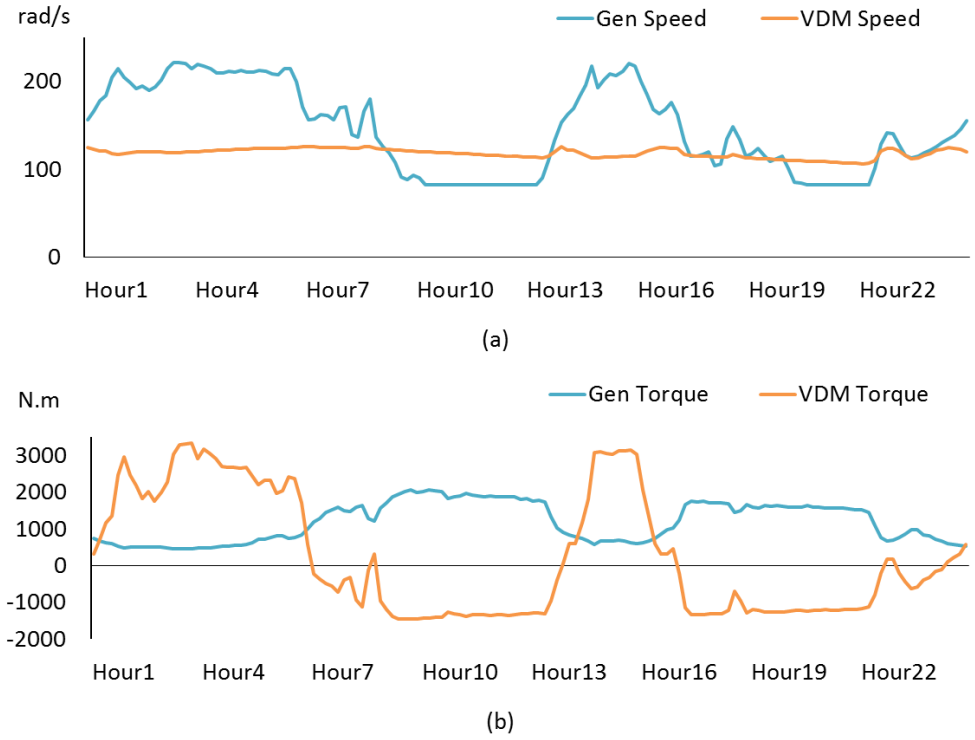

Figure 3.28: The generator and VDM operational details of a) rotation speed and b) torque.

3.6. Chapter Summary

In this chapter, the fundamentals of a compressed-air-assisted wind energy conversion system were introduced and explained. The core component of the system is a variable displacement machine, which serves as a buffer to compensate for the discrepancy between the mechanical power from the wind and the electric power to the load. The references of the control variables, such as the wobble angle and the neutral piston displacement, are calculated by the mesh-grid method.

According to the seven-day numerical case study, the generation of the proposed system is increased by 39.2%, compared to a traditional wind turbine under the same circumstances. It covers 97.08% of the load, compared to 69.76% covered by a traditional

wind turbine. The proposed system recovers most of the power dips caused by the mismatch between the wind energy and the load. Moreover, whenever the wind speed is beyond the operational range, the variable displacement machine is able to drive the generator and supply the load independently. The operational variables, such as the speed references for the blade and generator, are also obtained by the algorithm.

CHAPTER 4. OPTIMAL SIZING

The sizing problem of the proposed system includes determining the optimal combination of appropriate components to form a system for energy management and economical operation under a stochastic environment of variable wind speed and a dynamic power market.

An analytical approach is developed to determine the optimal capacities of the generator, variable displacement machine (VDM), and air tank, respectively, by using the option list of each component. Proper sizing of the proposed system is a challenge to the designer due to a large number of options for each component. The stochastic property of a wind resource adds additional complexity to the problem.

Consequently, the decision maker faces the uncertainties of intermittent wind energy and a volatile power market, while taking into consideration several technical constraints associated with selected components. Meanwhile, to evaluate possible performance solutions, the decision maker has to deduce an operation policy corresponding to the optimal solution.

4.1. Optimal Sizing Problem Review

As mentioned in Section 3.2, a new configuration is proposed to capture mechanical spillage and convert it into compressed air storage. Because of the uniqueness of the system, research on this type of sizing problem is scant. However, even though various types of energy storage systems (ESSs) have been developed to couple with intermittent renewable energy, the relevant literature has been found on the topics of sizing 1) battery storage or pumped hydro storage for a wind farm, 2) large-scale compressed air energy storage

(CAES), and 3) generation and storage in a microgrid. The search methods fall into three categories: exhaustive, heuristic, and deterministic algorithm.

4.1.1. Exhaustive Search

An exhaustive search means to evaluate every possible solution to the problem through finite possible candidates in the search space. A cost-benefit approach was established to determine the most profitable rating for ESSs of existing wind farms, where an exhaustive search is applied to find an optimal solution through all possible combinations of sizing options [60]. A model for a solar-home-system with CAES was developed to represent the sizing problem of compressed air storage, where an exhaustive search through feasible options for tank size was used to determine the optimal solution [57]. An improved optimal sizing method for a wind-solar-battery hybrid system was developed [61], considering the power reliability and fluctuation requirement, for which an exhaustive search was conducted to find the optimal combination for the number of wind turbines, solar panels, and battery units. However, since the number of combinations increases as the number of component options increases, a complete enumeration of solutions could be impractical considering a large number of possible combinations in the search space.

4.1.2. Heuristic Search

To avoid the intensive computation associated with an exhaustive search through all possible solutions, heuristic methods are usually suggested to solve sizing problems. A genetic algorithm (GA) optimization methodology was proposed in [62] to minimize the energy cost and maximize the renewable energy penetration. An evolutionary strategy (ES)

was developed to solve the optimal selection and sizing problem in a power system consisting of microgrid clusters [63]. A tabu search (TS)-based evolutionary technique was used to optimize the size of the ESS, considering the unit commitment scheduling of the thermal units [64]. A hybrid of simulated annealing (SA) and tabu search (TS) was proposed to take advantage of both metaheuristic methods while escaping from the short-sighted confines of both [65]. However, the selection of appropriate parameters for the heuristic method is a sensitive procedure. For example, the choice of tabu size in TS, the temperature decrease coefficient in SA, or the crossover fraction in GA could determine the success or failure in finding the optimal solution. In general, the quality of a solution obtained from a heuristic search depends on the careful selection of iteration parameters and the smoothness of the search space.

4.1.3. Deterministic Algorithm

The optimal sizing problem becomes complex if the variables involve not only the size of storage but also the operation strategy for the generators and other regulations. The mixed integer linear programming (MILP) method was used to optimize the size and operation strategy of a storage system for a microgrid, consisting of wind power, solar power, and fuel cell and battery storage, in which the unit commitment was considered [66]. The integer constraints were meaningful for some variables because, for example, the number of battery units cannot be a decimal. The reliability consideration was brought to the MILP model, adding the constraint of loss-of-load expectation (LOLE) [67]. The relationship between the cost of ESS and the total energy cost of the microgrid was established. The balance point between investment cost and operational cost of an ESS in a microgrid was studied. Typical scenarios with uneven probability were set up as a

stochastic environment. The final result provided the optimal size of storage and its optimal operation schedule.

4.2. Model Formulation

To address the optimal sizing problem of the proposed system, a stochastic environment is established to evaluate the performance of various configurations. In a stochastic programming framework, the uncertainties of wind speed and electricity price are represented by countable sets of joint scenarios. Each joint scenario is comprised of two vectors: wind speed and electricity price. Each vector includes 168 spot values, representing hourly wind speed or electricity price in a week. The stochastic programming approach is employed to generate a deterministic equivalent of the original problem, while taking into account each possible scenario with a probability. The mixed integer linear programming (MILP) method is employed to solve the problem. Techniques, such as piecewise linearization and the auxiliary binary variable method, are usually used to linearize the objective function and constraints.

4.2.1. Two-Stage Stochastic Programming

Stochastic programming is a framework to model the optimization problems which involve environmental uncertainty before making a decision. In this chapter, the wind energy resources and electricity prices are treated as stochastic variables in a time-based series model. As long as the stochastic process can be described by probability, representative scenarios can be generated to account for the environmental uncertainty. Then the problem is converted to s a linear programming problem, called deterministic equivalent.

The decision process of this problem can be divided into two stages. The first stage decision or here-and-now decision is made before the realization of the stochastic process, representing the sizes of key components, i.e., generator, VDM, and air tank. The second stage decision, or wait-and-see decision, is made after the realization of the stochastic processes, representing the operation detail in each time step under a given scenario. Thus, making a second stage decision depends on the joint realization of the stochastic process and the first stage decision. It is remarked that as a price taker a single wind turbine does not have the power to influence the market price. Therefore, no bidding or penalty are considered in the sizing problem.

4.2.2. Discounting Cost

Equipment cost usually involves a one-time initial investment and annual operational and maintenance (O&M) costs. Since the economic life of the equipment and the planning horizon of the model are not identical, the equipment cost needs to be converted to the value that fits for the planning horizon. This involves a two-step conversion process. First, the investment is converted to an annual basis by considering the economic life of the equipment and the minimum attractive rate of return. Second, the annual equivalent of the investment and the O&M costs are linearly scaled to fit the time window of the planning horizon chosen for the model. The calculation is expressed in (4.1),

$$C = \frac{N^h h}{365 \times 24}\left(\mathrm{CI} \,/\left[\frac{1}{r} - \frac{1}{r(1+r)^L}\right] + \mathrm{CM}\right) \tag{4.1}$$

where the price, the annual O&M cost, and discounted cost for the related hardware are represent by CI, CM, $and\ C$, respectively. The annual interest rate and the economic life

are represented by *r* and *L*, respectively. The number and duration of the time step in the planning horizon are represented by N^h and *h*, respectively.

4.2.3. Decision Variables

The system design includes selecting the appropriate components from the option list, considering its corresponding cost. The selections of the i^{th} option of generator and j^{th} option of VDM are represented by binary decision variable x_i^G and x_j^V, of which the values one and zero represent selection and nonselection, respectively, of a specific option. The the air storage capacity is identified by an integer variable y^T where the integer value refers to the number of prespecified air storage tank.

4.2.4. Objective Function

The objective function maximizes the expected revenue from the production of electricity and minimizes the summation of component costs over a planning horizon, as shown in (4.2).

$$Max\ Z = \sum_{\omega=1}^{N^{\varphi}} \varphi_{\omega} \sum_{t=1}^{N^h} e_{t,\omega}^{rt} \cdot P_{t,\omega}^{Go} \cdot h - \sum_{i=1}^{N^G} C_i^G \cdot x_i^G - \sum_{j=1}^{N^V} C_j^V \cdot x_j^V - C^{TU} \cdot y^T \tag{4.2}$$

where the probability of scenario ω is φ_{ω}; the real-time market price at time *t* under scenario ω is represented by $e_{t,\omega}^{rt}$; the discounted cost of the i^{th} option of generator, the j^{th} option of the VDM, and the storage tank units are represented by $C_i^G, C_j^V,$ and C^{TU}, respectively; an integer number of air tanks is represented by y^T; and the output power of a wind generator at time *t* under scenario ω is represented by $P_{t,\omega}^{Go}$. The total number of

scenarios under consideration is represented by N^{φ}. The numbers of generator and VDM options are represented by $N^{G}$and N^{V}.

The first term of the objective function represents the expected value of revenue from sales of electricity; this is the expected value of the product of the electricity rate, output power, and hours h within each time step of the N^{h} time steps in the planning horizon. The second and third terms represent the discounted cost of the generator and the VDM during the planning horizon, respectively. The fourth term is the discounted cost of storage tank(s). It should be noted that, as a price taker, a single wind turbine does not have the power to influence the market price. Therefore, no bidding or penalty costs are considered in this formulation.

4.2.5. Constraints

- Unitary Constraint

Only one option is allowed for a component of generator or VDM, respectively. Therefore, the constraints are expressed in (4.3)–(4.5).

$$\sum_{i=1}^{N^{G}} x_i^{G} \leq 1 \tag{4.3}$$

$$\sum_{j=1}^{N^{V}} x_j^{V} \leq 1 \tag{4.4}$$

$$x_i^{G} \in \{0,1\}, x_j^{V} \in \{0,1\} \tag{4.5}$$

- Blade Power Envelope Constraint

The maximum power that can be captured by the blades and delivered to the gearbox is a function of wind speed expressed in (3.1). The corresponding power curve is defined as the blade power envelope, which means the wind turbine is free to operate with the area of the envelope. However, the constraint brings nonlinearity into the model since a term of a cube of the wind speed exists.

A new variable $\theta_t = \frac{1}{2}\rho v_t{}^3$ is defined to linearize the expression in (3.1). With the substitution, the blade power at time *t* under scenario ω is represented by (4.6), where the parameters $a_i = C_p A^w$ and $b_i = f^{loss}$ are defined to represent the parameters of the i^{th} option of the generator, and θ_t becomes constant for a given wind speed.

$$P_{t,\omega}^{B} \leq \sum_{i=1}^{N^G} \left(a_i \theta_{t,\omega} - b_i\right) \cdot x_i^G \tag{4.6}$$

Since each wind turbine has its own cut-in speed, below which a conventional wind turbine stands still, this characteristic adds a conditional requirement to the linear blade power as represented by (4.7).

$$P_{t,\omega}^{B} \leq \begin{Bmatrix} \sum_{i=1}^{N^G} \left(a_i \theta_{t,\omega} - b_i\right) \cdot x_i^G \text{ , If } \sum_{i=1}^{N^G} \left(a_i \theta_{t,\omega} - b_i\right) \cdot x_i^G \geq 0 \\ 0 \text{ , } Otherwise \end{Bmatrix} \tag{4.7}$$

The *either/or* aspect of constraint (4.7) could be linearized by adding an auxiliary binary variable, as shown in (4.8)–(4.11), where M_{11} and M_{12} are big positive numbers, and

u_1 is a binary decision variable. Switching u_1 between 0 and 1 makes either (4.8)–(4.9) or (4.10)–(4.11) nonbinding.

$$\sum_{i=1}^{N^G}\left(a_i\theta_{t,\omega}-b_i\right)\cdot x_i^G+M_{11}(1-u_1)\geq 0 \tag{4.8}$$

$$P_{t,\omega}^B \leq \sum_{i=1}^{N^G}\left(a_i\theta_{t,\omega}-b_i\right)\cdot x_i^G+M_{11}(1-u_1) \tag{4.9}$$

$$\sum_{i=1}^{N^G}\left(a_i\theta_{t,\omega}-b_i\right)\cdot x_i^G<M_{12}u_1 \tag{4.10}$$

$$P_{t,\omega}^B \leq M_{12}u_1 \tag{4.11}$$

Another way to linearize either/or constraints is to pretreat the wind power for each option of the wind turbine before entering the optimization phase. The maximum blade power that a wind turbine can capture is computed by (4.12) since wind power density is assumed to be known variables after the scenario generation process. Then, the blade power constraint in (4.7) is reduced to a linear one as shown in (4.13). The benefit of the pretreatment method includes the elimination of an additional auxiliary variable.

$$P_{t,\omega}^{B,L,i} = \begin{Bmatrix} a_i\theta_{t,\omega}-b_i, \text{If } a_i\theta_{t,\omega}-b_i\geq 0 \\ 0\,, else \end{Bmatrix} \tag{4.12}$$

$$P_{t,\omega}^B \leq \sum_{i=1}^{N^G} P_{t,\omega}^{B,L,i}\cdot x_i^G \tag{4.13}$$

As auxiliary binary variable u_1 represents the engagement/disengagement of states of the clutch, among the aforementioned two paths, the auxiliary binary variable method is chosen to formulate the problem in this chapter.

- Mechanical Power Balance on the Gearbox

The power balance on the gearbox under various scenarios are depicted in (4.14)–(4.15), where blade power, VDM expansion power, VDM compression power, and generator input power at time t under scenario ω are represented by $P_{t,\omega}^{B}$, $P_{t,\omega}^{Vp}$, $P_{t,\omega}^{Vc}$, and $P_{t,\omega}^{Gi}$, respectively. The fundamental of the gearbox is explained in Section 3.2.3.

$$P_{t,\omega}^{B} + P_{t,\omega}^{Vp} = P_{t,\omega}^{Gi} + P_{t,\omega}^{Vc} \tag{4.14}$$

$$P_{t,\omega}^{Vp} \cdot P_{t,\omega}^{Vc} = 0 \tag{4.15}$$

Obviously, the constraint in (4.15) introduces nonlinearity to the formulation. Simply eliminating this constraint may create several alternative optimal solutions because, mathematically, identical VDM output power could result from multiple pairs of compression power and expansion power. This situation could be eliminated by adding compression power and expansion power into the objective function and assigning them small negative coefficients. Minimizing both compression power and expansion power could guarantee one of them is maintained at zero. The artificial penalty coefficient ε is selected for this purpose. By adding artificial penalty term in the objective function, the constraint (4.15) can be eliminated from the optimization model. Thus, the new objective function is represented by (4.16).

$$Max\ Z_1 = \sum_{\omega=1}^{N^{\varphi}} \varphi_{\omega} \sum_{t=1}^{N^{h}} e_{t,\omega}^{rt} \cdot P_{t,\omega}^{Go} \cdot h - \sum_{i=1}^{N^{G}} C_i^G \cdot x_i^G - \sum_{j=1}^{N^{V}} C_j^V \cdot x_j^V - C^{TU} \cdot y^T - \varepsilon \sum_{t=1}^{N^{h}} \left(P_{t,\omega}^{Vp} + P_{t,\omega}^{Vc}\right) \tag{4.16}$$

- Storage Tank Energy Balance

As stated in Section 3.2.4, for a given storage tank, the characteristic is analogous to a battery pack. The energy balance under different scenarios is calculated by (4.17), where the energy in the tank in the current and next time steps are represented by E_t^T and E_{t+1}^T, respectively. A minimum pressure may be required for normal operation [56].

$$E_{t+1,\omega}^T = \eta^T E_{t,\omega}^T + \eta^{Vc} P_{t,\omega}^{Vc}\, h - P_{t,\omega}^{Vp}\, h/\eta^{Vp} \tag{4.17}$$

- Capital Expenditure Constraint

The investment is limited by an upper bound on the available capital C^{IC}, as shown in (4.18), where the prices of the i^{th} option of generator, j^{th} option of VDM, and the tank unit are represented by CI_i^G, CI_j^V and CI^{TU}, respectively.

$$\sum_{i=1}^{N^{G}} \mathrm{CI}_i^G\, x_i^G + \sum_{j=1}^{N^{V}} \mathrm{CI}_j^V x_j^V + \mathrm{CI}^{TU} y^T \le C^{IC} \tag{4.18}$$

- Other Constraints

The generator input and output power constraits are shwon in (4.19) and (4.20), respectively. The VDM compression power and expansion power are depicted in (4.21) and (4.22), respectively. The tank storage capacity limit and minimum pressrue restriction

are shwon in (4.23) and (4.24), respectively. The mechanical survival threshold is arbitrarily assumed as three times the generator rated power, as it is shown in (4.25). The non-negativity constraint and integer constraint are expressed in (4.26) and (4.27), respectively.

$$P_{t,\omega}^{Go} \leq \sum_{j=1}^{N^G} P_i^G x_i^G \tag{4.19}$$

$$P_{t,\omega}^{Go} \leq \eta^G P_{t,\omega}^{Gi} \tag{4.20}$$

$$\eta^{Vc} P_{t,\omega}^{Vc} \leq \sum_{j=1}^{N^V} P_j^V x_j^V \tag{4.21}$$

$$P_{t,\omega}^{Vp} \leq \sum_{j=1}^{N^V} P_j^V \, x_j^V \tag{4.22}$$

$$E_{t,\omega}^{T} \leq E^{TU} y^T \tag{4.23}$$

$$E_{t,\omega}^{T} \geq 10\% \cdot E^{TU} y^T \tag{4.24}$$

$$P_{t,\omega}^{B} \leq 3 \sum_{j=1}^{N^G} P_i^G x_i^G \tag{4.25}$$

$$P_{t,\omega}^{B}, P_{t,\omega}^{Go}, P_{t,\omega}^{Vc}, P_{t,\omega}^{Vp}, E_{t,\omega}^{T} \geq 0 \tag{4.26}$$

$$y^T = 0, 1, 2, 3, 4 \ldots \ldots \tag{4.27}$$

4.2.6. Formulation Summary

According to the previous explanation, the formulation of the optimal sizing problem for the proposed system could be summarized as a mixed integer linear programming problem as follows,

$$Max\ Z_1 = \sum_{\omega=1}^{N^{\varphi}} \varphi_{\omega} \sum_{t=1}^{N^h} e_{t,\omega}^{rt} \cdot P_{t,\omega}^{Go} \cdot h - \sum_{i=1}^{N^G} C_i^G \cdot x_i^G - \sum_{j=1}^{N^V} C_j^V \cdot x_j^V - C^{TU} \cdot y^T - \varepsilon \sum_{t=1}^{N^h} \left(P_{t,\omega}^{Vp} + P_{t,\omega}^{Vc}\right)$$

Subject to:

- Unitary constraint

$$\sum_{i=1}^{N^G} x_i^G \leq 1$$

$$\sum_{j=1}^{N^V} x_j^V \leq 1$$

- Investment upper limit

$$\sum_{i=1}^{N^G} \mathrm{CI}_i^G\, x_i^G + \sum_{j=1}^{N^V} \mathrm{CI}_j^V x_j^V + \mathrm{CI}^T y^T \leq C^{IC}$$

- Mechanical balance

$$P_{t,\omega}^{B} + P_{t,\omega}^{Vp} = P_{t,\omega}^{Gi} + P_{t,\omega}^{Vc}$$

- Energy storage update

$$E_{t+1,\omega}^{T} = \eta^{T} E_{t,\omega}^{T} + \eta^{Vc} P_{t,\omega}^{Vc}\, h - P_{t,\omega}^{Vp}\, h/\eta^{Vp}$$

- Cut-in speed condition linearization

$$\sum_{i=1}^{N^G} \left(a_i \theta_{t,\omega} - b_i\right) \cdot x_i^G + M_{11}(1 - u_1) \geq 0$$

$$P_{t,\omega}^{B} \leq \sum_{i=1}^{N^G} \left(a_i \theta_{t,\omega} - b_i\right) \cdot x_i^G + M_{11}(1 - u_1)$$

$$\sum_{i=1}^{N^G} \left(a_i \theta_{t,\omega} - b_i\right) \cdot x_i^G < M_{12} u_1$$

$$P_{t,\omega}^{B} \leq M_{12} u_1$$

- Blade power limit

$$P_{t,\omega}^{B} \leq 3 \sum_{j=1}^{N^G} P_i^G x_i^G$$

- Generator capacity

$$P_{t,\omega}^{Go} \leq \sum_{j=1}^{N^G} P_i^G x_i^G$$

$$P_{t,\omega}^{Go} \leq \eta^{G} P_{t,\omega}^{Gi}$$

- VDM compression and expansion capacity

$$\eta^{Vc} P_{t,\omega}^{Vc} \leq \sum_{j=1}^{N^V} P_j^V x_j^V$$

$$P_{t,\omega}^{Vp} \leq \sum_{j=1}^{N^V} P_j^V x_j^V$$

- Storage upper and lower limits

$$E_{t,\omega}^{T} \leq E^{TU} y^T$$

$$E_{t,\omega}^{T} \geq 10\% \cdot E^{TU} y^T$$

- Non-negativity constraint

$$P_{t,\omega}^{B}, P_{t,\omega}^{Go}, P_{t,\omega}^{Vc}, P_{t,\omega}^{Vp}, E_{t,\omega}^{T}, E_{t+1,\omega}^{T} \geq 0$$

- Integer and binary constraints

$$x_i^G, x_j^V, u_1 \in \{0,1\}$$

$$y^T = 0, 1, 2, 3, 4 \ldots \ldots$$

4.3. A Numerical Case Study

The proposed wind turbine is assumed to be connected to an infinite bus. Therefore, the grid can accept all of the amount of wind power generated, and no congestion on

transmission line is considered. In this case, there is electrical spillage, however, mechanical spillage still exists.

Sixty options for the wind turbines, twenty options for the VDMs, and one option for the air tank are considered in the study. A sample of eight options for the wind turbines is shown in Table 4.1; a sample of five options for VDMs are listed in Table 4.2; and the option for the air tank is shown in Table 4.3. The efficiencies for each component are given in Table 4.4. It is noted that the tank leakage is assumed as 0.5% during an hourly cycle. Thus the energy retaining coefficient for the compressed-air storage is obtained as 99.5%.

Table 4.1: Wind Turbine List

No.	P_i^G (kW)	v_0 (m/s)	v_{r1} (m/s)	CI_i^G	CM_i^G	C_i^G
2	400	2.7	10.0	$ 680,000	$ 3,400	$ 942
3	400	3.0	10.0	$ 640,000	$ 3,200	$ 886
4	500	2.7	11.0	$ 800,000	$ 4,000	$ 1,108
5	500	3.2	11.0	$ 700,000	$ 3,500	$ 969
6	500	3.5	10.0	$ 700,000	$ 3,500	$ 969
7	600	2.7	11.0	$ 960,000	$ 4,800	$ 1,330
8	600	3.0	9.0	$ 1,020,000	$ 5,100	$ 1,413

.
.
.

Table 4.2: VDM List

No.	P_j^V (kW)	CI_j^V	CM_j^V	C_j^V
1	300	$ 127,500	$ 956	$ 183
2	350	$ 140,000	$ 1,050	$ 201
3	400	$ 140,000	$ 1,050	$ 201
4	450	$ 135,000	$ 1,013	$ 193
5	500	$ 150,000	$ 1,125	$ 215

.
.
.

Table 4.3: Air Tank Information

No.	E_L^{TU} (kWh)	CI^T	CM^T	C^{TU}
1	100	$ 2,500	$ 13	$ 3

Table 4.4: System Component Efficiencies

	η^G	η^T	η^{Vc}	η^{Vp}
Value	99.0%	99.5%	65.0%	65.0%

The same economic lives and zero salvage values are assumed for all components. The planning horizon N^h is set at 168 hours with a one-hour interval. The capital expenditure limit is set as $1.5 million. It is assumed that the annual interest rate is 3% and the life cycle of equipment is 20 years.

The wind speed vectors are generated from the historical records of wind speed in Stuart, Nebraska [68]. In each season, a 7-day, hourly wind speed vector is selected from the first week of the second month. Each vector consists of 168 wind speed values (7 days × 24 hourly spot wind speeds). The electricity price vectors corresponding to the time of the wind speed vectors are extracted from the PJM Energy Market [69]. In total, four joint scenarios are considered in the optimization. Each includes hourly wind speed and electricity price values for 168 hours. Equal probability is assigned to each scenario. Because the infinite bus is assumed to be connected to the system in this study, the generation reference is the capacity of the generator. The representative wind speed vectors and corresponding electricity rate vectors in each season are shown in Figure 4.1 and Figure 4.2, respectively.

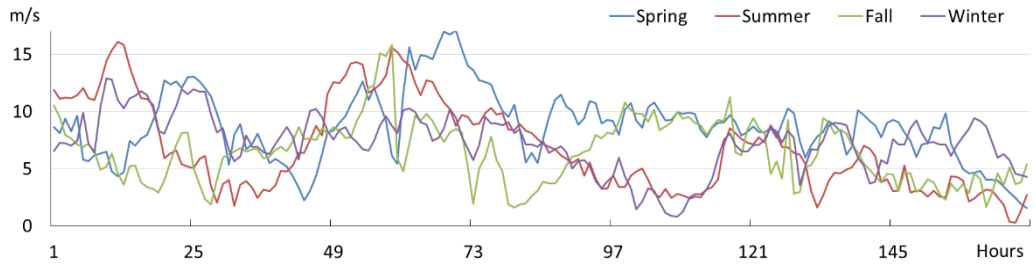

Figure 4.1: Representative wind speed vectors in different seasons.

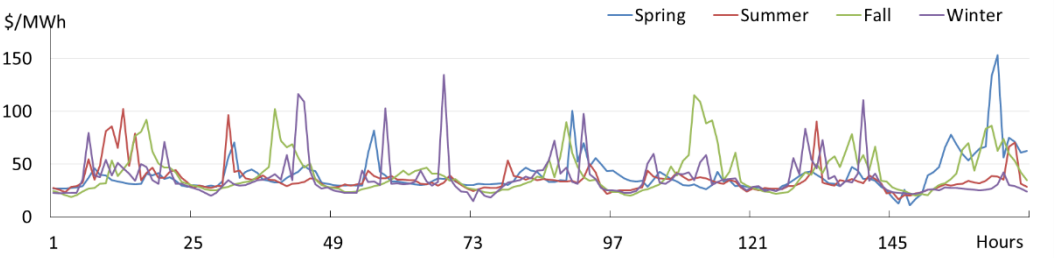

Figure 4.2: Electricity rate vectors corresponding to wind speed vectors.

The cost of wind turbine is $1,300 to $2,000 per kW, depending on the capacity of the generator and the size of the blades. The cost of the VDM is derived from cost of the small size air machine ranging from $300 to $450 per kW.

The problem is developed and solved by optimization solver ‘intlinprog’ in MATLAB R2014a. The numerical solution is performed on a 2.40GHz dual core processor with 6.00G RAM.

Two cases are considered for comparison. Case 1 represents the proposed system that includes a compressed-air storage while Case 2 represents the traditional wind turbine without storage. Both systems are connected to the grid, meaning all of the generation could be accepted by the grid at the real-time electricity rate. Thus, congestion and electrical spillage are not considered.

4.3.1. Optimal Solution

The results show the optimal size of the wind turbine is 500kW with a cut-in speed (v_{in}) of 3.5 m/s and electrical rated speed (v_{r1}) of 7.0 m/s. The optimal capacity of the VDM is 450kW. Seventy-one sets of the 100kWh air tanks, forming a total of 7100kWh storage, is needed for optimal operation under four representative seasonal conditions. The initial cost is $1,162,500, and the annual O&M cost is $6,150, as shown in Table 4.5. The potential annual revenue generated by this investment is $138,157.

Table 4.5: Optimal System Configuration

Component	*Capacity*	CI	CM	*C*
Generator	500 kW	$ 850,000	$ 4,250	$ 1,177
VDM	450 kW	$ 135,000	$ 1,013	$ 193
Storage	7100 kWh	$ 177,500	$ 888	$ 246
Sum	n/a	$ 1,162,500	$ 6,150	$ 1,616

The revenue corresponding to the final optimal solution is $2,650, consisting of $1,102 expected profit and $1,548 depreciation, as shown in Figure 4.3. A detailed comparison of the breakdown of the revenue is given in Figure 4.4. The expected revenue is $2,140 in Case 2, including $1,616 in hardware cost and $1,033 in net profit.

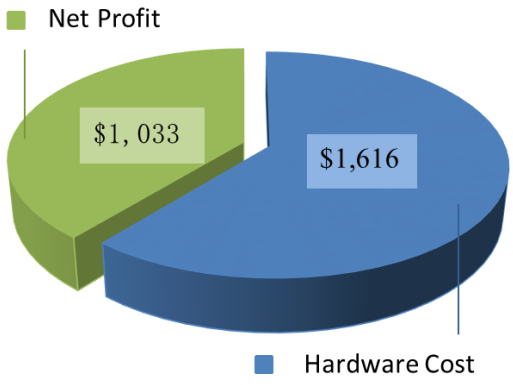

Figure 4.3: Revenue splits.

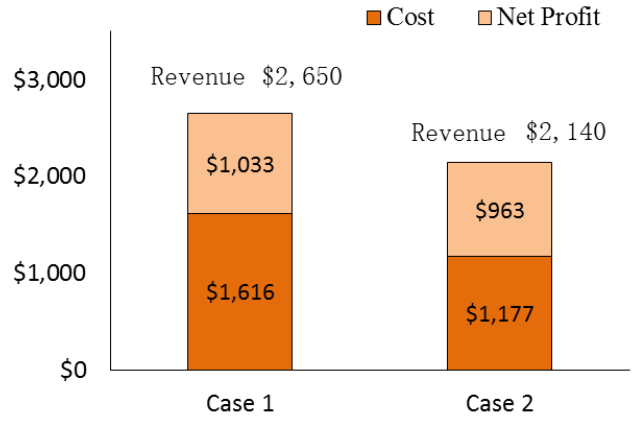

Figure 4.4: Revenue breakdown comparison between Case 1 and 2.

4.3.2. Discounted Payback Period

The payback period defines the time when the revenue recovers the cost, creating a positive cash flow for the first time. To determine the discounted payback period, the future value of the costs are calculated as a function of time. Then, the future value of the revenue is calculated and compared. The cost and revenue curves are depicted in Figure 4.5, and a discount rate of 3% is used. The intersection point indicates a discounted payback period of ten years.

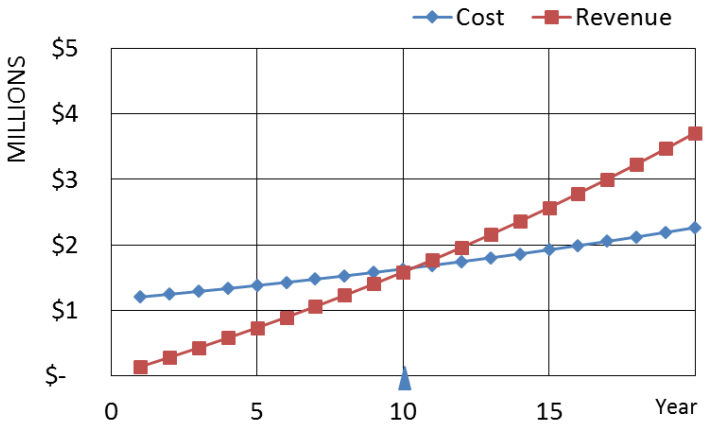

Figure 4.5: Discounted payback period.

4.3.3. System Operation Profile

The operational profiles for Case 1 and Case 2 are determined by the optimal values of the second stage decision variables after the size parameters are determined. The power generation curves for both cases in spring scenario are shown in Figure 4.6. The comparison shows that the proposed system eliminates most of the power drops during the 50th hour to the 160th hour. The capacity factor in this scenario increases from 84% to 96%.

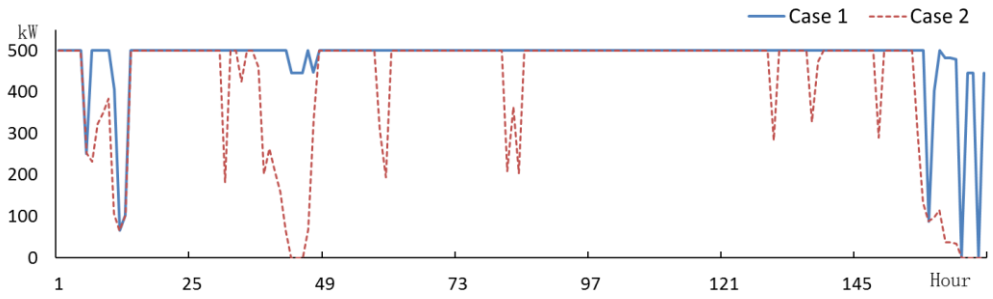

Figure 4.6: Generation comparison in spring scenario.

An episode of VDM operation under the same scenario is depicted in Figure 4.7, whereas VDM compressed the air while the wind is high and expands the air while the wind is low. The corresponding air tank state is depicted in Figure 4.8.

4.3.4. Seasonal Comparison

After the optimal sizes were determined, the system performances are compared under four different seasonal scenarios, respectively, for comparison. The seasonal power generations are given in Figure 4.9 (a), and their corresponding revenues are given in Figure 4.9 (b). The seasonal comparison shows that the power generation in Case 1 is increased by 15%, 17%, 18%, and 14%, respectively, over Case 2; and the corresponding revenue increments are 23%, 24%, 30%, and 19%, respectively.

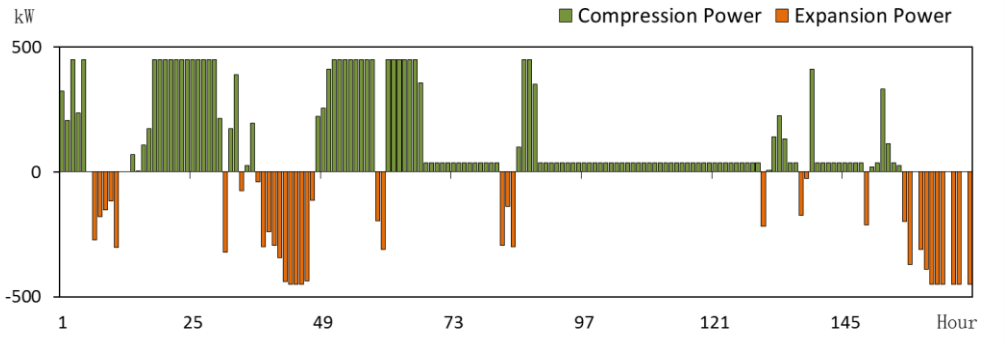

Figure 4.7: VDM operation in spring scenario.

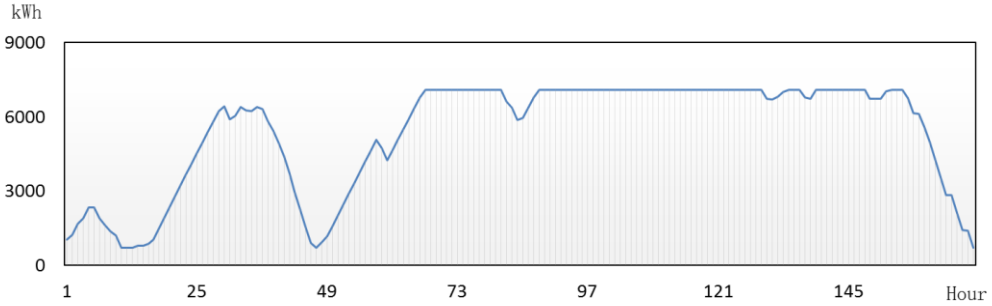

Figure 4.8: Tank storage energy condition in spring scenario.

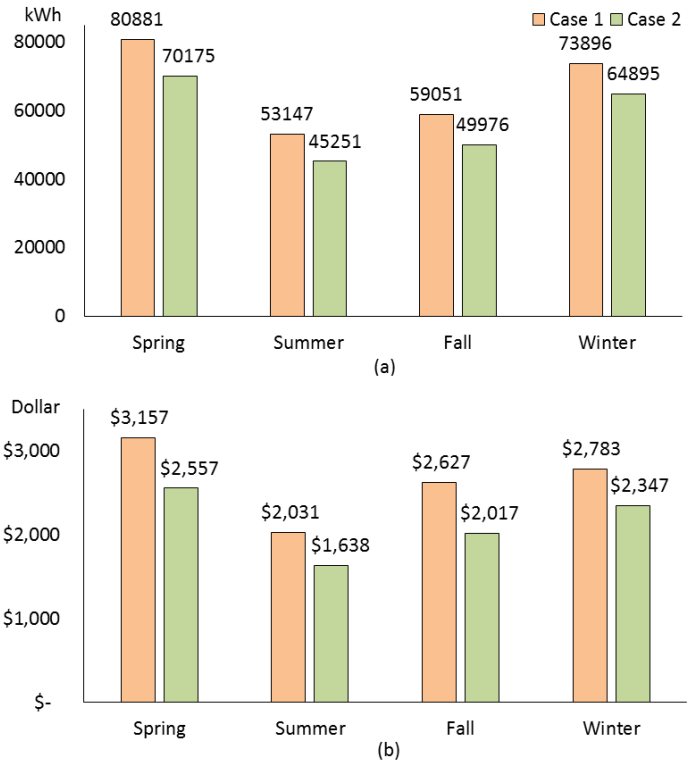

Figure 4.9: Seasonal comparisons for a) power generations and b) revenues.

4.4. Sensitivity Analysis

In this section, a sensitivity analysis is conducted to evaluate the cost-effectiveness of the proposed wind turbine project compared to a traditional wind turbine project. Three parameters are varied for comparison.

4.4.1. Wind Speed Sensitivity

To evaluate the impact from the strength/abundance of the wind resource, the wind speed is varied by ±30% and reevaluate the project's profit. The result is shown in Figure 4.10. Both profit curves increase with the wind speed; however, they experience a saturation effect if the wind speed is too high. While the wind speed is within the range of –20% to +40% (estimated) variation, the profit curve for Case 1 surpasses that of Case 2. If the wind speed decreases more than 20%, Case 2 could be an optimal option. This is because if the wind speed is too low, the proposed system does not have enough wind power to build up the storage; and if the wind speed is too high, the wind turbine is naturally working at a very high capacity factor, thus here is a very little capacity vacancy to be used.

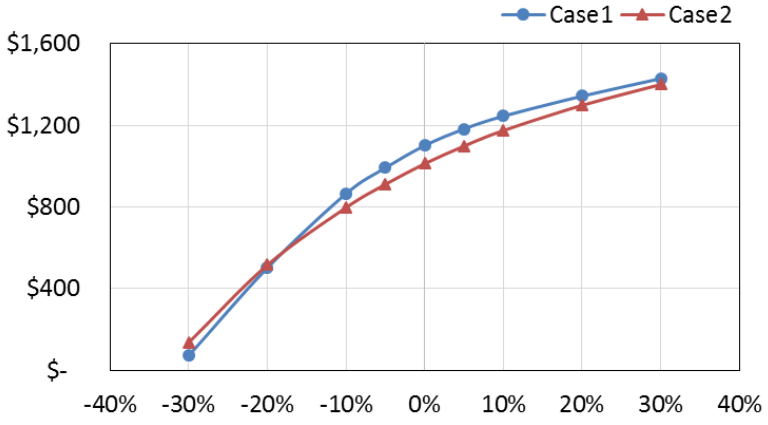

Figure 4.10: Wind speed sensitivity comparison.

4.4.2. Hardware Cost Sensitivity

To evaluate hardware cost sensitivity, the hardware cost is varied by ±30%; and the profit curves are shown in Figure 4.11. The curves indicate that if the hardware cost is increased by more than 22%, the profit of the proposed system is below that of a traditional wind turbine system.

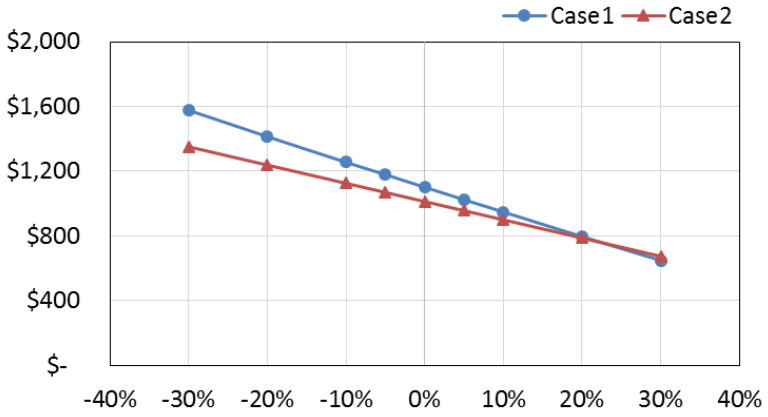

Figure 4.11: Hardware sensitivity comparison.

4.4.3. Electricity Rate Sensitivity

Electricity rate is another factor that impacts the profit of the project. To evaluate electricity rate sensitivity, the electricity rate is varied by ±30% for all scenarios, and the profits are proportional to the electricity rate as shown in Figure 4.12. If the electricity rate is decreased by 18% or more, the proposed system is unable to recover the additional cost through additional revenue from the extra power generation, compared to a traditional wind turbine system.

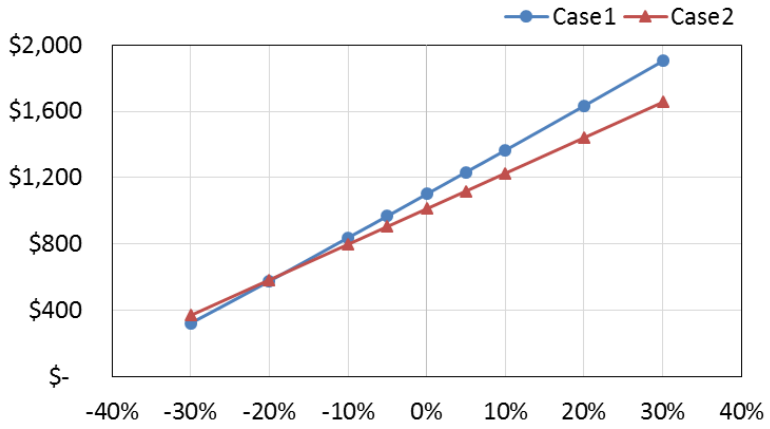

Figure 4.12: Electricity rate sensitivity comparison.

4.5. Chapter Summary

This chapter studies the sizing problem of a CA-WECS. To determine the sizes of each component, the two-stage scholastic programming method is employed. The stochastic environment is represented by a countable set of scenarios, and the performance is evaluated by the net profit for the planning period. The proposed system with storage and the traditional system without storage are compared.

The problem is solved by the MILP method. The resulting algorithm presents not only the optimal sizes of each component but also the corresponding operational details under different scenarios. The comparison showed that the expected revenue increased by 23.8%, resulting from a 15.9% increment of generation, compared to the traditional system.

CHAPTER 5. OPTIMAL OFFERING

The offer of power generation to the day-ahead market for a wind energy producer involves submitting the quantitative offer vector of generation twenty-four hours ahead, before knowing exact wind generation and electricity market prices. Optimal offering problem is to find out the optimal offer vector under an uncertain environment, taking different types of scenarios into consideration. Any mismatch between the offering and generation could cause an imbalance penalty, including over generation and under generation. Because the wind energy is traditionally considered to be a non-dispatchable resource, the development of optimal offering strategies is crucial for all wind power producers to maximize their profits, while facing high uncertainty in wind energy resource.

The electricity industry over the world is experiencing the shift from regulated power market to a competitive one, although it was organized as a regulated and vertically integrated natural monopoly not long ago. Electricity market framework was developed to break down this monopoly and to stimulate the growth of competitive energy producers.

Because the electricity is a special commodity that the generation has to match consumption simultaneously, a power market has to have at least two levels of the market, namely, day-ahead market and real-time market (or balancing market). In day-ahead market, producers and consumers agents submit the curves of their production offers and consumption bids, respectively. Afterward, the market is cleared according to the cumulative offering and bidding for each hour, determining the market clearing price and the set of acceptance for their offers and bids. Typically, the day-ahead market for day *n* is cleared at noon at day *n-1*. The clearance price and amount are determined by the

intersection where offer meets the demand on an hourly basis. The real-time market is cleared in the same way as the day-ahead market does, except that it is used to mitigate deviations between the offering in day-ahead market and real-time demand. This competitive framework is established to promote operational efficiency while fulfilling the reliability constraints of the power system.

Wind power producer is a special group of participants in the electricity market. The following three aspects differentiate them with the conventional producers: zero emission, zero fuel cost, and nondispatchability. The zero emission property gives the wind energy the priority to enter the power pool of an electricity market. The zero fuel cost property indicates that the energy cost is decoupled from the amount of generation. However, nondispatchability introduces additional uncertainty to the power system and introduces risk to the decision on power offering.

Therefore, wind energy producers participate in the different trading floors, in which they are paid the day-ahead market clearance price if they generate the promised amount of electricity, while being subjected to imbalance penalties for any real-time energy deviations. In short, they are price takers in the day-ahead market and the real-time market.

Imbalance penalty will be imposed on the energy producers if they cannot produce the exact amount of energy submitted and accepted in the power pool, for instance, either over production or under production in real-time. The detail of power market framework for wind energy is stated in [70, 71].

For traditional wind energy producer, the underestimation is adapted in wind forecasting to avoid under production, and pitching control is implemented on real-time to

avoid over production. Both methods help to create a safety margin but at the cost of energy spillage, since a great amount of kinetic energy in the wind is trimmed away. Integrating energy storage system is another way to mitigate the mismatch and recover the energy spillage. Options could include battery energy storage (BES), pumped hydro energy storage (PHES), compressed air energy storage (CAES), etc. The surplus energy exceeding the forecasting in the wind is directed to the storage and serves as power supply while under generation is about to happen.

A single wind turbine is not large enough to participate in the electricity market. In this chapter, it is assumed that a wind farm, consisting of a group of proposed size-optimized wind energy conversion system, acts as a single agent to make the offer. While treating wind speeds at different locations in the wind farm as interdependent variables, the offer vector of the wind farm is formed by cumulating offers of all wind turbines in the farm.

Because of environmental-friendliness, wind energy producer is assumed as a prior supplier in the market, meaning that all amount of power offering that a renewable energy producer submitted to the power pool is accepted at the market clearing price of that hour. Additionally, as a small party in the market, wind energy supplier is still considered as a price taker, placing no influence on speculation of market price. Thus, wind energy producer only submits an offer for the hourly quantity of generation instead of a quantity-price pair [72, 73].

5.1. Optimal Offering Strategy Review

The configuration of proposed system has not been shown in any previous publications. Therefore the literature of optimal offering strategy problem on proposed system is scant. The relevant literature was found on the topics of wind energy optimal offering with conventional CAES, BES, PHES and so forth.

A case of operation schedule for a BES with WTs under Time-of-Use (TOU), electricity rate environment, is studied [74], where a multi-pass dynamic programming method is proposed to solve the problem. TOU represents the segmented electricity price policy where electricity is priced at a high level for on-peak load and low level for the off-peak load. A modified particle swarm optimization (PSO) is integrated to improve the computational effectiveness and solution quality in each round of iteration. However, obtaining the optimal schedule depends on the correct selections of particle parameters. Moreover, a more dynamic power market framework is not considered.

The uncertainty of wind resource and market price is included in [75], where a two-stage stochastic programming framework is proposed for the optimal offering strategy. Risk preference is defined and measured by conditional value-at-risk (CVaR), which exists in the objective function to weight between expected profit and risk of loss. However, the strategy and model are for a traditional wind turbine; the impact of storage is not considered and thus not thoroughly studied.

Additionally, demand response (DR) is introduced to mitigate the deviation of the wind power generation caused by the intermittency of wind resources [72, 76]. The joint operation of wind power and DR is proposed so that any deviation on wind power

generation could be offset or compensated by DR operation, in order to fulfill the economic operational goal and reliability requirement. However, risk preference issue is not tackled by this approach, and the decrease of customer satisfaction associated with DR is not evaluated.

The optimal offering strategy for a group of thermal and hydro units are studied in [77], where a two-stage stochastic framework is set up to account for market uncertainty. The risk aversion is taking into consideration as CVaR measure in the objective function. However, the strategy is for a traditional generation, in which performance of renewable energy and storage are not included. And the cumulative offer is not established.

The coordinated operation of wind power and pumped storage units is proposed to improve economic performance and hedge against uncertainty from wind resource and market prices [78]. This model could be used by a system of wind power integrated with CAES. However, it ignored risk management of wind energy producers.

5.2. Model Formulation

Suppose a wind farm with a group of CA-WECSs is planning to participate in the electricity market. A schematic of such a system is shown in Figure 5.1. The wind farm, as a single wind power producer, is making a N^h time period aggregated offer to the day-ahead market. The duration and the number of time slots in a day is represented by h and N^h, respectively; and $h \times N^h$ covers a 24-hour period in one day. If the duration is one hour, there should be twenty-four hourly offers. The wind farm is paid at the day-ahead market price if the offered amount is provided but may be subject to imbalance penalties if either a positive or a negative deviation from the accepted offer amount occurs.

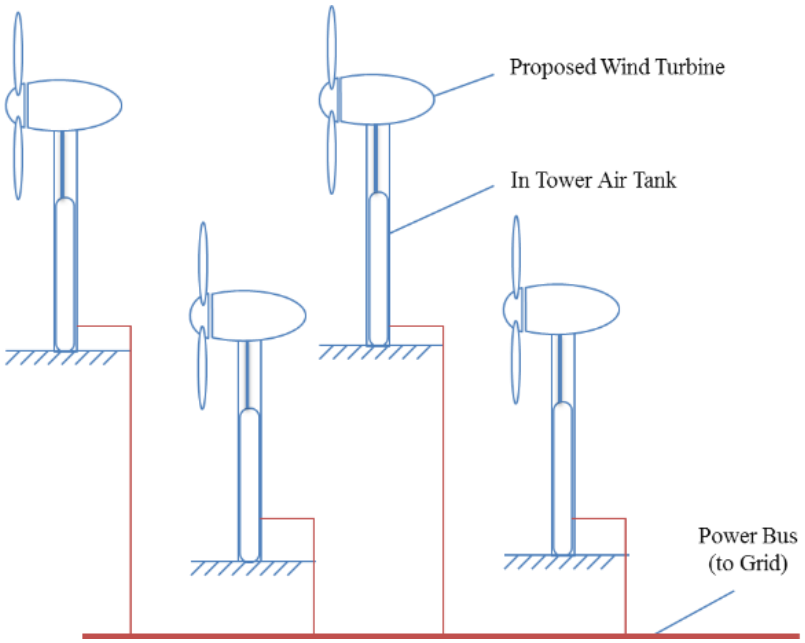

Figure 5.1: Wind farm layout and connections.

A two-stage stochastic programming framework is used to address this offering problem. Different from the operation of traditional wind turbines, i.e., underestimation or blade-pitching, the proposed wind farm could utilize the CAES system to mitigate real-time deviations. Thus, the wind power producer can submit the greater amount of offer to the market, and make steadier real-time generation binding to the offer. Similar to the model in Section 4.2, the problem is solved by the linear programming method. Maximization of the expected revenue is sought for participation in the day-ahead market.

5.2.1. Two-Stage Stochastic Programming Model

As mentioned in Section 4.2.1, two stage stochastic programming is a framework to solve the optimization problem under uncertainty. As to the optimal offering problem, the first-stage decision represents an offer that is submitted to the market, before knowing the exact wind speeds and electricity prices, while the second-stage decision represents the

real-time operation detail after the realization of wind speeds and electricity market prices. The objective is to maximize the profit of the wind farm.

Different from the case in Section 4.2.1, the conditions influencing the revenue of the wind farm include not only the wind speed but also the day-ahead market price and the real-time imbalance ratio. Their uncertainties are represented by a countable set of joint scenarios in this study. Each joint scenario is comprised of three vectors: wind speed, electricity price, and imbalance ratio. Since the time interval is chosen as one hour, each vector includes 24 spot values.

Two day-ahead electricity price scenarios, four real-time imbalance ratio scenarios, and six wind speed scenarios are considered; thus, the total number of joint scenarios is N^{φ}=2×4×6=48. The probability of each joint scenario is calculated by multiplying the probabilities of a specific day-ahead price scenario, a specific real-time imbalance ratio scenario, and a specific wind speed scenario, as it is shown in Figure 5.2.

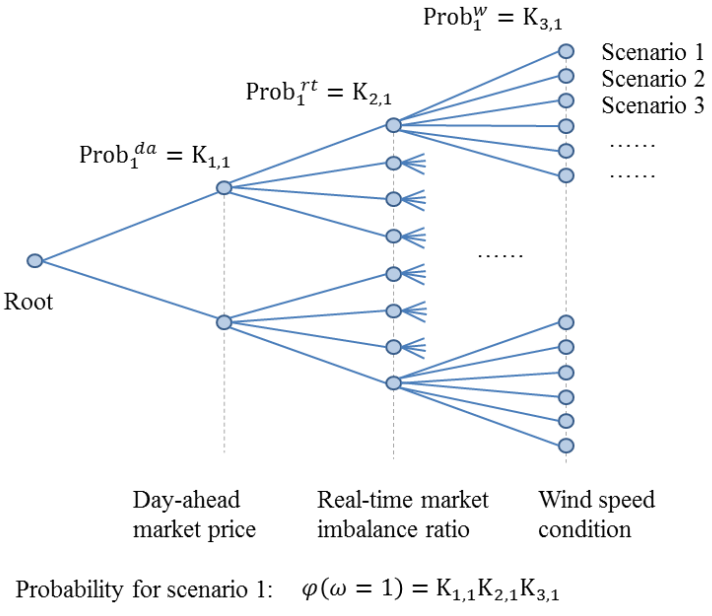

Figure 5.2: Composition of the scenarios.

5.2.2. Risk Measurement Model

Two ways to measure the risk in a stochastic process are value-at-risk (VaR) and CVaR. Value-at-risk is defined as the minimum profit that a decision maker could believe to be guaranteed within a confidence level, while CVaR is defined as the expected profit under worst-case scenarios beyond the confidence level. Conditional value-at-risk is selected for risk management of this problem because it does not require an additional binary variable and can be modeled by simple linear constraints, compared to VaR [75, 79]. Moreover, if CVaR and the scenario probabilities are obtained, VaR can also be calculated.

Mathematically, CVaR is computed as the expected value of the profit that is smaller than $(1-\alpha)$-quantile of the profit distribution, as shown in (5.1) and (5.2).

$$\text{CVaR} = Max\left(\xi - \frac{1}{1-\alpha}\sum_{\omega=1}^{N^{\varphi}} \varphi_{\omega} s_{\omega}\right) \tag{5.1}$$

$$s_{\omega} = \left\{ \begin{array}{c} 0\text{ , If } p_{\omega} \geq \xi \\ \xi - p_{\omega}\text{, If } p_{\omega} < \xi \end{array} \right\} \tag{5.2}$$

where variable ξ is an auxiliary variable whose optimal value is VaR and the confidence level is predefined as α; and variable s_{ω} is an auxiliary variable that has conditional value. The variable s_{ω} is equal to zero if the profit under scenario ω is larger than ξ, otherwise s_{ω} is equal to the difference between ξ and the corresponding profit [70, 80]. The profit function for a specific offer vector is p_{ω} under the scenario ω.

5.2.3. Decision Variables

The first-stage decision variables are the amounts of power offered to the day-ahead market during time period *t* as represented by P_t^r. The real-time generation during period *t* is the aggregated output of all wind turbines in the farm, as represented in (5.3), and the deviation between the amount of power offered and the power generated is defined by (5.4),

$$P_{t,\omega}^F = \sum_{k=1}^{N^K} P_{t,\omega}^{Go,k} \tag{5.3}$$

$$P_{t,\omega}^{dF} = P_{t,\omega}^F - P_t^r \tag{5.4}$$

where the power output of the k^{th} wind turbine in the wind farm at time *t* under scenario ω is represented by $P_{t,\omega}^{Go,k}$, and the wind farm generation and power deviation at time *t* under scenario ω are represented by $P_{t,\omega}^F$ and $P_{t,\omega}^{dF}$, respectively. The total number of wind turbines in the farm is represented by N^K.

This deviation is subject to symmetrical penalty, i.e., a function of the ratio of the real-time and day-ahead prices of electricity. This penalty, $C_{t,\omega}^{PT}$, is defined by a conditional equation shown in (5.5). If the deviation is positive, the imbalance penalty ratio is $r_{t,\omega}^+$ <1, while a negative deviation is subject to an imbalance penalty ratio of $r_{t,\omega}^- > 1$ [70]. The positive and negative penalty ratios are defined in (5.6) and (5.7), where the day-ahead and real-time market prices at time t under scenario ω are represented by $e_{t,\omega}^{da}$ and $e_{t,\omega}^{rt}$, respectively.

$$C_{t,\omega}^{PT} = \begin{cases} e_{t,\omega}^{da}\left(1 - r_{t,\omega}^{+}\right)\left|P_{t,\omega}^{dF}\right|h, \text{If } P_{t,\omega}^{dF} \geq 0 \\ \\ e_{t,\omega}^{da}\left(r_{t,\omega}^{-} - 1\right)\left|P_{t,\omega}^{dF}\right|h, \text{If } P_{t,\omega}^{dF} < 0 \end{cases} \quad (5.5)$$

$$r_{t,\omega}^{+} = \max\left\{\frac{e_{t,\omega}^{rt}}{e_{t,\omega}^{da}}, 1\right\} \quad (5.6)$$

$$r_{t,\omega}^{-} = \min\left\{\frac{e_{t,\omega}^{rt}}{e_{t,\omega}^{da}}, 1\right\} \quad (5.7)$$

Since conditional constraint and absolute values are included in (5.5)–(5.7), one way to linearize the equation is to separate the absolute value into two strictly positive variables: positive balance and negative balance [75]. Subsequently, power deviation and its absolute value can be represented by the linear function of two nonnegative variables: positive deviation $P_{t,\omega}^{dF^+}$ and negative deviation $P_{t,\omega}^{dF^-}$, as it is in (5.8) and (5.9). Those two nonnegative variables are subject to the additional zero-product constraint in (5.10).

$$P_{t,\omega}^{dF} = P_{t,\omega}^{dF^+} - P_{t,\omega}^{dF^-} \quad (5.8)$$

$$\left|P_{t,\omega}^{dF}\right| = P_{t,\omega}^{dF^+} + P_{t,\omega}^{dF^-} \quad (5.9)$$

$$P_{t,\omega}^{dF^+} \cdot P_{t,\omega}^{dF^-} = 0 \quad (5.10)$$

Thus, the spot revenue for time period *t* under scenario ω can be rewritten as it is in (5.11), representing the income from the day-ahead market and from positive deviation and the cost of negative deviation. It is noted that the second term on the right side of the equation is considered as a penalty because this amount of power could deserve a higher

income if offered to the day-ahead market because the imbalance ratio $r_{t,\omega}^{+}$ is always no larger than one.

$$e_{t,\omega}^{da} P_{t,\omega}^{F} h - C_{t,\omega}^{PT} = \left[e_{t,\omega}^{da} P_{t}^{r} + e_{t,\omega}^{da} r_{t,\omega}^{+} P_{t,\omega}^{dF^{+}} - e_{t,\omega}^{da} r_{t,\omega}^{-} P_{t,\omega}^{dF^{-}}\right] h \tag{5.11}$$

5.2.4. Objective Function

The expected revenue is a weighted average of daily revenue through all considered scenarios. The objective of the optimal offering problem is to maximize both the revenue of the wind farm and the CVaR, as expressed in (5.12),

$$\begin{aligned} Max\ Z_2 = (1-\beta) \sum_{\omega=1}^{N^{\varphi}} \varphi(\omega) \sum_{t=1}^{N^{h}} \Big[& e_{t,\omega}^{da} P_{t}^{r} + e_{t,\omega}^{da} r_{t,\omega}^{+} P_{t,\omega}^{dF^{+}} \\ & - e_{t,\omega}^{da} r_{t,\omega}^{-} P_{t,\omega}^{dF^{-}} \Big] h + \beta \cdot CVaR \end{aligned} \tag{5.12}$$

where $\beta \in [0, 1]$ is the risk aversion coefficient assigned to scale the portion between part a), the expected revenue under all scenarios, and part b), the expected revenue under several worst-conditions beyond a given confidence level, measured as CVaR. The probability of scenario ω is represented by φ_{ω}.

The risk measure related constraints in (5.1)–(5.2) are reformatted as linear inequalities, as shown in (5.13)–(5.14), where the profit function is replaced by the revenue from the day-ahead market, plus income from positive output deviation, minus the cost of negative output deviation. Finally, the objective function is expressed as (5.15).

$$\xi - \sum_{t=1}^{N^h} \left[e_{t,\omega}^{da} P_t^r + e_{t,\omega}^{da} r_{t,\omega}^{+} P_{t,\omega}^{dF^+} - e_{t,\omega}^{da} r_{t,\omega}^{-} P_{t,\omega}^{dF^-} \right] h \leq s_\omega \tag{5.13}$$

$$s_\omega \geq 0 \tag{5.14}$$

$$\begin{aligned} Max\ Z_2 = (1-\beta) \sum_{\omega=1}^{N^\varphi} \varphi(\omega) \sum_{t=1}^{N^h} \left[e_{t,\omega}^{da} P_t^r + e_{t,\omega}^{da} r_{t,\omega}^{+} P_{t,\omega}^{dF^+} \right. \\ \left. - e_{t,\omega}^{da} r_{t,\omega}^{-} P_{t,\omega}^{dF^-} \right] h + \beta \left(\xi - \frac{1}{1-\alpha} \sum_{\omega=1}^{N^\varphi} \varphi_\omega s_\omega \right) \end{aligned} \tag{5.15}$$

5.2.5. Constraint

- Power Density Treatment

It is assumed that the size and type of wind turbine have been selected using the sizing optimization, thus, the turbine's two key parameters, power density discount factor a_i and friction loss b_i, are known fixed values. All wind turbines in the farm have identical parameters, i.e., $a_i = a_0$ and $b_i = b_0$. Thus, the blade upper bound power for k^{th} wind turbine at time t under scenario ω can be written as (5.16)–(5.17),

$$P_{t,\omega}^{B,k,L} \leq \begin{Bmatrix} a_0 \theta_{t,\omega}^k - b_0, \text{If } a_0 \theta_{t,\omega}^k - b_0 \geq 0 \\ 0\ , \text{If } else \end{Bmatrix} \tag{5.16}$$

$$P_{t,\omega}^{B,k,L} \leq 3\ P_L^G \tag{5.17}$$

where the power density at the k^{th} wind turbine at time t under scenario ω is represented by $\theta_{t,\omega}^k$. The mechanical survival threshold is arbitrarily assumed as three times the generator rated power.

Because representative wind speed scenarios are generated prior to solving of the optimization model, the wind power density $\theta_{t,\omega}^{k}$ can be calculated from the value of the wind speed and assumed to be a known parameter. Thus, the blade upper bound power, $P_{t,\omega}^{B,L,k}$, can be numerically determined using the minimum value of the available power in the wind and the blade mechanical capacity, as shown in (5.18). Consequently, the blade power constraint can be expressed as in (5.19),

$$P_{t,\omega}^{B,L,k} = \begin{Bmatrix} min\left(a_0\theta_{t,\omega}^{k} - b_0, 5\ P_L^G\right), \text{If } a_0\theta_{t,\omega}^{k} - b_0 \geq 0 \\ 0\ , \text{If } else \end{Bmatrix} \tag{5.18}$$

$$P_{t,\omega}^{B,k} \leq P_{t,\omega}^{B,L,k} \tag{5.19}$$

where the blade power for the k^{th} wind turbine at time t under scenario ω is represented by $P_{t,\omega}^{B,k}$. Wind power density pertaining to the location where the k^{th} wind turbine has been installed is represented by $\theta_{t,\omega}^{k}$. Because wind turbines are in the same wind farm, under the same scenario ω, and at the same time t, the wind power densities in different locations are interdependent.

- Power and Energy Constraints

The wind turbines in wind farm retain the power and energy constraints as they are mentioned in Section 4.2.5. Constraints associated with capacity and efficiency limits of generator, blades and VDM are shown in (5.20)–(5.24). The upper and lower limits of tank storage is defined in (5.25) and (5.26), respectively. The storage energy updates and the power balance in the gearbox are shown in (5.27) and (5.28), respectively. The non-negativity constraint is given in (5.29).

The system parameters or variables pertaining to the size of the component are assumed as known values from the sizing problem. The capacities of generator power, VDM power, and storage energy are represented by P_L^G, P_L^V and E_L^T, respectively.

$$P_{t,\omega}^{Go,k} \leq P_L^G \tag{5.20}$$

$$P_{t,\omega}^{Go,k} = \eta^G P_{t,\omega}^{Gi,k} \tag{5.21}$$

$$\eta^{Vc} P_{t,\omega}^{Vc,k} \leq P_L^V \tag{5.22}$$

$$P_{t,\omega}^{Vp,k} \leq P_L^V \tag{5.23}$$

$$P_{t,\omega}^{B,k} \leq 3\, P_L^G \tag{5.24}$$

$$E_{t,\omega}^{T,k} \leq E_L^T \tag{5.25}$$

$$E_{t,\omega}^{T,k} \geq 10\% \cdot E_L^T \tag{5.26}$$

$$E_{t+1,\omega}^{T,k} = \eta^T E_{t,\omega}^{T,k} + \eta^{Vc} P_{t,\omega}^{Vc,k}\, h - P_{t,\omega}^{Vp,k}\, h/\eta^{Vp} \tag{5.27}$$

$$P_{t,\omega}^{B,k} + P_{t,\omega}^{Vp,k} = P_{t,\omega}^{Gi,k} + P_{t,\omega}^{Vc,k} \tag{5.28}$$

$$P_{t,\omega}^{B.k}, P_{t,\omega}^{Vp,k}, P_{t,\omega}^{Gi,k}, P_{t,\omega}^{Vc,k}, E_{t,\omega}^{T,k}, E_{t+1,\omega}^{T,k} \geq 0 \tag{5.29}$$

5.2.6. Formulation Summary

According to the previous formatting and treatment, the formulation of the optimal offering problem of proposed wind farm could be summarized as the linear programming problem as follows,

$$Max\ Z_2 = (1-\beta)\sum_{\omega=1}^{N^{\varphi}}\varphi(\omega)\sum_{t=1}^{N^{h}}\left[e_{t,\omega}^{da}P_t^r + e_{t,\omega}^{da}r_{t,\omega}^{+}P_{t,\omega}^{dF^+} - e_{t,\omega}^{da}r_{t,\omega}^{-}P_{t,\omega}^{dF^-}\right]h$$

$$+\beta\left(\xi - \frac{1}{1-\alpha}\sum_{\omega=1}^{N^{\varphi}}\varphi_{\omega}s_{\omega}\right) - \varepsilon\sum_{t=1}^{N^{h}}\sum_{t=1}^{N^{K}}\left(P_{t,\omega}^{Vp,k} + P_{t,\omega}^{Vc,k}\right)$$

Subject to:

- Wind farm generation

$$P_{t,\omega}^{F} = \sum_{k=1}^{N^{K}} P_{t,\omega}^{Go,k}$$

- Power deviation

$$P_{t,\omega}^{dF} = P_{t,\omega}^{F} - P_t^r$$

- Power deviation splits

$$P_{t,\omega}^{dF} = P_{t,\omega}^{dF^+} - P_{t,\omega}^{dF^-}$$

- Mechanical power balance on gearbox

$$P_{t,\omega}^{B,k} + P_{t,\omega}^{Vp,k} = P_{t,\omega}^{Gi,k} + P_{t,\omega}^{Vc,k}$$

- Storage update

$$E_{t+1,\omega}^{T,k} = \eta^{T}E_{t,\omega}^{T,k} + \eta^{Vc}P_{t,\omega}^{Vc,k}\,h - P_{t,\omega}^{Vp,k}\,h/\eta^{Vp}$$

- CVaR axillary constraint

$$\xi - \sum_{t=1}^{N^h} \left[e_{t,\omega}^{da} P_t^r + e_{t,\omega}^{da} r_{t,\omega}^{+} P_{t,\omega}^{dF^+} - e_{t,\omega}^{da} r_{t,\omega}^{-} P_{t,\omega}^{dF^-} \right] h \leq s_\omega$$

- Blade power upper limit

$$P_{t,\omega}^{B,k} \leq P_{t,\omega}^{B,L,k}$$

- Generator power capacity and efficiency

$$P_{t,\omega}^{Go,k} \leq P_L^G$$

$$P_{t,\omega}^{Go,k} = \eta^G P_{t,\omega}^{Gi,k}$$

- VDM compression and expansion power capacity

$$\eta^{Vc} P_{t,\omega}^{Vc,k} \leq P_L^V$$

$$P_{t,\omega}^{Vp,k} \leq P_L^V$$

- Upper and lower limits of storage

$$E_{t,\omega}^{T,k} \leq E_L^T$$

$$E_{t,\omega}^{T,k} \geq 10\% \cdot E_L^T$$

- Non-negativity constraint

$$P_{t,\omega}^{B.k}, P_{t,\omega}^{Vp,k}, P_{t,\omega}^{Gi,k}, P_{t,\omega}^{Vc,k}, , E_{t,\omega}^{T,k}, E_{t+1,\omega}^{T,k}, P_{t,\omega}^{dF^+}, P_{t,\omega}^{dF^-}, s_\omega \geq 0$$

5.3. Numerical Study

The wind farm consists of four wind turbine systems with compressed air tanks and is connected to the same power bus as depicted in Figure 5.1. The bus is assumed to be an infinite bus to the grid, meaning no congestion is considered. The configuration and system parameters are given in Table 5.1.

Table 5.1: System Parameters

Parameter	Value	Parameter	Value
Generator rated power	500kW	VDM rated power	450kW
Cut-in speed	3.5m/s	Compression efficiency	65.0%
Rated speed	7.0m/s	Expansion efficiency	65.0%
Blade diameter	107m	Storage rated capacity	2500kWh
Generator efficiency	99.0%	Tank storage efficiency	99.5%

A confidence level of $\alpha = 0.95$ is selected to ensure the robustness of the decision. A risk aversion coefficient of β=0.2 is used to weigh the expected profit against the risk intolerance. Since all constraints have been linearized, the problem is solved by the linear programing method.

Twenty-four hours of wind speed records from Stuart, Nebraska, from 1996 are retrieved from the historical data and serve as the reference for the day-ahead wind speed forecasting. It is assumed that the wind speed at time *t* is a random variable, and it follows a normal distribution with a mean corresponding to the reference to wind speed forecasting and a variation of the logarithmic function described by (5.30).

$$v_t \sim N\left(v_t^f, c_1 \cdot \log(t + t_0)\right) \tag{5.30}$$

where the real-time wind speed and the forecasted wind speed are represented by v_t and v_t^f, respectively; and the magnitude coefficient and time-lag constant are represented by c_1 and t_0, respectively. It is noted that the variance increases with the lead time, which indicates that the possible error between the forecasted wind and real wind speed is greater as the lead time increases.

Two hundred wind speeds are sampled from the normal distribution. A fast-forward selection algorithm [81] is used to reduce the number of scenarios. Six representative scenarios with respective probabilities are shown in Figure 5.3.

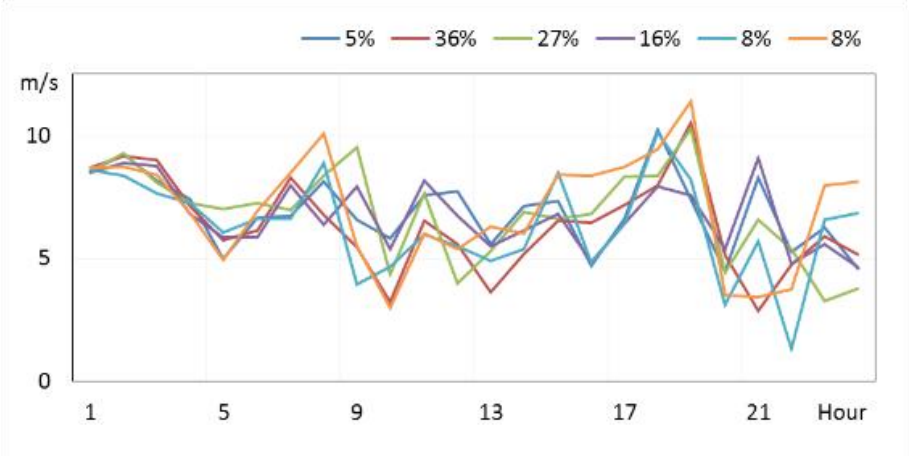

Figure 5.3: Wind speed scenarios.

Given the wind speed scenarios for the wind farm, the wind speed variation coefficients of [0.90, 0.95 1.05, and 1.10] are assigned to individual wind turbines to describe their location differences within the farm. The two real-time market price scenarios and four imbalance ratio scenarios are obtained from the records in the NE-ISO power pool.

5.3.1. Offer Curve

The first-stage decision gives the optimal offer under a risk aversion level of $\beta = 0.2$, as shown in Figure 5.4.

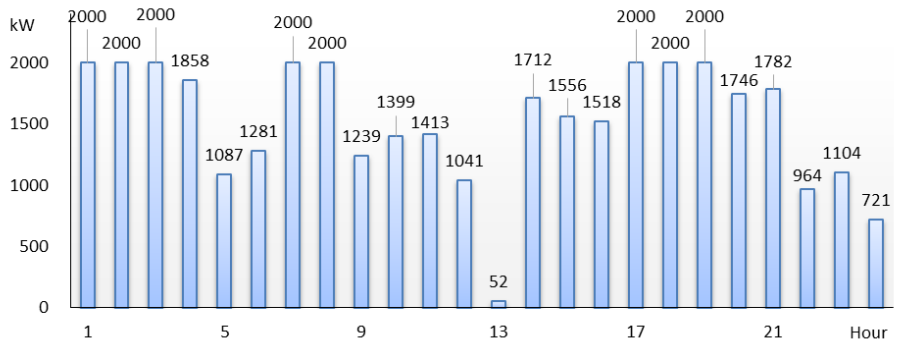

Figure 5.4: Offer curve to the market for risk aversion level $\beta = 0.2$.

It should be noted that the offer vector in Figure 5.4 maximizes the expected profit over all of the scenarios but is not necessarily the optimal for a specific scenario. The comparisons of the optimal offer and the real generation in two scenarios are depicted in Figure 5.5 a) and b). It is noted that both scenarios have identical market price and imbalance ratio condition, however, the wind speed condition is different.

5.3.2. Profit Analysis

The optimal offer results in \$1,762 of expected profit, the corresponding CVaR is \$1,557. This means the optimal offer gains, on average, \$1,762 in revenue from selling electricity to the grid; meanwhile, in the worst 5% of cases, a profit of \$1,557 is guaranteed. The optimal value of ξ gives the corresponding VaR of \$1,560, interpreting that the decision indicates 95% confidence that the profit is larger than \$1,560.

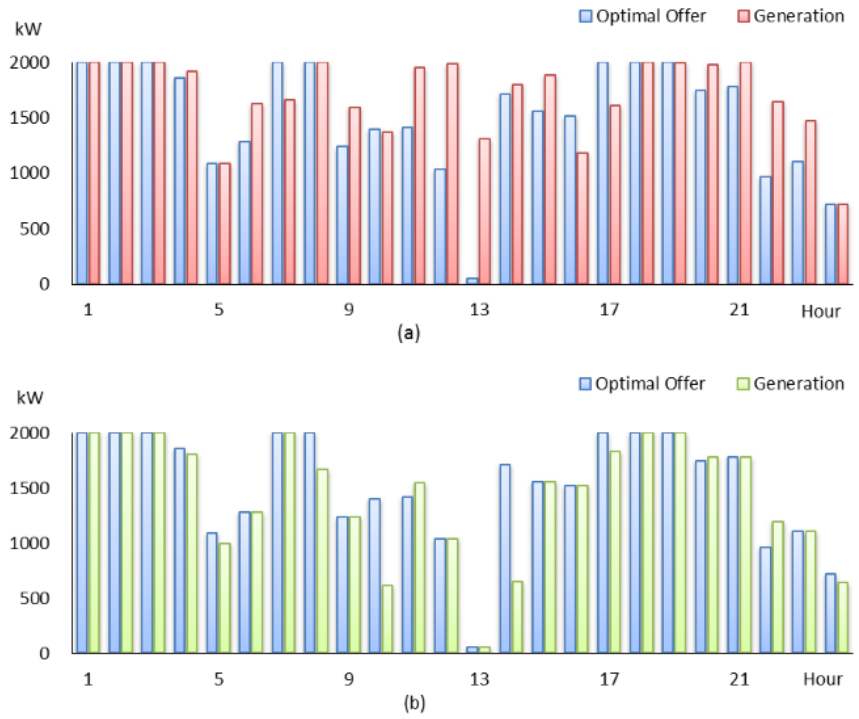

Figure 5.5: Optimal offer vs. real generation in a) Scenario 1 and b) Scenario 2.

After the optimal offer is determined, the system performance under each scenario is evaluated. Sorting the profits from large to small gives the profit spectrum for all 48 scenarios, as shown in Figure 5.6. The values of expected profit, VaR, and CVaR are marked in Figure 5.6 as the dashed line, dotted line, and the solid line, respectively. According to the profit distribution, the CDF of profit is plotted in Figure 5.7.

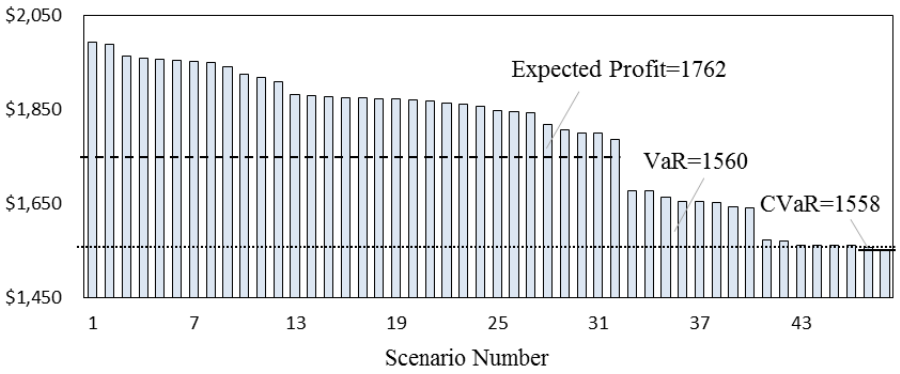

Figure 5.6: Profit distribution for risk aversion level $\beta = 0.2$.

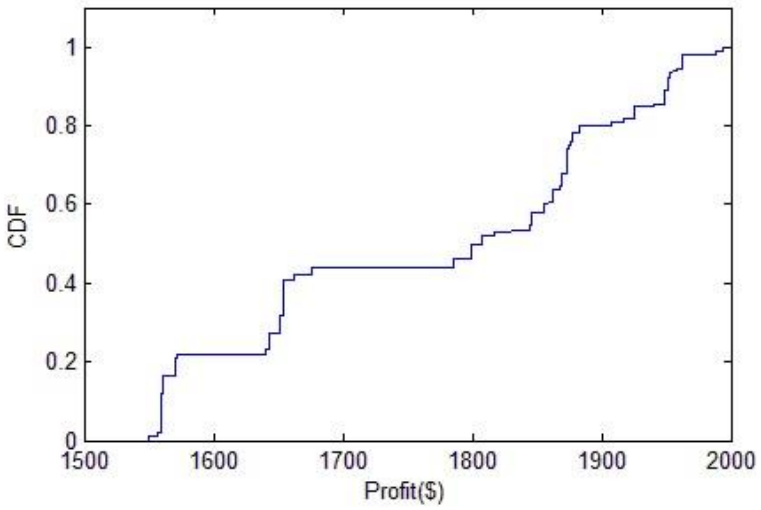

Figure 5.7: CDF of profit for risk aversion level $\beta = 0.2$.

5.3.3. Power Generation

Because of the wind speed variations associated with WT locations, the wind powers on different WTs are not identical. Individual power generations are given by the second-stage decisions of the optimization. Generation profiles under Scenario 1 are depicted in Figure 5.8. The corresponding power deviations of the wind farm are depicted in Figure 5.9.

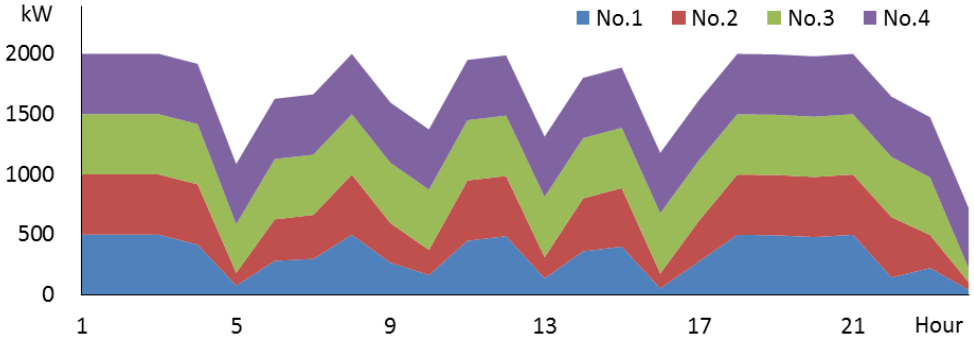

Figure 5.8: Individual wind turbine generations.

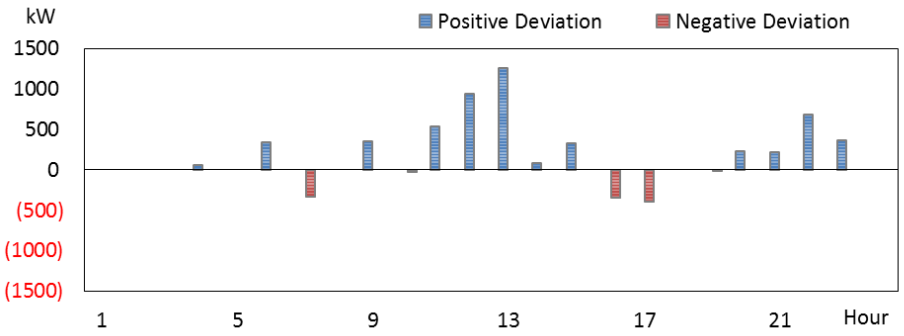

Figure 5.9: Wind farm power deviation.

5.3.4. Operation Profile

Besides the optimal offer curve, the two-stage stochastic programming also gives the hourly operation details resulting in the profit in each scenario. Choosing WT3 in Scenario 2, for example, the VDM operation and air tank state for each hour are shown in Figure 5.10 a) and b), respectively.

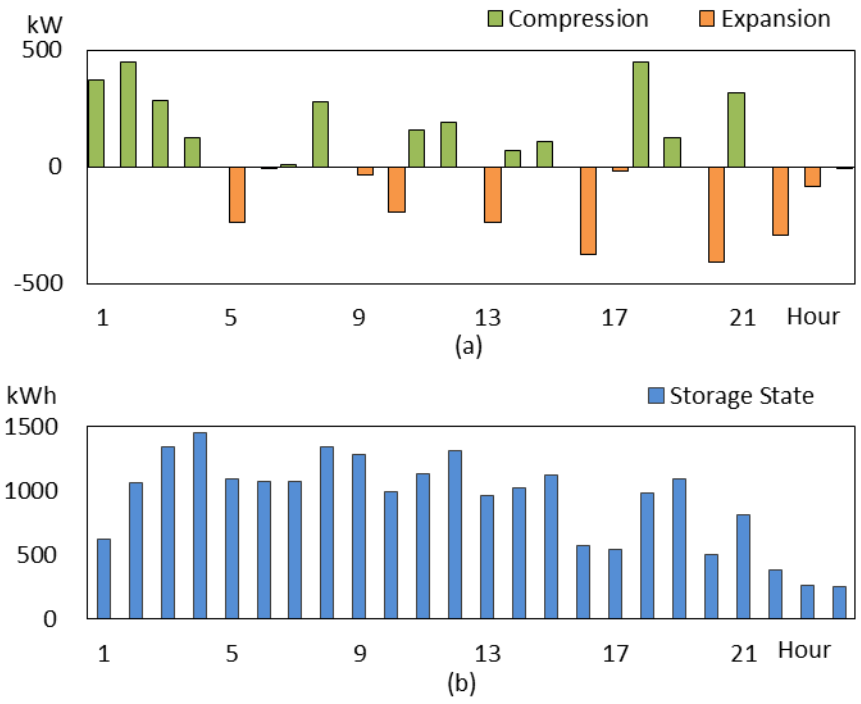

Figure 5.10: a) VDM operation and b) tank storage states.

The proposed system exhibits the designed function of converting the mechanical spillage to storage while the wind is at a surplus and generating electricity from the storage while the wind is a deficit.

5.3.5. Risk Aversion Attitude

In terms of risk aversion attitude, the decision maker has to make a trade-off between a better average profit and the risk of low profit in worst scenarios. The expected profits for different levels of risk considerations are shown in Table 5.2.

It is obvious that CVaR increases with β, while the expected profit decreases with β. This trend indicates that the wind farm sacrifices part of the average profit to ensure a better profit beyond the confidence level. Converting the table to the efficient frontier results in the plot in Figure 5.11. The expected profit decreases from \$1,763 to \$1,754; and the CVaR increases from \$1,554 to \$1,565, while the risk aversion coefficient changes from 0% to 100%.

Table 5.2: Objective Value under Various Risk Aversion Level

β	Expected Profit	CVaR	Objective Value
0%	\$ 1,763.08	\$ 1,553.68	\$ 1,720.82
20%	\$ 1,762.62	\$ 1,557.41	\$ 1,720.82
40%	\$ 1,761.03	\$ 1,561.60	\$ 1,680.50
60%	\$ 1,758.12	\$ 1,564.34	\$ 1,641.09
80%	\$ 1,757.33	\$ 1,564.77	\$ 1,602.52
100%	\$ 1,753.54	\$ 1,565.06	\$ 1,566.22

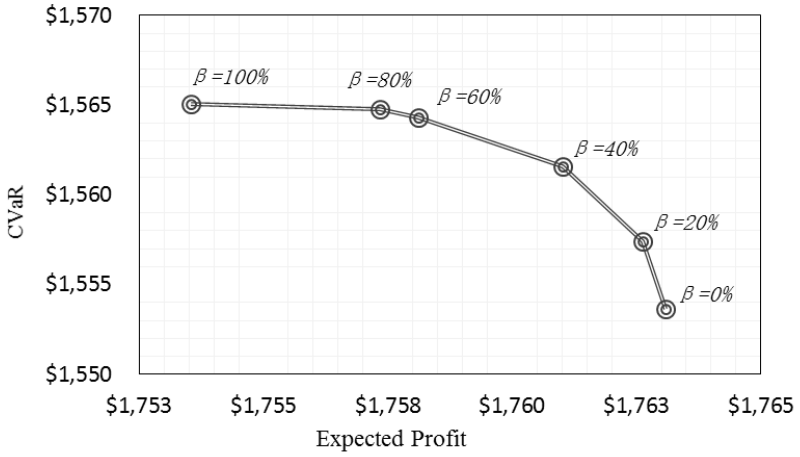

Figure 5.11: Efficient frontier for various risk aversion level.

5.3.6. Case Comparison

A wind farm with the proposed systems is evaluated thoroughly through the previous analysis. A wind farm, consisting of wind turbines with the same capacity under the identical environment/scenarios but without VDM and a storage system, is set up as a benchmark to evaluate the benefit of integrating the proposed compressed air system with the conventional wind turbines.

In the analysis, the total amount of offering to the day-ahead market for the benchmark farm is 29 MWh. Compared to 36 MWh for the CA-WECS farm, integration of the compressed air system brings a 25% increment in power generation. The offer comparisons are shown in Figure 5.12. The CDFs of expected profits for two cases are compared in Figure 5.13 under a risk aversion level of $\beta = 0.2$. It is noted that the proposed system first-order stochastically dominates the benchmark system without storage. From the comparison, the average increment of profit is around $300, measured by the average distance between two curves on the x axis.

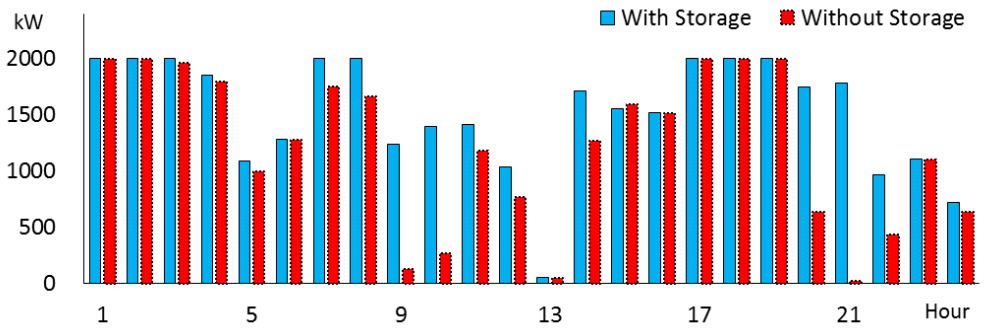

Figure 5.12: Offer comparison between proposed system and benchmark system.

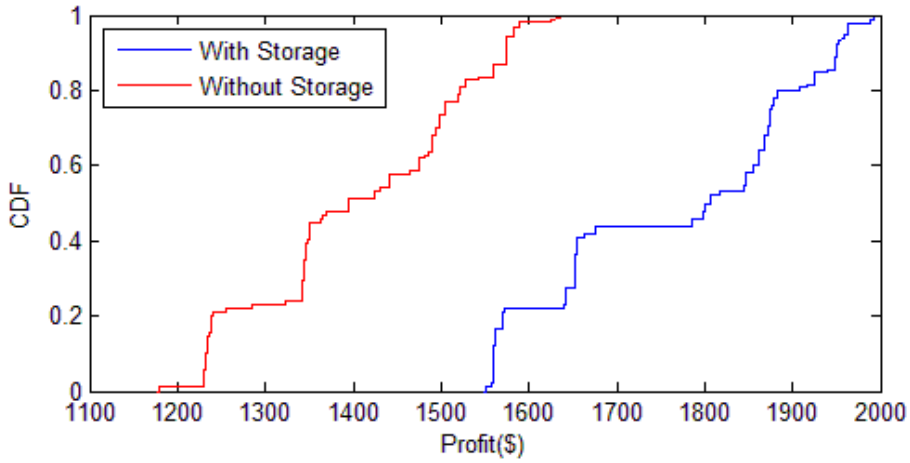

Figure 5.13: CDF comparison for the proposed CA-WECS farm and the benchmark farm under risk aversion level $\beta = 0.2$.

5.4. Chapter Summary

This chapter addressed the offering problem of a wind farm consisting of compressed-air-assisted wind energy conversion systems. The compressed-air-assisted wind energy conversion system integrates a compressed-air mechanism into a conventional wind turbine, providing a buffer between mechanical power from the wind and the electric power on the generator. The configuration can provide energy storage without impairing the overall generation.

A stochastic framework is set up to model the uncertainty of the environment. A linear program (LP) is employed to solve the problem, while several methods are used to linearize the constraints and objective function. The risk aversion attitude is introduced into the model and measured by CVaR, counting the average profit beyond the confidence level.

The optimal results give the hourly optimal offer, as well as the corresponding operational detail in each scenario. The power offering and profit distribution are compared with the benchmark, which is a wind farm consisting of conventional wind turbines without a storage system. The results showed the offering amount to the day-ahead market is increased by 25%, and the proposed system first-order stochastically dominates its counterpart by approximate $300 increments in the profit under all scenarios.

CHAPTER 6. APPLICATION TO MICROGRID EXPANSION

In a traditional power distribution system, as the community expands, the system designer plans to upgrade the capacity of the transmission line to the load center. However, integrating a distributed energy resource and distributed energy storage could be an alternative to decrease the microgrid's dependence on the transmission line upgrading.

In this chapter, the CA-WECS is considered to increase the local power generation. It can provide both distributed energy resource and distributed energy storage to the microgrid. A stochastic programming framework is proposed to assist the decision among upgrading the transmission line, integrating the CA-WECS or the combination of both.

6.1. Planning Microgrid application

Microgrid expansion decision generally involves the choices of expanding the connectivity to the grid and/or enhancing the local generation capabilities. For example, Figure 6.1 shows a small community that has local generation capability in the form of wind energy and is connected to the grid through a point of common coupling (PCC). Suppose options to improve the community power supply are twofold. One option is to enhance the wind energy availability by installing a CA-WECS, while the other one is to upgrade the transmission line to the microgrid. To address expansion planning problem under the various condition, a stochastic environment framework needs to be employed. To determine the optimal expansion plan, a mathematical program is formulated.

Generally, equipment cost involves a one-time initial investment and annual operational and maintenance (O&M) costs. The formulation is the same as in (4.1) in Section 4.2.2.

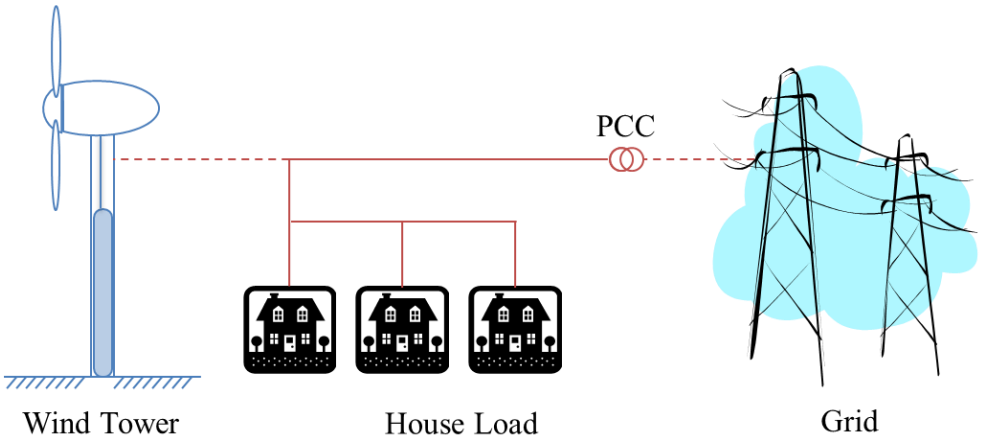

Figure 6.1: Microgrid expansion options.

6.1.1. Decision Variables

Each choice of CA-WECS or transmission line upgrade is represented by a binary decision variable. However, no more than one choice is allowed in each category. The constraints for the decision variable are expressed in (6.1)–(6.3).

$$\sum_{m=1}^{N^D} x_m^D \leq 1 \tag{6.1}$$

$$\sum_{n=1}^{N^U} x_n^U \leq 1 \tag{6.2}$$

$$x_m^D \in \{0,1\}, x_n^U \in \{0,1\} \tag{6.3}$$

where the selections of m^{th} option of CA-WECS and n^{th} option of transmission upgrade are represented by x_m^D and x_n^U, respectively.

6.1.2. Objective Function

The objective function minimizes the summation of hardware costs and payment to the grid for electricity over a planning horizon as shown in (6.4).

$$Min\ Z = \sum_{\omega=1}^{N^{\varphi}} \varphi_{\omega} \sum_{t=1}^{N^{h}} e_{t,\omega}^{rt} \cdot \left(P_{t,\omega}^{LD} - P_{t,\omega}^{Go}\right) \cdot h + \sum_{m=1}^{N^{D}} C_m^D \cdot x_m^D + \sum_{n=1}^{N^{U}} C_n^U \cdot x_n^U + C^{TU} \cdot y^T \tag{6.4}$$

where the probability of scenario ω is represented by φ_{ω}. The real-time market price at time *t* under scenario ω is represented by $e_{t,\omega}^{rt}$. The discounted cost of m^{th} option of CA-WECS and n^{th} option of transmission line upgrade are represented by C_m^D, C_n^U and C^{TU}, respectively. The number of air tank is represented by y^T (an integer). The power load of the community and the output power of wind generator at time *t* under scenario ω are represented by $P_{t,\omega}^{LD}$ and $P_{t,\omega}^{Go}$, respectively.

The first term represents the expected value of payment to the grid for electricity; this is the expected value of the product of the electricity rate, output power, and hours in each time step for N^h steps in the planning horizon. The second and third terms represent the discounted cost of the CA-WECS and transmission upgrade plan during the planning horizon, respectively. The fourth term is the discounted cost of storage tank(s). It is remarked that, as a price taker, a single wind turbine does not have the power to influence the market price. Therefore, no bidding and penalty are considered in this problem.

6.1.3. Constraints

Power and energy constraints include the blade power envelope constraints in (4.8)–(4.11), mechanical power balance on gearbox constraints in (4.14)–(4.15), storage energy update constraint in (4.17) and the capacity limits (4.19)–(4.27). Those constraints are thoroughly discussed in Section 4.2.5.

Additionally, the PCC flow is constrained by the selected upgrade plan, as it is defined in (6.5),

$$\left|P_{t,\omega}^{Go} - P_{t,\omega}^{LD}\right| \leq \sum_{n=1}^{N^U} P_n^U \, x_n^U \tag{6.5}$$

where the capacity limit of n^{th} option of transmission upgrade is represented by P_n^U.

The capital investment should be less than the budgeted capital threshold as discussed in (4.18). The mechanical survival power of the blade structure is assumed as five times that of the generator rated power. All the variables are subject to non-negative number constraints.

6.2. Numerical Case Study

A numerical example is used to select the components of the proposed system and evaluate its performance. It is assumed there are five options for the CA-WECS, five options for the transmission line, and only one option for the tank unit. The available options are shown in Table 6.1, Table 6.2 and Table 6.3, respectively, where the capacity of m^{th} option of generator and VDM are represented by P_m^G and P_m^V, respectively; and the corresponding cut-in speed and rated speed associated with rate electric power are

represented by v_{in} and v_{r1}. The rated storage capacity of the available air tank unit is represented by E_L^{TU}.

Table 6.1: CA-WECS Options

No.	P_i^G (kW)	v_0 (m/s)	v_{r1} (m/s)	P_i^V (kW)	CI_i^D	CM_i^D	C_i^D
1	200	2.7	7.0	180	$ 490,000	$2,675	$ 683
2	250	3.0	11.0	225	$ 556,250	$3,047	$ 775
3	400	3.0	7.0	360	$ 880,000	$4,800	$1,226
4	500	3.5	10.0	450	$ 925,000	$5,063	$1,289
5	600	2.7	11.0	540	$1,290,000	$6,900	$1,795

Table 6.2: Transmission Options

No.	P_i^U (kW)	CI_i^U	CM_i^U	C_i^U
1	300	$ –	$ 300	$ 6
2	500	$ 125,000	$ 625	$ 173
3	750	$ 225,000	$1,125	$ 312
4	1000	$ 350,000	$1,750	$ 485
5	1250	$ 500,000	$2,500	$ 692

Table 6.3: Air Tank Information

No.	E_L^{TU} (kWh)	CI^{TU}	CM^{TU}	C^{TU}
1	100	$ 2,000	$ 10	$ 3

The planning horizon N^h is set at 168 hours, and the limit of the available capital is $1.5M. In each season, a 7-day, hourly wind speed vector for the rural community of Stuart, Nebraska is selected from the first week of the second month. Each vector consists of 168 wind speed values (7 days × 24 hourly spot wind speeds). The wind speed vectors and electricity rate vectors corresponding to the time of the wind speed vectors are extracted from the PJM Energy Market, as they were shown in Figure 4.1 and Figure 4.2, respectively. The corresponding load vectors are extracted from the PJM Energy Market as it is shown in Figure 6.2.

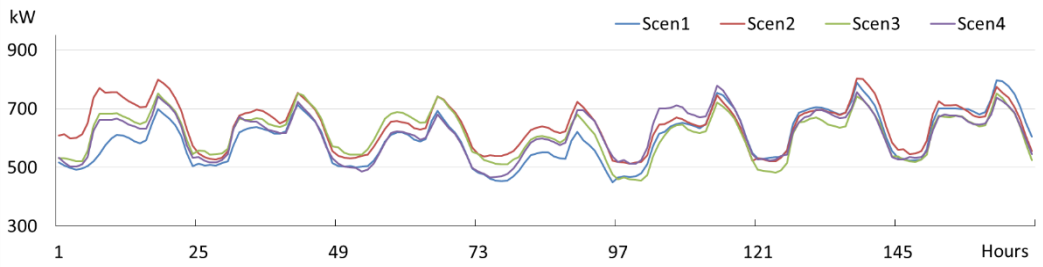

Figure 6.2: Load patterns for different scenarios.

Equal probability is assigned to each scenario. Two planning cases are considered. In Case 1, both CA-WECS and transmission upgrade, or a combination of the two is allowed; while in Case 2, only transmission upgrade is permissible. Infinite bus is assumed in this study, thus, no congestion/curtailment will be considered. The local load consumes the local wind power generation first, if there is a deficit, extra power will be supplied from the grid.

6.2.1. Optimal Results

The optimal decisions for both cases, obtained by solving the mixed integer linear program, are presented in Table 6.4. The optimal solution for Case 1 includes a 400kW wind turbine with the cut-in speed of 3.0 m/s and electrical rated speed of 7.0 m/s; a 360kW VDM; and 5500kWh storage consisting of fifty-five units of the 100kWh air tank. The transmission line capacity is 750kW. The optimal result for Case 2 shows the capacity requirement for the transmission line is 1000kW.

Table 6.4: Optimal Result for the Two Planning Cases

No.	P_L^G (kW)	P_L^V (kW)	E_L^T (kWh)	P_L^U (kW)	*Cost*
Case 1	400	360	7000	750	$3,624
Case 2	n/a	n/a	n/a	1000	$4,533

6.2.2. Operations

The power generation detail for the proposed system under scenario 1 is depicted by the solid red curve in Figure 6.3. The red dash line represents the generation pattern for a wind turbine without a storage system.

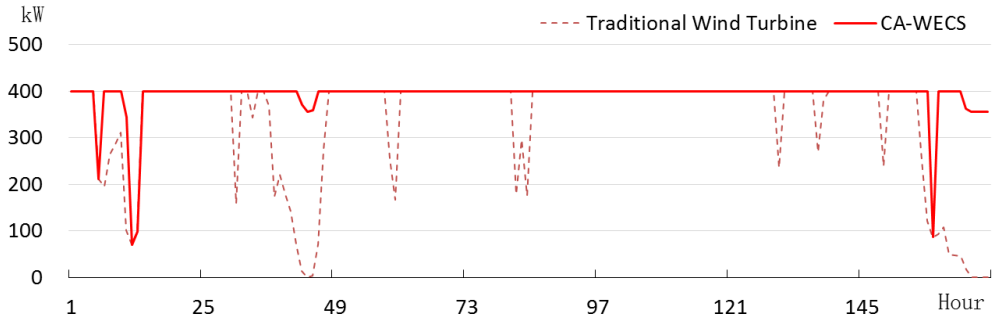

Figure 6.3: Power generation under Scenario 1.

The comparison between the solid and dashed lines shows that the proposed system eliminates the majority of power dips while wind speed is low, and increases the capacity factor of the generator. The operational details of VDM are also given by the optimization method.

6.2.3. Performance Comparison

The amounts of power purchased (power flows through PCC for Case 1 and Case 2 under four typical scenarios are given by Figure 6.4. It can be seen that the average power flow through PCC is reduced by 65%, 41%, 47% and 58%. Converting the power generation to the income gives the comparison in Figure 6.5.

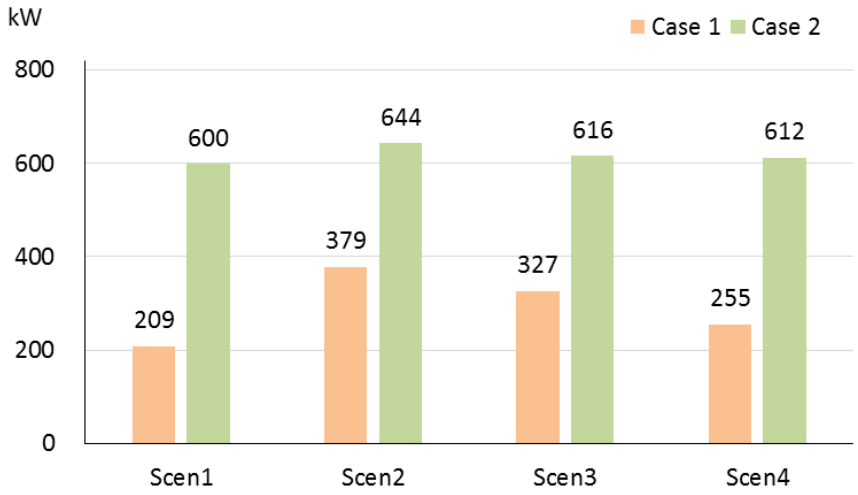

Figure 6.4: Comparison of PCC average flows under different scenarios.

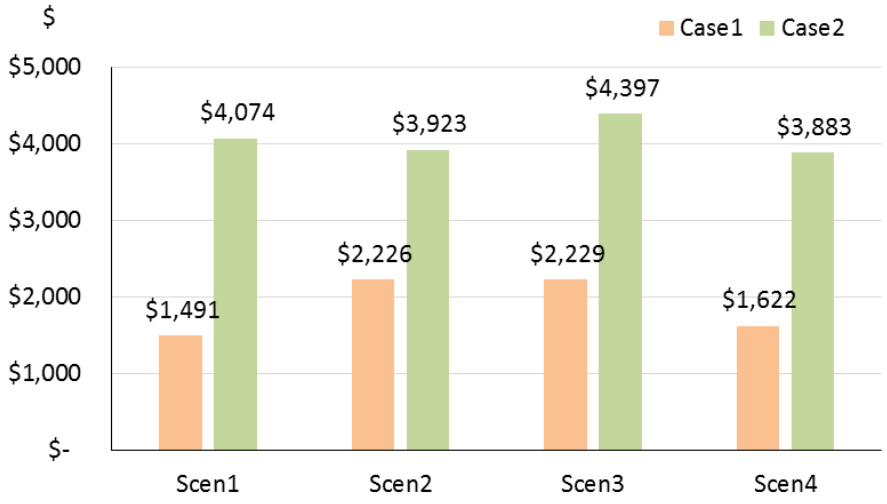

Figure 6.5: Comparison average income under different scenarios.

The breakdown of the cost reveals that, for Case 1, the expected energy cost of $3,579 consists of $1,630 hardware cost and $1,949 payment to the grid; while for Case 2, the expected energy cost of $4,533 consists of $464 hardware cost and $4,069 payment to the grid, as shown in Figure 6.6. This accounts for 21% reduction on annual energy cost.

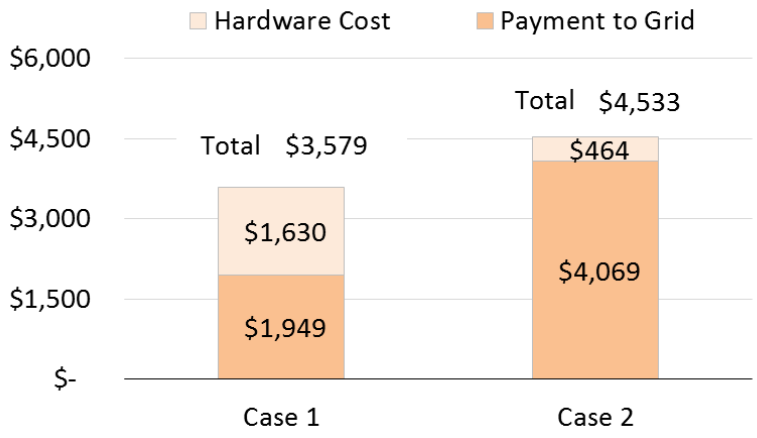

Figure 6.6: Energy cost decomposition comparison.

6.3. Chapter Summary

In this chapter, an application of CA-WECS in the microgrid expansion planning was studied. A mathematical program is used to develop the optimal system. The optimal power capacity, and storage capacity of CA-WECS, and the capacity of the transmission line to the microgrid are determined by solving the mixed integer linear program. A numerical example is investigated to evaluate the performance of the new system. The comparison result shows that integration of a CA-WECS can largely decrease the demand on the transmission line. Thus the capacity of the transmission line is decreased from 1000kW to 750kW for the identical load pattern. The average power flow through the point of common coupling is reduced by around 50%. The energy cost of the community is reduced by 21%.

CHAPTER 7. CONCLUSIONS AND FUTURE WORKS

The term “dispatchable generation” refers to a generation unit that can adjust its output according to a reference command. A traditional wind turbine is considered to be a nondispatchable power source because of the random availability of wind. Thus, relying on wind energy could result in power control and quality challenges, such as overvoltage, undervoltage, and frequency excursion. Furthermore, a wind turbine may not be able to ride through an external fault because of insufficient spin reserve or black start capacity.

Turbine blades are designed to capture wind energy proportional to the cube of the wind speed. However, this energy can be trimmed by the generator capacity. If this limit were removed, the wind energy could be extrapolated to a higher level. The amount of energy which could be captured by the blade but trimmed away by the pitching control is defined as the mechanical spillage. On the other hand, when wind speed is below the rated wind speed, the generator is unable to operate at its full capacity. The idle capacity in this area is defined as the capacity vacancy.

This dissertation proposes a novel configuration of a compressed-air-assisted wind energy conversion system, integrating an adaptive structure into a traditional wind turbine. The key component of the system involves a variable displacement machine, which can convert surplus wind energy into compressed air when the wind speed is high and supplement power generation using the energy stored as compressed air when the wind speed is low. When the wind speed is below the cut-in speed or above the cut-out speed, the clutch is disengaged and blades are locked; and the VDM and the generator form an independent system to generate electricity.

Compared to traditional compressed air storage, the compressor and gas turbine are merged into one variable displacement machine. The new design eliminates the gas turbine generator by utilizing the idle capacity of the wind turbine generator.

The configuration of the VDM establishes a direct mechanical linkage between the wind power and the compressed air power. From an energy point of view, the storage system serves as a buffer between the mechanical power supply of the wind and the electric power demand of the load, providing another degree of freedom for energy management. The new configuration decouples the mechanical power of the blade and electric power of the generator, letting the new system "perform like" a dispatchable unit.

The contributions of this work include:

- A compact system designed to integrate a compressed air storage system into a wind energy conversion system.
- A novel VDM design for compression and expansion under variable torque, power, and tank pressure conditions.
- A scheme for dispatchable generation of a wind energy conversion unit.
- A flexible transmission system to couple/accommodate power to the desired shaft(s) smoothly.
- A model for optimal sizing of the system with economic consideration.
- A model for an optimal offering strategy with risk management.
- A model for an optimal decision on transmission line upgrade options in a microgrid environment.

Besides the dispatchable generation, the compressed air storage also serves as operating reserve to provide a broad range of regulation capacities in a microgrid environment. The expected benefits include:

- Mitigating uncertainty and improving predictability of power generation.
- Enhancing the dispatchability of a wind turbine.
- Improving the robustness of a wind turbine system to external disturbances.
- Increasing wind power harvesting.
- Providing spinning reserve and black start capability.
- Increasing low voltage ride through capacity.
- Increasing the renewable energy penetration percentage.
- Reducing the investment in a transmission upgrade.

This technology has broad application, for example:

- On-shore wind power with in-tower or underground storage tanks.
- Off-shore wind power with underwater storage tanks.
- A microgrid, either in an island mode or with a grid connection, in a remote area.
- A wind farm sharing underground storage.

The abundant wind resource and vast open plain in Nebraska also facilitate the application of the proposed system. This technology could be extended to farms, ranches, and communities in the Great Plains area.

Recommendations for future research are as follows:

- A system model under steady state was discussed in this dissertation. To better understand the dynamic performance of the proposed system, future work could be extended to the control model for transient state analysis. A PID controller for the VDM will be needed to tune the transient response of the system.
- Since the proposed system integrates energy storage for renewable energy, it has additional resources to regulate the voltage and frequency. Future research can extend to the issues/ability of power quality management of the proposed system.
- Since the proposed system can provide spinning reserve, nonspinning reserve, and black start capability to the grid/microgrid. The proposed system can participate in the ancillary market for additional income/revenue. Research on the performance in the ancillary market will be desirable.
- Because of the storage system, the additional energy resource from the storage can increase the wind turbines low-voltage-ride-through (LVRT) ability during a crucial/critical external event. Investigation of this issue will be expected in future work.
- An offering problem for the wind farm consisting of a group of the proposed systems is studied in Chapter 5. However, sharing the storage tank among turbines within the farm has potential to increase the reliability of power generation following the offer. Future research on shared storage is desirable.

- The proposed system provides dispatchable renewable resources to the power system. The optimization issue in grid scheduling and load dispatching will be of great interest to the system operator.
- The proposed system can be considered as an option when planning a microgrid, especially in the island mode. The optimization operation will be of great interest to the system planner.
- The cost effectiveness analysis could also be a critical issue because it can determine the economic performance of the project. A detailed analysis toward the levelized cost of electricity (LCOE) is recommended.

BIBLIOGRAPHY

[1] The European Parliament and the Council of the European Union, “EU 2020 renewable energy targets,” *Off. J. Eur. Union*, vol. L 140/16, pp. 16–62, 2009.

[2] “Compressed air energy storage power plants,” *BINE Information Service*, 20 07. [Online]. Available: http://www.bine.info/fileadmin/content/Publikationen/Englische_Infos/projekt_0507_engl_internetx.pdf.

[3] “Wind vision: a new era for wind power in the United States,” Rep. DOE/GO-102015-4640, Department of Energy, 2014.

[4] S. Succar and R. Williams, “Compressed air energy storage : theory , resources , and applications for wind power,” Princeton Environmental Institute, Princeton University, 2008.

[5] L. Dye, “Wind is fastest growing energy resource.” [Online]. Available: http://abcnews.go.com/Technology/story?id=99611.

[6] J. Weiner, “Study finds that the price of wind energy in the United States is at an all-time low, averaging under 2.5¢/kwh,” 2015.

[7] Electricity Advisory Committee, “Bottling electricity: storage as a strategic tool for managing variability and capacity concerns in the modern grid,” The Electricity Advisory Committee, 2008.

[8] R. G. Pratt, “Transforming the U.S. electricity system,” *IEEE PES Power Syst. Conf. Expo. 2004.*, pp. 1–6, 2004.

[9] H. Ibrahim, A. Ilinca, and J. Perron, "Energy storage systems-Characteristics and comparisons," *Renew. Sustain. Energy Rev.*, vol. 12, no. 5, pp. 1221–1250, 2008.

[10] D. Rastler, "Electricity energy storage technology options: a white paper primer on applications, costs and benefits," Rep. 1020676, Electric Power Research Institute, 2010.

[11] J. Paska, P. Biczel, and M. Klos, "Technical and economic aspects of electricity storage systems co-operating with renewable energy sources," *2009 10th Int. Conf. Electr. Power Qual. Util.*, pp. 1–6, 2009.

[12] D. O. Akinyele and R. K. Rayudu, "Review of energy storage technologies for sustainable power networks," *Sustain. Energy Technol. Assessments*, vol. 8, pp. 74–91, 2014.

[13] A. Joseph and M. Shahidehpour, "Battery storage systems in electric power systems," *Power Eng. Soc. Gen. Meet.*, pp. 1–8, 2006.

[14] J. L. Neumiller, "Reservoir simulation of combined wind energy and compressed air energy storage in different geologic settings," Ph.D. dissertation, Colorado School of Mines.

[15] Y. V. Makarov, B. Yang, J. G. DeSteese, S. Lu, C. H. Miller, P. Nyeng, J. Ma, D. J. Hammerstrom, and V. V. Viswanathan, "Wide-area energy storage and management system to balance intermittent resources in the Bonneville power administration and California ISO control areas," *Bonnev. Power Adm.*, p. 127, 2008.

[16] S. J. Hayes, “Technical analysis of pumped storage and integration with wind power in the Pacific Northwest final report,” Rep. MWH-HDC-T12, MWH Americas, Inc., 2009.

[17] “Licensed pumped storage projects.” Federal Energy Regulatory Commission, 2015.

[18] S. Eckroad, “EPRI-DOE Handbook of energy storage for transmission & distribution applications,” Rep. 1001834, Electric Power Research Institute, 2003.

[19] G. Manfrida and R. Secchi, “Performance prediction of a small-size adiabatic compressed air energy storage system,” *27th Int. Conf. Effic. Cost, Optim. Simul. Environ. Impact Energy Syst. Jun 15-19, Turku, Finl.*, pp. 1–14, 2014.

[20] S. D. Lim, A. P. Mazzoleni, J. Park, P. I. Ro, and B. Quinlan, “Conceptual design of ocean compressed air energy storage system,” *Oceans*, pp. 1–8, 2012.

[21] G. Grazzini and A. Milazzo, “A Thermodynamic Analysis of Multistage Adiabatic CAES,” *Proc. IEEE*, vol. 100, no. 2, pp. 461–472, 2012.

[22] H. Chen, T. N. Cong, W. Yang, C. Tan, Y. Li, and Y. Ding, “Progress in electrical energy storage system: A critical review,” *Prog. Nat. Sci.*, vol. 19, no. 3, pp. 291–312, 2009.

[23] K. Zach, H. Auer, and G. Lettner, “Facilitating energy storage to allow high penetration of intermittent renewable energy,” Intelligent Energy Europe, 2012.

[24] R. D. Moutoux, “Wind integrated compressed air energy storage in Colorado,” Master thesis, Dept.t of Elect.l Eng., University of Colorado, Boulder, CO, 2007.

[25] J. Taylor and A. Halnes, “Analysis of compressed air energy storage,” *PCIC Eur. Conf. Rec.*, pp. 1–5, 2010.

[26] H. Hoffeins, “Huntorf air storage gas turbine power plant,” *Energy Supply - Brown Boveri Mittelungen*, no. D GK 90 202 E. 1994.

[27] M. Khatibi and M. Jazaeri, “An analysis for increasing the penetration of renewable energies by optimal sizing of pumped-storage power plants,” *2008 IEEE Electr. Power Energy Conf.*, 2008.

[28] H. Daneshi, A. K. Srivastava, and A. Daneshi, “Generation Scheduling with Integration of Wind Power and Compressed Air Energy Storage,” *IEEE PES Transm. Distrib. Conf. Expo.*, pp. 1–6, 2010.

[29] A. Daneshi, N. Sadrmomtazi, H. Daneshi, and M. Khederzadeh, “Wind power integrated with compressed air energy storage,” *2010 IEEE Int. Conf. Power Energy (PECon2010), Nov, 2010, Kuala Lumpur, Malaysia*, pp. 634–639, 2010.

[30] “The economic impact of CAES on wind in TX, OK, and NM,” Ridge Energy Storage & Grid Services L.P., 2005.

[31] G. Shi, “Cost optimal selection of storage tanks in LPG vaporization station,” *Nat. Resour.*, vol. 03, no. 03, pp. 164–169, 2012.

[32] H. P. Loh, J. Lyons, and C. W. White III, “Process equipment cost estimation final report,” Rep. DOE/NETL-2002/1169, National Energy Technology Laboratory, 2002.

[33] D. Heimiller, S. Haymes, M. Schwartz, and W. Musial, “Offshore wind resource potential of the United States,” *Ocean. 2007*, pp. 1–8, 2007.

[34] S. D. Lim, “Ocean compressed air energy storage (OCAES) integrated with offshore renewable energy sources,” Master Thesis, North Carolina State University, 2013.

[35] S. Zhang, “The plan to store wind energy in giant underwater air bubbles,” 2015. .

[36] P. Dvorak, “Underwater compressed-air storage making good progress,” 2014. .

[37] P. Y. Li, E. Loth, T. W. Simon, J. D. Van de Ven, and S. E. Crane, “Compressed air energy storage for offshore wind turbines,” in *Proc. International Fluid Power Exhibition (IFPE), Las Vegas, U.S.*, 2011.

[38] M. Saadat, F. A. Shirazi, and P. Y. Li, “Revenue maximization of electricity generation for a wind turbine integrated with a compressed air energy storage system,” in *American Control Conference (ACC), Portland, Oregon, U.S.*, 2014.

[39] “Offshore wind energy with compressed air energy storage-A DNV innovation project,” Det Norske Veritas.

[40] H. Sun, J. Wang, S. Guo, and X. Luo, “Study on Energy Storage Hybrid Wind Power Generation Systems,” in *World Congress on Engineering (WCE), London, U.K.*, 2010, vol. II, pp. 833–838.

[41] M. Martínez, M. G. Molina, and P. E. Mercado, “Dynamic performance of compressed air energy storage (CAES) plant for applications in power systems,” *2010 IEEE/PES Transm. Distrib. Conf. Expo. Lat. Am.*, no. August, pp. 496–503, 2010.

[42] V. Vongmanee, “The renewable energy applications for uninterruptible power supply based on compressed air energy storage system,” in *2009 IEEE Symposium*

on Industrial Electronics & Applications (ISIEA 2009), Kuala Lumpur, Malaysia, 2009, vol. 2, pp. 827–830.

[43] J. F. Manwell, J. G. McGowan, and A. L. Rogers, *Wind Energy Explained: Theory, Design and Application, 2nd Edition*. 2010.

[44] M. Cirrincione, M. Pucci, and G. Vitale, "Neural MPPT of variable-pitch wind generators with induction machines in a wide wind speed range," *IEEE Trans. Ind. Appl.*, vol. 49, no. 2, pp. 942–953, 2013.

[45] N. W. Miller, J. J. Sanchez-Gasca, W. W. Price, and R. W. Delmerico, "Dynamic modeling of GE 1.5 and 3.6 MW wind turbine-generators for stability simulations," *2003 IEEE PES Gen. Meet. (IEEE Cat. No.03CH37491)*, vol. 3, no. July, pp. 1977–1983, 2003.

[46] B. Limit, "Understanding coefficient of power (Cp) and Betz Limit," *Kidwind Science Snack*, pp. 3–5.

[47] O. Alizadeh and A. Yazdani, "A strategy for real power control in a direct-drive PMSG-based wind energy conversion system," *IEEE Trans. Power Deliv.*, vol. 28, no. 3, pp. 1297–1305, 2013.

[48] Yu Zou, M. E. Elbuluk, and Y. Sozer, "Stability Analysis of Maximum Power Point Tracking (MPPT) Method in Wind Power Systems," *IEEE Trans. Ind. Appl.*, vol. 49, no. 3, pp. 1129–1136, 2013.

[49] J. Cheng and F. Choobineh, "The joint design of a compressed air and wind energy system for mechanical spillage recovery," in *The 8th Annual IEEE Energy Conversion Congress & Exposition (ECCE 2016)*, to be published.

[50] J. Cheng and F. Choobineh, “Wind energy to compressed air conversion system to extend wind turbine power generation capabilities,” U.S. Provisional Patent Application Number 62 272 405, 2015.

[51] J. Gordon, “Cooling system : variable displacement A/C compressor,” *Teardown*, no. April, 2005.

[52] “Variable displacement piston pumps,” *mekanizmalar.com*. [Online]. Available: http://www.mekanizmalar.com/variable_displacement_piston_pump.html.

[53] M. Fischetti, “No more gears,” *Scientific American*, 2006. [Online]. Available: http://www.scientificamerican.com/article/no-more-gears/.

[54] D. Pratte, “Continuously variable transmissions-rubber band gearboxes be gone,” 2014. [Online]. Available: http://www.superstreetonline.com/.

[55] “XTRONIC CVT technology overview,” NISSAN.

[56] T. Das, V. Krishnan, Y. Gu, and J. D. McCalley, “Compressed air energy storage: State space modeling and performance analysis,” in *2011 IEEE Power and Energy Society General Meeting*, 2011, pp. 1–8.

[57] A. Setiawan, A. Priyadi, M. Pujiantara, and M. H. Purnomo, “Sizing compressed-air energy storage tanks for solar home systems,” in *2015 IEEE International Conference on Computational Intelligence and Virtual Environments for Measurement Systems and Applications (CIVEMSA), Shenzhen, China*, 2015, pp. 1–4.

[58] U.S. National Renewable Energy Laboratory, “Obtaining the eastern wind da taset,” *NREL: Transmission grid integration*, 2016. [Online]. Available: http://www.nrel.gov/electricity/transmission/eastern_wind_methodology.html.

[59] ISO New England Inc., “Independent system operator New England: Real-ti me maps and charts,” 2016. [Online]. Available: http://www.iso-ne.com/isoexpress/web/charts.

[60] H. T. Le and T. Q. Nguyen, “Sizing energy storage systems for wind power firming : an analytical approach and a cost-benefit analysis,” in *IEEE PES General Meeting on Conversion and Delivery of Electrical Energy in the 21st Century*, 2008, pp. 1–8.

[61] L. Xu, X. Ruan, C. Mao, B. Zhang, and Y. Luo, “An improved optimal sizing method for wind-solar-battery hybrid power system,” *IEEE Trans. Sustain. Energy*, vol. 4, no. 3, pp. 774–785, 2013.

[62] E. I. Vrettos and S. a. Papathanassiou, “Operating policy and optimal sizing of a high penetration RES-BESS system for small isolated grids,” *IEEE Trans. Energy Convers.*, vol. 26, no. 3, pp. 744–756, 2011.

[63] T. Logenthiran and D. Srinivasan, “Optimal selection and sizing of distributed energy resources for distributed power systems,” *J. Renew. Sustain. Energy*, vol. 4, no. 5, 2012.

[64] S. Chakraborty, T. Senjyu, H. Toyama, A. Y. Saber, and T. Funabashi, “Determination methodology for optimising the energy storage size for power system,” *IET Gener. Transm. Distrib.*, vol. 3, no. 11, p. 987, 2009.

[65] Y. A. Katsigiannis, P. S. Georgilakis, and E. S. Karapidakis, “Hybrid simulated annealing-tabu search method for optimal sizing of autonomous power systems with renewables,” *IEEE Trans. Sustain. Energy*, vol. 3, no. 3, pp. 330–338, 2012.

[66] S. X. Chen, H. B. Gooi, and M. Q. Wang, “Sizing of energy storage for microgrids,” *IEEE Trans. Smart Grid*, vol. 3, no. 1, pp. 142–151, 2012.

[67] S. Bahramirad, W. Reder, and A. Khodaei, “Reliability-constrained optimal sizing of energy storage system in a microgrid,” *IEEE Trans. Smart Grid*, vol. 3, no. 4, pp. 2056–2062, 2012.

[68] High Plains Regional Climate Center, “Wind Data Retrieval.” [Online]. Available: http://hprcc6.unl.edu/cgi-bin/winddr.cgi.

[69] PJM, “PJM- Energy market,” 2016. [Online]. Available: http://www.pjm.com/markets-and-operations/energy.aspx.

[70] A. J. Conejo, M. Carrion, and J. M. Morales, *Decision making under uncertainty in electricity markets*. Springer, 2010.

[71] Federal Energy Regulatory Commission, *Energy primer-A handbook of energy market basics*. 2012.

[72] J. Mohammadi, A. Rahimi-Kian, and M. S. Ghazizadeh, “Aggregated wind power and flexible load offering strategy,” *IET Renew. Power Gener.*, vol. 5, no. 6, p. 439, 2011.

[73] S. Dutta and T. J. Overbye, “Optimal storage scheduling for minimizing schedule deviations considering variability of generated wind power,” *2011 IEEE/PES Power Syst. Conf. Expo. PSCE 2011*, 2011.

[74] T.-Y. Lee, “Operating schedule of battery energy storage system in a time-of-use rate industrial user with wind turbine generators: a multipass iteration particle swarm optimization approach,” *IEEE Trans. Energy Convers.*, vol. 22, no. 3, pp. 774–782, Sep. 2007.

[75] J. P. S. Catalão, H. M. I. Pousinho, and V. M. F. Mendes, “Optimal offering strategies for wind power producers considering uncertainty and risk,” *IEEE Syst. J.*, vol. 6, no. 2, pp. 270–277, 2012.

[76] N. Mahmoudi, S. Member, T. K. Saha, S. Member, and M. Eghbal, “Wind power offering strategy in day-ahead markets : employing demand response in a two-stage plan,” *IEEE Trans. Power Syst.*, pp. 1–9, 2014.

[77] C. K. Simoglou, P. N. Biskas, and A. G. Bakirtzis, “Optimal offering strategies in day-ahead electricity markets under uncertainty,” in *8th Mediterranean Conference on Power Generation, Transmission, Distribution and Energy Conversion (MEDPOWER 2012)*, 2012, pp. 1–6.

[78] J. García-González, L. M. S. Rocío Moraga Ruiz de la Muela, and A. M. González, “Stochastic joint optimization of wind generation and pumped-storage units in an electricity market,” *IEEE Trans. Power Syst.*, vol. 23, no. 2, pp. 460–468, 2008.

[79] A. J. Conejo, M. Carrion, and J. M. Morales, *Decision making under uncertainty in electricity markets*. 2010.

[80] A. J. Conejo, R. García-Bertrand, M. Carrión, Á. Caballero, and A. de Andrés, “Optimal involvement in futures markets of a power producer,” *IEEE Trans. Power Syst.*, vol. 23, no. 2, pp. 703–711, 2008.

[81] W. Römisch, “Scenario reduction techniques in stochastic programming,” *Lect. Notes Comput. Sci. (including Subser. Lect. Notes Artif. Intell. Lect. Notes Bioinformatics)*, vol. 5792 LNCS, no. 2, pp. 1–14, 2009.